Final Report
ONR GRANT / CONTRACT INFORMATION

Grant / Contract Title:	Shock Survivability of Dynamical Systems
Performing Organization:	Boston University
Principal Investigator:	Dr. Paul E. Barbone
Contract Number:	N00014-95-1-0283
PR Number:	97PR02090-01
ONR Scientific Officer:	Dr. Geoffrey Main

REPORT DOCUMENTATION PAGE

Form Approved
OMB No. 0704-0188

1. AGENCY USE ONLY (Leave blank)	2. REPORT DATE	3. REPORT TYPE AND DATES COVERED
	5 May 1999	Final Report

4. TITLE AND SUBTITLE
Shock Survivability of Dynamical Systems

5. FUNDING NUMBERS
No: N00014-95-1-0283
PR: 97PR02090-01

6. AUTHOR(S)
Paul E. Barbone

7. PERFORMING ORGANIZATION NAME(S) AND ADDRESS(ES)
Department of Aerospace and Mechanical Engineering
Boston University
110 Cummington St.
Boston, MA 02215

8. PERFORMING ORGANIZATION REPORT NUMBER
AM-99-006

9. SPONSORING/MONITORING AGENCY NAME(S) AND ADDRESS(ES)
Office of Naval Research
Ballston Tower One
800 North Quincy St.
Arlington, VA 22217

10. SPONSORING/MONITORING AGENCY REPORT NUMBER

11. SUPPLEMENTARY NOTES

12a. DISTRIBUTION/AVAILABILITY STATEMENT
Openly available as BU/AME Report No. AM-99-006

12b. DISTRIBUTION CODE

13. ABSTRACT (Maximum 200 words)

We have studied the dynamic response of very complicated structures to transient shock-related excitation. We have defined a notion of complexity of dynamical substructures. We found that in the limit of infinite complexity, substructures can be accurately represented as very low order dynamical subsystems. We have obtained error bounds and estimates for these approximate representations, and derived older preexisting approximations as special cases of ours.

14. SUBJECT TERMS
Effective dynamical properties, dynamic reduction, Fuzzy structures, high modal density, modal overlap, substructures, dynamic condensation.

15. NUMBER OF PAGES
158

16. PRICE CODE

17. SECURITY CLASSIFICATION OF REPORT	18. SECURITY CLASSIFICATION OF THIS PAGE	19. SECURITY CLASSIFICATION OF ABSTRACT	20. LIMITATION OF ABSTRACT
Unclassified	Unclassified	Unclassified	Unlimited

Contents

1 Research Objectives

We have been studying the problem of quantifying equipment survivability to high amplitude impulsive inputs. We are providing a general theory by which the analysis of such systems can be systematically simplified. The simplification eases the analytical burden associated with large scale dynamical simulations. We are developing a theoretical foundation for the study of large classes of equipment and its potential failure mechanisms.

2 Technical Approach

We have considered the problem of trying to compute the response of a large scale system, say an entire submarine or a section of such, to a shock related input. The entire system can be regarded as being comprised of a main structure to which several smaller but complex subsystems (i.e. the equipment) are attached. We divide the problem into two parts: (1) modeling the effect of the subsystem on the dynamics of the main structure; (2) modeling the response (and survivability) of a subsystem given its environmental loading.

Satisfactory results on step (1) is a prerequisite for proceeding to step (2). Thus, the focus of our efforts during the project period has been on addressing part (1). If the equipment is dynamically "simple", i.e. has few resonant modes in the frequency band of interest, then a relatively simple modal description of the equipment is feasible and practical. Standard dynamic reduction techniques, e.g. *component mode synthesis*, can be utilized to construct an efficient and physically accurate model of the subsystem. It is usually the case, however, that the equipment can be described as "complex", by which we define as having many (possibly but not necessarily overlapping) resonances in the frequency band of interest. Our approach to this problem is to exploit its main complication. We have obtained an asymptotic model for the effect of a subsystem in the limit when the subsystem is "infinitely complicated."

3 Review of Progress & Accomplishments

We conceived the idea of representing subsystems through time-domain DtN maps as described in [5]. We later developed time-domain DtN maps to represent several classes of subsystems, including:

1. Linear, undamped, discrete mechanical subsystems with arbitrary number of attachment point degrees of freedom [3].
2. Linear, damped, discrete mechanical subsystems with arbitrary number of attachment point degrees of freedom [7].
3. Slightly nonlinear, undamped, discrete mechanical subsystems with a single attachment point [4].

These maps have been extensively studied. Their main drawbacks to use in practice are that:

1. They are computationally expensive to evaluate initially.
2. They depend on too much detailed information about the equipment they represent.
3. They are computationally expensive to utilize in practice.

In an attempt to address the first drawback, we examined the high modal density limit. We showed in [3] that replacing an undamped system with its "fuzzy" counterpart leads to $O(1)$ error in a time scaling with $t = o(\epsilon^{-1})$. Such a model still required an "infinite" amount of information, in that an entire mass-frequency distribution was required to construct the fuzzy DtN map, but didn't require a detailed eigenvalue analysis of the subsystem.

We then addressed the issue of information. We posed the question, suppose we replaced the system not by its fuzzy counterpart, but any "smooth" system. What characteristics do we need to build into our smooth approximation in order to accurately model the real system? The answer to this question was eventually obtained, and we identified a small sequence of parameters (three, for a system with a single attachment point) necessary to accurately model a system to a time $t = o(\epsilon^{-1})$.

The "final" issue was that of implementation. The time-domain DtN is in the form of a convolution equation in time. When this is inserted into an equation of motion, the resulting equation is an integro-differential equation (IDE) of the Volterra type. Time marching schemes for such equations are an area of active research, and stability problems are notorious. We developed a stabilized explicit time marching scheme for Volterra IDEs [6]. The method was only first order accurate, but fully explicit and has a large critical time-step.

The IDE marching, however, was displaced by the development of the effective dynamical system theory described in [2] and [1]. In [2], we also present for the first time: bounds on the symbol of the DtN in the Laplace domain in terms of its Pade' approximants; a maximum entropy approximation for the DtN in the time domain; a derivation of a self-similar mass-frequency distribution for built-up subsystems; proven upper bounds on the dissipation constant; estimated bounds on the dissipation constant; and the first formal presentation of the three-parameter model.

In [1], we examine the application of the effective dynamical system theory to continuous systems, and show that the limit of infinitely many modes is well represented in the theory.

4 Conclusions

We have developed an effective vibratory system theory which is analogous to the effective medium theory of composites. Both are asymptotic theories; both are most accurate when the properties of the system under consideration have a lot of fine detail (lots of layers in the composite, or lots of modes in the substructure); both have finite ranges of validity in terms of the independent variable.

The benefits of using effective dynamical parameters to describe a subsystem include: (1) The model requires relatively few effective parameters to be measured or predicted. (2) The parameters are independent of the master structure to which the subsystem is to be attached. (3) The error incurred from using the approximate model has been well studied [2]. (4) The effective vibratory system model is much simpler than the full model. The drawbacks of the effective vibratory system model include: (1) The model is valid for finite time, in the absense of sufficient subsystem dissipation. (2) The effective subsystem model does not predict the displacement amplitudes inside the subsystem itself.

5 Relevance to the Navy

Numerically modeling the time-domain response of naval structures can allow the simulation of explosion studies without the cost of experimental model testing. This has value in shock

hardening modifications to existing structures, the design of new structures, and the design of ordinance to excite specific motions in unfriendly structures.

Much of the shock energy absorbed by a large structure is transmitted into the substructures. Modeling the response of the main structure thus requires an appropriate representation of the response of the substructures. The specific advances made to date allow substructures to be modeled with the addition of a few differential equations, depending on just a few parameters each.

The anticipated prediction and general modeling of equipment failure modes will provide a firm theoretical foundation to develop shock-hardness tests of equipment. This is a necessary step in certifying COTS (commercial-off-the-shelf) equipment for naval applications.

6 References

1. Paul E. Barbone, "Effective Dynamical Properties," *Proceedings of the 1998 International Mechanical Engineering Congress*, Anaheim, CA, November 15–20, 1998.

2. Paul E. Barbone, A. Cherukuri, and D. Goldman. "Canonical representations of complex vibratory subsystems: Time domain Dirichlet to Neumann Maps," *Int. J. Solids and Struct.*, accepted November, 1998.

3. A. Cherukuri and P. E. Barbone. "High Modal Density Approximations for Equipment in the Time Domain," *J. Acoust. Soc. Am.*, Vol 104, No 4, October 1998.

4. Daniel Goldman and Paul E. Barbone. "Dirichlet to Neumann Maps for the Representation of Equipment with Weak Nonlinearities," Proc. ASME Noise Control and Acoustics Division, Vol. NCA22, pp. 71–76, Proceedings of the 1996 International Mechanical Engineering Congress, Atlanta, GA, November 17–22, 1996.

5. "Equipment Representations for Shock Calculations: Time Domain Dirichlet to Neumann Maps," Paul E. Barbone, *Acoustics, Vibrations, and Rotating Machines*, Vol. 3, Part B, pp. 223–228, Proceedings of the 1995 Design Engineering Technical Conferences, Sept. 17–20, 1995. ASME Press, New York.

6. Paul E. Barbone, "Implementation of Time Domain Fuzzy Structure Representations," **J. Acoust. Soc. Am.** Vol. 101, No. 5, Pt. 2, May 1997, page 3043.

7. Aravind Cherukuri and Paul E. Barbone, "Time Domain Dirichlet to Neumann Maps for Representing Complex Dynamical Subsystems," BU Dept. Aerospace & Mechanical Engineering Technical Report No. AM-96-018, 1996.

A List of publications, reports and presentation

A.1 Refereed Papers (Life of grant)

1. Paul E. Barbone, "Effective Dynamical Properties," *Proceedings of the 1998 International Mechanical Engineering Congress*, Anaheim, CA, November 15–20, 1998.

2. Paul E. Barbone, A. Cherukuri, and D. Goldman. "Canonical representations of complex vibratory subsystems: Time domain Dirichlet to Neumann Maps," *Int. J. Solids and Struct.*, accepted November, 1998.

3. A. Cherukuri and P. E. Barbone. "High Modal Density Approximations for Equipment in the Time Domain," *J. Acoust. Soc. Am.*, Vol 104, No 4, October 1998.

4. Daniel Goldman and Paul E. Barbone. "Dirichlet to Neumann Maps for the Representation of Equipment with Weak Nonlinearities," Proc. ASME Noise Control and Acoustics Division, Vol. NCA22, pp. 71–76, Proceedings of the 1996 International Mechanical Engineering Congress, Atlanta, GA, November 17–22, 1996.

5. "Equipment Representations for Shock Calculations: Time Domain Dirichlet to Neumann Maps," Paul E. Barbone, *Acoustics, Vibrations, and Rotating Machines*, Vol. 3, Part B, pp. 223–228, Proceedings of the 1995 Design Engineering Technical Conferences, Sept. 17–20, 1995. ASME Press, New York.

A.2 Non-Refereed Papers/Reports (Life of grant)

1. Paul E. Barbone, A. Cherukuri, and D. Goldman. "Canonical representations of complex vibratory subsystems, Part I: Single Attachment Point," BU Dept. Aerospace & Mechanical Eng. Technical Report No. AM-98-027, June 1998.

2. A. Cherukuri, *Time domain Dirichlet to Neumann Maps for representing complex dynamical subsystems.* M.Sc. Thesis, Dept. of Aerospace & Mechanical Eng., Boston University, Boston, MA. 1996.

3. "High Modal Density Approximations for Equipment in the Time Domain," Aravind Cherukuri and Paul E. Barbone, BU Dept. Aerospace & Mechanical Engineering Technical Report, AM-90-013, June 3, 1996.

4. Aravind Cherukuri and Paul E. Barbone, "Time Domain Dirichlet to Neumann Maps for Representing Complex Dynamical Subsystems," BU Dept. Aerospace & Mechanical Engineering Technical Report No. AM-96-018, 1996.

5. Paul E. Barbone, "Equipment Representations for Shock Calculations: Time Domain Dirichlet to Neumann Maps," BU Dept. Aerospace & Mechanical Engineering Technical Report No. AM-95-012,

A.3 Presentations (Life of grant)

A.3.1 Invited

1. Paul E. Barbone, "How complex is a complex subsystem?" invited (by Dr. S. Wu) as part of *Symposium on Innovative Computational Methods Applied to Linear Structural Mechanics and Acoustics*, Sponsored by Noise Control and Acoustics Division, ASME,

1998 International Mechanical Engineering Congress and Exposition, Anaheim, CA, November 15–20, 1998.

2. Paul E. Barbone, "Computational Representations of Complicated Linear Dynamical Subsystems: High Modal Density Asymptotics," BU Dynamical Systems Seminar Series, BU Mathematics Department, Sept. 28, 1998.

3. Paul E. Barbone, "Computational Representations of Complicated Subsystems in Structural Dynamics Simulations," Special Seminar, BU College of Engineering, April 15, 1998.

4. Paul E. Barbone & Aravind Cherukuri, "Equipment Representations for Shock Calculations: Time Domain Dirichlet to Neumann Maps," *invited seminar*, Engineering Technology Center, Mystic, CT, December 18, 1995.

A.3.2 Contributed presentations:

1. Paul E. Barbone and Allan D. Pierce, "Asymptotic Models of Complex Vibratory Subsystems," 13^{th} US National Congress of Applied Mechanics, Gainsville, FL, June 22, 1998.

2. Paul E. Barbone, "Implementation of time-domain fuzzy structure representations," 133^{rd} *Meeting of the Acoustical Society of America*, State College, PA, June 15–20, 1997.

3. Daniel Goldman and Paul E. Barbone. "Dirichlet to Neumann Maps for the Representation of Equipment with Weak Nonlinearities," *ASME Noise Control and Acoustics Division, 1996 International Mechanical Engineering Congress,* Atlanta, GA, November 17–22, 1996.

4. Paul E. Barbone, Aravind Cherukuri and Daniel Goldman, "Equipment Representations for Shock Calculations: Time Domain Dirichlet to Neumann Maps," *ONR Structural Dynamics Meeting*, Naval Surface Warfare Center, David Taylor Modeling Basin, Carderock, MD, October 17, 1996.

5. Aravind Cherukuri & Paul E. Barbone, "Equipment Representations as Time Domain Fuzzy Structures," 131^{st} *Meeting of the Acoustical Society of America*, Indianapolis, IN, May 13–17, 1996.

6. Paul E. Barbone, "Equipment Representations for Shock Calculations: Time Domain Dirichlet to Neumann Maps," *ASME Design Technical Conference*, Boston, MA, Sept. 17–20, 1995.

B List of Honors/Awards

Name of Person Receiving Award	Recipient's Institution	Name, Sponsor and Purpose of Award
Paul E. Barbone	Boston University	1999 R. Bruce Lindsay Award Acoust. Soc. Am.†
Aravind Cherukuri	Boston University	ASA Student Paper Competition††
Paul E. Barbone	Boston University	Young Investigator Award ONR†††

† R. Bruce Lindsay Award: Award presented annually to a member of the ASA who is under 35 years of age and who, ... has contributed substantially, through published papers, to the advancement of theoretical and/or applied acoustics. March, 1999.

†† Second-Best Student Paper in Structural Acoustics and Vibration, Awarded by ASA Structural Acoustics and Vibration Technical Committee, May 1996.

††† Award won for proposal "Hybrid asymptotic-numerical methods in scattering," 1995.

C Reprinted papers

This section contains reprints of papers that resulted from the current project in reverse chronological order. Where substantial duplication between journal papers and reports occurs, only the journal paper is included. The most complete overview of the project is contained in papers C.2 and C.5. A summary of the effective dynamical subsystem theory is described in paper C.1.

C.1 Effective Dynamical Properties

Paul E. Barbone, "Effective Dynamical Properties," *Proceedings of the ASME Noise Control and Acoustics Division*, Vol. NCA25, pp. 333-338, Proceedings of the 1998 International Mechanical Engineering Congress, Anaheim, CA, November 15–20, 1998.

NCA-Vol. 25, Proceedings of the ASME
Noise Control and Acoustics Divsion
ASME 1998

EFFECTIVE DYNAMICAL PROPERTIES

Paul E. Barbone *
Department of Aerospace and Mechanical Engineering
Boston University
110 Cummington St.
Boston, MA 02215

ABSTRACT

We discuss effective dynamical properties of complicated vibratory subsystems. A complicated vibratory subsystem is one in which the resonance structure contains a lot of fine detail. The first part of this paper describes an analogy between the effective vibratory subsystem theory and the effective medium equations used to model composite materials. The second part of this paper presents an example application of the effective vibratory subsystem theory. The effective subsystem theory is used to model a continuous elastic rod. Features of the nonuniform limit $\omega \to \infty$ are shown to be reproduced by the effective vibratory subsystem theory.

INTRODUCTION

We describe the modeling of a complicated vibratory subsystem in terms of an "equivalent" effective vibratory subsystem. The "effective vibratory subsystem" is that subsystem which is characterized by the "effective dynamical properties" (mass, stiffness, damping) of the subsystem under consideration. Modeling a subsystem in this way is analogous to modeling a composite material in terms of an effective medium. In the next few paragraphs, we try to explore this analogy to provide some background to the effective vibratory system theory. We follow this with an example which shows how the effective vibratory system theory can be applied. The example chosen reveals an interesting feature of the modal description of subsystems: nonuniformity of the limit $\omega \to \infty$ and $N \to \infty$. We study this limit in detail in the context of the example of an elastic rod subsystem.

Financially supported by Office of Naval Research.

EFFECTIVE MEDIUM ANALOGY

The mechanical properties of composite materials are often described in terms of "effective" material constants. The effective medium description of the composite is accurate when the length scale of deformation is much larger than the typical length scale of the microstructure. The effective medium theory is much easier to work with than the complete 3-D description of the composite material. Not only is it easier to perform an analysis with the effective medium equations, but it is much easier to measure effective material constants than it is to measure the full 3-D microstructural geometry and properties.

A well known simple example of an effective medium theory is that describing *long* waves in a *finely* layered elastic rod. The displacement field $u(x,t)$ in the rod satisfies the equation:

$$(E(x)u'(x,t))' - \rho(x)\ddot{u}(x,t) = 0. \tag{1}$$

Here, $E(x)$ is the Young's modulus of the rod and $\rho(x)$ is the mass density. We let h denote the distance over which the properties of the rod change substantially (i.e. $E(x)/E'(x) = O(h)$) and we let l denote a reference length in the rod. Then the effective medium description of the displacement field is given by:

$$u(x,t) \sim \bar{u}(x,t) + O(h/l, xh^2/l^3) \tag{2}$$

$$E_{eff}\bar{u}''(x,t) - \rho_{eff}\ddot{\bar{u}}(x,t) = 0. \tag{3}$$

$$E_{eff}^{-1} = \lim_{L\to\infty} L^{-1} \int_0^L E(x)^{-1}\, dx \tag{4}$$

$$\rho_{eff} = \lim_{L\to\infty} L^{-1} \int_0^L \rho(x)\, dx \tag{5}$$

By solving (3), one obtains an approximation of $u(x,t)$ as described in (2). The approximation is most accurate when the elastic properties of the rod have a lot of fine detail; i.e. when $h/l \ll 1$. Two simple measurements are required to evaluate the effective medium coefficients, E_{eff} and ρ_{eff}.

In analogy with the effective medium theory, Barbone, *et al.* (1998) have introduced an effective vibratory system theory to describe complicated vibratory systems. A complicated vibratory system is one in which the resonance structure has a lot of fine detail. The effective vibratory system theory has similar advantages to the effective medium theory: it is easier to model the effective system, and the effective coefficients are much simpler to measure.

Just as in the case of the effective medium theory, the effective vibratory system theory is an asymptotic theory. It is valid in the limit $\epsilon \equiv \Delta\omega/\Omega_0 \to 0$, where $\Delta\omega$ is the mean spacing between natural frequencies of the vibratory system and Ω_0 is a reference frequency parameter of the vibratory system.

We can extend the analogy further by noting that both theories have limited regions of validity in terms of the independent variables. In the case of the effective medium theory, small dispersion errors build up over distance leading to $O(1)$ contributions when

$$x = O(l^3/h^2). \tag{6}$$

Since, by assumption, $h/l \ll 1$, this distance is very large. For the effective vibratory system theory, small phase differences gradually add up to give $O(1)$ error when

$$t = O(\Delta\omega/\Omega_0^2). \tag{7}$$

Again, by assumption, $\Delta\omega/\Omega_0 \ll 1$, so this time is very large.

An effective medium theory that corrects for the dispersion effects just mentioned can be constructed (Shuman & Barbone, 1998). The equation for $\bar{u}$ takes the form (Shuman & Barbone, 1998):

$$E_{eff}\bar{u}''(x,t) - \rho_{eff}\ddot{\bar{u}}(x,t) + (h^2/l^2)\left[\alpha\ddot{\bar{u}}''(x,t) + \beta\ddot{\ddot{\bar{u}}}(x,t)\right] = 0. \tag{8}$$

We see from (8) that the effective medium is no longer a simple elastic rod, but has additional terms in the equation. The two new coefficients, α and β, depend on higher order correlations of the medium properties. An effective vibratory system theory that is valid for undamped systems beyond $O(\Delta\omega/\Omega^2)$ has not yet been developed, and is still an active area of research.

From this discussion, we conclude that the effective vibratory system theory of Barbone, *et al.* (1998) is analogous to the effective medium theory used in composites. The challenge of extending the theory to a wider range of validity, and exploring the limitations of the theory as it exists remain. In the remainder of this paper, we shall briefly describe our effective vibratory subsystem theory in the context of a specific example problem. Then we will apply the theory to a case which is formally outside its region of validity: modeling a continuous system.[1] In particular, we shall show that the nonuniform limit at $\omega = \infty$, $N = \infty$, where N is the number of modes, is reproduced exactly by the effective vibratory system theory. This buoys our confidence that the effective theory, though derived for finite dimensional systems, remains valid for infinite dimensional systems.

EFFECTIVE DYNAMICAL SUBSYSTEM THEORY

Here we describe the effective vibratory subsystem theory of Barbone, *et al.* (1998). We shall do so in the context of the simplest possible example of a "master system" which can interact with a "complicated substructure." The "master structure" is a linear harmonic oscillator. The motivation for using an effective model for the substructure is our interest in determining $x_0(t)$, the displacement history of the harmonic oscillator (master structure). The oscillator is coupled to a complicated substructure through a single attachment point. All motion is assumed to be restricted to be unidirectional. Analogous systems have been studied recently by Weaver (1996,1997), Strasberg and Feit (1996), and Nagem *et al.* (1997). This is a special case of the systems studied by Barbone and coworkers in (Barbone, 1995; Barbone and Goldman, 1996; Cherukuri and Barbone, 1998; Barbone, *et al.*, 1998). The equations of motion for the entire system can be written in the following

[1] The effective vibratory system theory in Barbone, *et al.* (1998) is derived for systems with a finite number of degrees of freedom.

form:

$$M\,\ddot{x_0} + Kx_0(t) = f(t) - f_0(t). \quad (9)$$

$$k_o x_0(t) - \sum_{n=1}^{N} \kappa_n x_n(t) = f_0(t). \quad (10)$$

$$m_n, \ddot{x}_n + \kappa_n\, x_n(t) = \kappa_n\, x_0(t) \quad (11)$$

Here, M and K represent the mass and stiffness, respectively, of the master oscillator. $x_0(t)$ represents its displacement. The subsystem is characterized by the mass constants m_n and stiffness constants κ_n. Its configuration is described by the N dimensional vector $\boldsymbol{x} = \{x_i, i = 1, \ldots, N\}$, which is zero at equilibrium. The master system is coupled to the subsystem through the vector of coupling constants $\{\kappa_i, i = 1, \ldots, N\}$. k_o is related to κ_i by $k_o = \sum_{n=1}^{N} \kappa_n$. For a complete solution, initial conditions must be prescribed.

The equations of motion using the effective vibratory system theory are

$$M\,\ddot{\bar{x}}_0 + K\bar{x}_0(t) = f(t) - f_0(t), \quad (12)$$

$$f_0(t) = M_T\ddot{y}(t), \quad (13)$$

$$M_T\ddot{y}(t) + 2bM_T\Omega\dot{y}(t) + k_o y(t) = k_o\bar{x}_0(t), \quad (14)$$

$$x_0(t) \sim \bar{x}_0(t) + O(\epsilon^4 t^4) \quad (15)$$

Here $y(t)$ is a dummy (scalar) variable, which has the interpretation of being the displacement of an additional harmonic oscillator. The effective mass M_T, stiffness k_o and damping coefficients η_o, are (in general) given in terms of the mass constants of the subsystem under consideration. In this example, the *effective mass* is simply the total mass of the subsystem,

$$M_T = \sum_{n=1}^{N} m_n, \quad (16)$$

Here, m_n is the n^{th} mass of the subsystem. The *effective stiffness* is similarly simple in this example. It is the same as the high frequency stiffness, k_o:

$$k_o = \sum_{n=1}^{N} \kappa_n \equiv \sum_{n=1}^{N} m_n\omega_n^2. \quad (17)$$

$\omega_n = \sqrt{\kappa_n/m_n}$ is the n^{th} natural frequency of the subsystem (with its attachment point held fixed.) The effective mass and stiffness together define the subsystem frequency parameter $\Omega = \sqrt{k_o/M_T}$.

The *effective dissipation* constant η_o is given by

$$\eta_o = \sum_{n=1}^{N} m_n\omega_n. \quad (18)$$

The damping term appearing in (14) is written in terms of the *effective critical damping* fraction, b, which is given in terms of η_o by solving the equation (Barbone, *et al.*, 1998)

$$\eta_o = M_T\Omega(2\cosh^{-1} b)/\pi\sqrt{b^2 - 1}. \quad (19)$$

Thus we have replaced the original $(N+1)$ DOF (degrees of freedom) undamped system, (equations (9 - 11)) with a 2 DOF dissipative system (equations (12-15)). Equation (15) indicates that $\bar{x}_0(t)$ is a good approximation for $x_0(t)$ when $\epsilon \ll 1$, up to times $t = o(\epsilon^{-1})$. As described by Pierce, Sparrow and Russel (1993), Weaver (1996,1997), Strasberg (1996), Strasberg and Feit (1996), and Cherukuri and Barbone (1998), dissipation can render the above approximation valid for all time. The dissipation must be sufficient to cause significant decay before the error has time to build up. That is, the decay time must be shorter than $t = o(\epsilon^{-1})$; i.e. the intrinsic critical damping factor, η, of the subsystem must be $\eta \gg \epsilon$. (See Cherukuri and Barbone (1998), eqn. 27; Strasberg (1996), eqn. (10).)

We note that the effective dynamical properties are independent of the master structure to which the subsystem is attached. This is one of the benefits of the effective vibratory system theory which is not available in other "fuzzy structure" theories. Thus for the purposes of further exploring the properties of the effective vibratory system model, we shall work in terms of the input impedance, as in (Strasberg, 1996).

Exact and Effective Input Impedances

The exact and effective input impedances are not meant to approximate each other. Using $\mathcal{Z}_{eff}$, the effective input impedance, however, provides an estimate $\bar{x}_0(t)$ which approximates $x_0(t)$ as specified in equation (15), above. From equations (13) and (14) we find

$$f_0 = -i\omega\mathcal{Z}_{eff}\bar{x}_0, \quad (20)$$

$$\mathcal{Z}_{eff} = -i\omega M_T \frac{\Omega^2}{\Omega^2 - 2ib\Omega\omega - \omega^2}. \quad (21)$$

The exact impedance follows from transforming equations (10) and (11) and is

$$\mathcal{Z}_{exact} = -i\omega \sum_{n=1}^{N} m_n \frac{\omega_n^2}{\omega_n^2 - \omega^2}. \quad (22)$$

APPLICATION TO ELASTIC ROD

In the rest of this paper, we shall consider the subsystem to be an elastic rod. The continuous elastic rod can be approximated to any degree of accuracy by a sufficiently high number of vibrational modes. We denote the number of modes used to represent the elastic rod by N. As $N \to \infty$, we recover the exact representation of the rod.

For any *finite* value of N, we can replace the resulting N DOF subsystem by the 1 DOF "effective subsystem." The effective properties of the subsystem, however, become singular as $N \to \infty$. At first sight, this may seem to invalidate the effective system theory. We shall show, however, that this behavior is necessary to capture the *correct* infinite frequency limit as $N \to \infty$.

More specifically, let us denote the impedance of the elastic rod approximated by N vibrational modes by $\mathcal{Z}_{exact}(N)$. We note that the limit $N \to \infty$ of $\mathcal{Z}_{exact}(N)$ is nonuniform in ω. That is,

$$\lim_{N\to\infty}\lim_{\omega\to\infty} \mathcal{Z}_{exact} \neq \lim_{\omega\to\infty}\lim_{N\to\infty} \mathcal{Z}_{exact}. \qquad (23)$$

We shall find, however, that

$$\lim_{N\to\infty}\lim_{\omega\to\infty} \mathcal{Z}_{exact} = \lim_{N\to\infty}\lim_{\omega\to\infty} \mathcal{Z}_{eff} \qquad (24)$$

$$\lim_{\omega\to\infty}\lim_{N\to\infty} \mathcal{Z}_{exact} = \lim_{\omega\to\infty}\lim_{N\to\infty} \mathcal{Z}_{eff}. \qquad (25)$$

Nonuniformity of Exact Impedance as $\omega \to \infty$

Here we describe the nonuniformity in the limit of the exact impedance. We first consider N = fixed. Taking the limit of the exact impedance (22) as $\omega \to \infty$, we find

$$\mathcal{Z}_{exact} \sim \frac{i}{\omega}\sum_{n=1}^{N} m_n\omega_n^2 = ik_o/\omega \qquad \omega \to \infty; N = \text{fixed}. \qquad (26)$$

The above limit holds for any finite value of N. It shows that the impedance of the substructure at $\omega = \infty$ is always springlike, independent of the substructure.

Let us reconsider this limit in the context of the elastic rod. We suppose that the elastic rod is attached at its left end to the master structure and is free at the right end. The equations (9-11) still apply, but we must allow $N \to \infty$. Each oscillator represents one of the infinitely many vibrational modes of the fixed-free elastic rod. The drive point impedance at infinite frequency of an elastic rod is just that of the infinite rod:

$$\mathcal{Z}_{exact} \sim \rho cA \qquad N \to \infty; \omega \to \infty. \qquad (27)$$

Here, ρ is the mass density of the rod, A is its cross sectional area, and c is the wave speed in the rod.

Clearly, (26) and (27) disagree with each other. This demonstrates the nonuniformity expressed in equation (23). It is well known that the appropriate limit to capture the infinite degree of freedom system is to take $N \to \infty$ first, and then $\omega \to \infty$.

We shall now show that $\mathcal{Z}_{eff}$ is also nonuniform in the limit $N, \omega \to \infty$. Further, we shall show that it is nonuniform in precisely the same way that $\mathcal{Z}_{exact}$ is. This result gives us some confidence that the analysis in Barbone, *et al.* (1998), performed in the context of finite degree of freedom systems, can be applied to the limiting case of continuous systems as well.

BEHAVIOR OF $\mathcal{Z}_{eff}$ AS $\omega, N \to \infty$

The limit $\omega \to \infty$ with N = fixed is straightforward. From (26) we find

$$\mathcal{Z}_{eff} \sim \frac{i}{\omega} M_T\Omega^2 = ik_o/\omega \qquad \omega \to \infty; N = \text{fixed}. \qquad (28)$$

The fact that (26) and (28) agree shows that $\mathcal{Z}_{eff}$ accurately represents $\mathcal{Z}_{exact}$ in the limit $\omega \to \infty$ with N = fixed.

In order to evaluate the limit $N \to \infty$, we must consider the behavior of the indiviual effective dynamical coefficients appearing in $\mathcal{Z}_{eff}$ as functions of N. We shall examine the limiting behavior of each of the coefficients as $N \to \infty$.

The elastic rod and its modal description in the context of fuzzy structures was previously studied by Strasberg (1996). From his results, we obtain expressions for the modal mass coefficients and natural frequencies. These are:

$$\omega_n = (n - \frac{1}{2})\pi c/L \qquad (29)$$

$$m_n = 2\rho c^2 A/\omega_n^2 L. \qquad (30)$$

Here, the length of the rod is L. Using these allows us to define the effective dynamical coefficients *as functions of* N. We emphasize that N is the number of modes of the rod that are to be included in its modal description.

Behavior of M_T as $N \to \infty$:

The effective mass of the subsystem is given by (16), with the substitution (29) and (30):

$$M_T(N) = \sum_{n=1}^{N} m_n = 2\rho c^2 A/L \sum_{n=1}^{N} \omega_n^{-2}. \qquad (31)$$

This sum can be evaluated in closed form in terms of the Polygamma function.[2] Using Abramowitz and Stegun (1972, eqns. 6.4.5 & 6.4.12) helps us to write

$$M_T(N) = \rho AL[1 - \frac{2}{\pi^2}\psi'(N+\frac{1}{2})] \quad (32)$$

$$\sim \rho AL[1 - \frac{2}{\pi^2}N^{-1} - O(N^{-2})] \quad N \to \infty \quad (33)$$

Equation (33) shall be used shortly to evaluate $\mathcal{Z}_{eff}(N)$.

Behavior of k_o and Ω as $N \to \infty$:

The effective stiffness of the subsystem is given by (17) with (30):

$$k_o(N) = \sum_{n=1}^{N} m_n\omega_n^2 = 2\rho c^2 A/L \sum_{n=1}^{N} = (2\rho c^2 A/L)N \quad (34)$$

We note that the effective stiffness becomes infinite with N.

Given $k_o(N)$ and $M_T(N)$, we can determine $\Omega(N)$:

$$\Omega(N) = \sqrt{k_o(N)/M_T(N)} \quad (35)$$

$$\sim (c/L)\sqrt{2N(1+O(N^{-1}))}. \quad (36)$$

Behavior of η_o and b as $N \to \infty$:

Finally, we need to determine the behavior of $b(N)$ as $N \to \infty$. As a step to this, we must first find $\eta_o(N)$. From (18) and (29) and (30) we find

$$\eta_o(N) = \sum_{n=1}^{N} m_n\omega_n \quad (37)$$

$$= \frac{4\rho cA}{\pi}\sum_{n=1}^{N}(2n-1)^{-1} \quad (38)$$

$$\sim \frac{4\rho cA}{\pi}[\frac{1}{2}\log N + O(1)]. \quad (39)$$

In evaluting (38) we used Gradshteyn and Ryzhik (1965; eqn. 0.132, pg. 3).

To find $b(N)$, we substitute (39), (33) and (36) into (19). Simplifying this result yields

$$\frac{2}{\pi\sqrt{2}}\frac{\log N}{\sqrt{N}} \sim 2\cosh^{-1} b/\pi\sqrt{b^2-1}. \quad (40)$$

Equation (40) indicates that $b(N) \sim \beta\sqrt{N}$. We substitute this into (40) and solve to leading order to obtain

$$b \sim \sqrt{N/2}, \qquad N \to \infty. \quad (41)$$

[2]We used Mathematica to find this.

Evaluation of $\mathcal{Z}_{eff}(N)$:

We now substitute (33), (36) and (41) into equation (21) to find the effective impedance for large N:

$$\mathcal{Z}_{eff}(N) \sim \frac{-i\omega\rho AL(1+O(N^{-1})}{1-\frac{i\omega L}{c}(1+O(N^{-1/2})) - \frac{\omega^2L^2}{2c^2N}(1+O(N^{-1/2}))}. \quad (42)$$

It is easy to verify that the limit of (42) as $\omega \to \infty$ with $N =$ fixed recovers (28). It is similarly easy to see from (42) that the limit $N \to \infty$ with $\omega =$ fixed yields

$$\mathcal{Z}_{eff} \sim \frac{-i\omega\rho AL}{1-\frac{i\omega L}{c}}, \quad N \to \infty; \omega = \text{fixed}. \quad (43)$$

Taking the limit of (43) as $\omega \to \infty$ yields

$$\mathcal{Z}_{eff} \sim \rho cA \qquad N \to \infty; \omega \to \infty. \quad (44)$$

Equation (44) is in complete agreement with (27).

As an interesting aside, we note that the $\omega = 0$ limit of (43) yields

$$\mathcal{Z}_{eff} \sim -i\omega\rho AL = -i\omega M_T, \quad N \to \infty; \omega \to 0. \quad (45)$$

This agrees with the same limit of the exact impedance. Equations (44) and (45) show that in the limit $N \to \infty$, $\mathcal{Z}_{eff}(\omega)$ is "doubly asymptotic," at the $\omega = 0, \infty$ limits. This is also true at finite N, but the effective dissipation at finite N cannot be evaluated using this information alone.

We have thus shown that the effective impedance, predicted by the effective vibratory system theory, has the same nonuniform limiting behavior as $\omega \to \infty$ and $N \to \infty$ as does the exact impedance. That is we have shown that

$$\lim_{N\to\infty}\lim_{\omega\to\infty}\mathcal{Z}_{exact} = \lim_{N\to\infty}\lim_{\omega\to\infty}\mathcal{Z}_{eff}, \quad (46)$$

$$\lim_{\omega\to\infty}\lim_{N\to\infty}\mathcal{Z}_{exact} = \lim_{\omega\to\infty}\lim_{N\to\infty}\mathcal{Z}_{eff}. \quad (47)$$

CONCLUSIONS

We have described the effective vibratory system theory in terms of an analogy with effective medium theory of composites. We noted that both are asymptotic theories; both are most accurate when the properties of the system under consideration have a lot of fine detail (lots of layers in the composite, or lots of modes in the substructure); both have finite ranges of validity in terms of the independent variable.

The benefits of using effective dynamical parameters to describe a subsystem include: (1) The model requires relatively few effective parameters to be measured or predicted. (2) The parameters are independent of the master structure to which the subsystem is to be attached. (3) The error incurred from using the approximate model has been well studied (Barbone, *et al.*, 1998). (4) The effective vibratory system model is much simpler than the full model. The drawbacks of the effective vibratory system model include: (1) The model is valid for finite time, in the absense of sufficient subsystem dissipation. (2) The effective subsystem model does not predict the displacement amplitudes inside the subsystem itself.

We have also described an example subsystem: an elastic rod. Since the effective vibratory system theory has been derived in the context of finite dimensional subsystems, the applicability of that theory to this subsystem can be questioned. Nevertheless, the continuous subsystem can be represented as a limiting case of finite dimensional modal approximations. We have shown that the limiting effective impedance of this subsystem has the same behavior as the limiting exact impedance. This result boosts our confidence that the effective vibratory subsystem theory can be used for infinite dimensional as well as finite dimensional subsystems.

REFERENCES

Abramowitz, M. and Stegun, I. A., 1972. *Handbook of Mathematical Functions.* Dover Publications, New York.

Barbone, Paul E., 1995. Equipment representations for shock calculations: Time domain Dirichlet to Neumann maps. In *Acoustics, Vibrations, and Rotating Machines*, volume 3, Part B, pages 223–228, Boston, MA., September 1995. Proceedings of 1995 Design Engineering Technical Conferences, ASME Press, New York.

Barbone, Paul E., Cherukuri, Aravind, and Goldman, Daniel, 1998. Canonical representations of complex vibratory subsystems, Part I: Single attachment point. *Int. J. Solids & Struct.*, under consideration.

Cherukuri, Aravind and Barbone, Paul E., 1998. High modal density approximations for equipment in the time domain. *J. Acoust. Soc. Am.*, in press.

Goldman, Dan and Barbone, Paul E., 1996. Dirichlet to neumann maps for the representation of equipment with weak nonlinearities. In *Proc. ASME Noise Control and Acoustics Division, 1996 International Mechanical Engineering Congress*, volume NCA22, pages 71–76, Atlanta, GA, November 1996. ASME Press, New York.

Gradshteyn, I.S. and Ryzhik, I.M., 1965. *Table of Integrals, Series and Products.* Academic Press, New York.

Nagem, R.J., Veljkovic, I. and Sandri, G.v.H., 1997. Vibration damping by a continuous distribution of undamped oscillators. *J. Sound Vib.*, 207(3):429–434.

Pierce, A.D., 1995. Resonant-frequency-distribution of internal mass inferred from mechanical impedance matrices, with application to fuzzy structure theory. In *Proceedings of the ASME Symposium on Acoustics of Submerged Structures and Transduction Systems.* ASME Press, New York, September 17–21, 1995.

Pierce, A.D., Sparrow, V.W. and Russel, D.A., 1993. Fundamental structural-acoustic idealizations for structures with fuzzy internals. *ASME Transactions*, Paper No. 93-WA/NCA-17(ASME Winter Annual Meeting, New Orleans), November 1993.

Shuman, Rebecca B. and Barbone, Paul E., 1998. Forward and Inverse Acoustic Scattering in Media with Microstructure. Technical Report No. AM-98-025., Boston University, Dept. of Aerospace and Mechanical Engineering, Boston, May 1998.

Strasberg, M., 1996. Continuous structures as "fuzzy" substructures. *J. Acoust. Soc. Am.*, 100(5):3456–3459.

Strasberg, M. and Feit, D., 1996. Vibration damping of large structures induced by attached small resonant structures. *J. Acoust. Soc. Am.*, 99(1):335–344.

Weaver, R.L., 1996. The effect of an undamped finite degree of freedom "fuzzy" substructure: Numerical solutions and theoretical discussion. *J. Acoust. Soc. Am.*, 100(5):3159–3164.

Weaver, R.L., 1997. Mean and mean-square responses of a prototypical master/fuzzy structure. *J. Acoust. Soc. Am.*, 101(3):1441–1449.

C.2 Canonical representations of complex vibratory subsystems: Time domain Dirichlet to Neumann Maps

Paul E. Barbone, A. Cherukuri, and D. Goldman. "Canonical representations of complex vibratory subsystems: Time domain Dirichlet to Neumann Maps," *Int. J. Solids and Struct.*, accepted November, 1998.

CANONICAL REPRESENTATIONS OF COMPLEX VIBRATORY SUBSYSTEMS: TIME DOMAIN DIRICHLET TO NEUMANN MAPS.

By

Paul E. Barbone

Aravind Cherukuri[1]

Daniel Goldman[2]

4 June 1998

Department of Aerospace

& Mechanical Engineering

Boston University

Boston, MA 02215

Accepted, November 1998: International Journal of Solids and Structures

[1]Currently affiliated with Parametric Technologies Corporation, Waltham, MA.

[2]Currently affiliated with Biomedical Engineering Department, Johns Hopkins University.

1 Abstract

Large scale dynamic simulations can often be simplified by appropriately replacing large portions of the domain by a Dirichlet to Neumann, or DtN map [7]. Here we consider the problem of representing a linear dynamical subsystem by such a map. The exact DtN map is computed as a modal summation and its properties are studied. Bounds on the symbol of the DtN map in the Laplace domain are obtained. The exact map is then approximated, in particular in the high modal density regime. In the high modal density limit, we obtain the result that a subsystem can be accurately represented with just three parameters. Within such an approximation we obtain representations based on a maximum entropy representation, self-similar or fractal representation, and a rational function representation. The rational function representation leads to the interesting result that any complicated dynamical subsystem with a large number of degrees of freedom is asymptotically equivalent (in the limit of infinite modal density) to a single mass-dashpot-spring system. We end with numerical examples showing the efficiency of the rational function approximation.

Contents

1 Introduction

Substructuring and "reduction" or "condensation" procedures have been used to simplify large scale numerical calculations since the mid 1960's [9, 10]. In typical condensation procedures, one begins with a complete model of the so-called "slave" subsystem, and projects the response of the slave subsystem onto a relatively small subspace. The subspace is typically developed from a combination of rigid body modes, dynamic modes, and constraint modes [6].

Such techniques are especially useful when the subsystem has relatively few eigenvalues in the frequency range of interest of a given simulation. Then the subsystem can be represented by relatively few component modes, and its response is relatively simple to simulate and to understand. We are mainly concerned here, however, with the opposite case: that is when within any frequency range of interest, a very large number of eigenvectors of the subsystem are necessary to accurately characterize its response. We consider such a subsystem to be *complicated.*[3] This limit has been examined in the context of a specific example by Weaver [19, 20], Strasberg & Feit [18], Nagem, *et al.* [13], and in other special and more general cases by Pierce and coworkers [16, 15], and Barbone and coworkers [2, 5, 8].

Rather than the condensation approaches mentioned above, we choose to represent the substructure through its Dirichlet to Neumann, or *DtN* Map [7]. In the context of dynamic substructure representation, the DtN map takes displacement histories on the boundary of the substructure into current forces/tractions applied at the same boundary. Accordingly, the forces are the Neumann data, and the displacements are the Dirichlet data. Given the exact DtN map representing a slave substructure, the presence of that substructure is exactly taken into account when computing the dynamics of the master structure.

Though exact DtN representations of substructures may be available, approximate representations are often attractive. There are at least two reasons for this. First, the approximate representation may provide sufficient accuracy at greatly reduced computational cost. Second, and perhaps more importantly, an approximate representation may involve only a few gross parameters of the dynamical system, sometimes as few as three as we shall show. These parameters can be easily estimated, thus permitting simulations to be performed without detailed knowledge of the dynamic properties of the substructures. This is an especially important advantage when the substructure is very complicated.

In this paper, we consider the problem of constructing and approximating time-domain DtN

[3] Some authors refer to such subsystems as "fuzzy" substructures."

representations of very complicated substructures. We shall focus here on the special case of a substructure which is attached to the master through a single point. In section §2 we formulate the problem to be solved in order to find the DtN. We give the exact DtN in section §3, and discuss various of its properties in section §4. These include bounds on the DtN in the Laplace domain which are, we believe, presented for the first time here. We also derive various bounds on many of the gross dynamic properties of the subsystem in this section. We then move on to the special case of high modal density systems in §5. By expanding the DtN asymptotically in powers of the modal spacing, we find that an approximate DtN can be constructed that depends on as few as three parameters. We call these the "effective dynamical parameters," and their identification represents one of the central contributions of this paper. On the basis of our high modal density theory, we consider three "canonical representations" in section §6. These are: the maximum entropy representation, the self-similar or fractal representation, and the rational function representation. The rational function representation leads to a startling equivalence: That undamped but sufficiently complicated substructures are asymptotically equivalent (in the limit of zero modal spacing) to a single spring-dashpot-mass system, up to simulation times proportional to the inverse of the modal spacing. Specific formulas for the coefficients of the reduced system are given. Finally, we give some examples applying our theory for complicated subsystems in section §7.

2 Formulation

We consider a dynamical subsystem which has a quadratic potential energy function in the N degrees of freedom, x_n, $n = 1, \ldots, N$. We shall assume that the dynamical system is attached to the outside world at only one attachment point. The displacement of the attachment point from equilibrium is denoted by $x_0(t)$. We will denote by $f_0(t)$ the force that is applied to the attachment point. The "DtN" condition that we will derive represents a map from $x_0(t)$ to $f_0(t)$. Thus, the effect of the dynamical subsystem can be included in a dynamical simulation by employing the following boundary condition at the attachment point:

$$f_0(t) = \mathcal{M}[x_0(t)]. \tag{1}$$

Here, $\mathcal{M}$ denotes the DtN map.

In what follows, x_0 and x_n are purely unidirectional. The extension to many attachment points and three dimensional displacements follows in a future contribution.

In the case when $f_0 = 0$, we can write the potential energy function as

$$V(x_0, \mathbf{x}) = \frac{1}{2}[\mathbf{x} \cdot \mathbf{K}\,\mathbf{x} + 2x_0\,\boldsymbol{\kappa} \cdot \mathbf{x} + k_o {x_0}^2]. \tag{2}$$

Here, $\mathbf{x}$ is an N dimensional displacement vector, $\mathbf{K}$ is an $N \times N$ positive definite matrix, $\boldsymbol{\kappa}$ is an N dimensional vector of spring constants, and k_o is a coupling spring constant. The potential energy function must be invariant to rigid body translation [15]. Therefore, for all α

$$V(x_0 + \alpha, \mathbf{x} + \alpha p) = V(x_0, \mathbf{x}). \tag{3}$$

In (3), p is an N dimensional vector with each component equal to unity. Substituting (2) into (3) yields

$$\mathbf{K}\,p = -\boldsymbol{\kappa} \tag{4}$$

$$k_o = -p \cdot \boldsymbol{\kappa} = p \cdot \mathbf{K}\,p. \tag{5}$$

We introduce the positive definite mass matrix $\mathbf{M}$ which allows us to write the kinetic energy function as:

$$T(\dot{\mathbf{x}}) = \frac{1}{2}\left[m_o {\dot{x}_0}^2 + \dot{\mathbf{x}} \cdot \mathbf{M}\,\dot{\mathbf{x}}\right]. \tag{6}$$

Lagrange's dynamical equations of motion [11] gives us the equations of motion for our system as:

$$\mathbf{M}\,\ddot{\mathbf{x}} + \mathbf{K}\,\mathbf{x}(t) = -\boldsymbol{\kappa}\,x_0(t) \tag{7}$$

$$m_o \ddot{x_0} + \boldsymbol{\kappa} \cdot (\mathbf{x}(t) - p x_0(t)) = f_0(t). \tag{8}$$

3 Exact DtN map

An exact DtN map can be constructed by solving (7) exactly and substituting the result into (8). An exact solution of (7) can be constructed in terms of a Green's function. The Green's function itself shall be found in terms of the modes of vibration of the dynamical subsystem.

3.1 The Green's function

The Green's function, $g(t-\tau)$ satisfies

$$\mathbf{M}\ddot{g}(t-\tau) + \mathbf{K}g(t-\tau) = -\kappa\delta(t-\tau), \tag{9}$$

$$g(t-\tau) = \mathbf{0} \qquad t < \tau. \tag{10}$$

Equation (7), together with equations (9) and (10) show that $\mathbf{x}(t)$ is given by

$$\mathbf{x}(t) = \int_{-\infty}^{t} g(t-\tau)\, x_0(\tau)\, d\tau. \tag{11}$$

We now solve (9) for g in terms of a normal mode expansion. We begin by introducing a change of dependent variables

$$g(t) = \mathbf{M}^{-1/2}\, y(t). \tag{12}$$

Here, $\mathbf{M}^{1/2}$ is the unique positive definite matrix which satisfies $\mathbf{M}^{1/2}\,\mathbf{M}^{1/2} = \mathbf{M}$. We shall not have the need to calculate $\mathbf{M}^{1/2}$ explicitly here. Substituting (12) into (9) and left multiplying both sides by $\mathbf{M}^{-1/2}$ yields

$$\ddot{y}(t) + \mathbf{M}^{-1/2}\mathbf{K}\mathbf{M}^{-1/2}\, y(t) = -\mathbf{M}^{-1/2}\kappa\,(t). \tag{13}$$

The matrix $\mathbf{M}^{-1/2}\mathbf{K}\mathbf{M}^{-1/2}$ is $N \times N$, symmetric and positive definite. It therefore possesses N distinct, orthonormal eigenvectors $\boldsymbol{\xi}^{(n)}$, $n = 1, \ldots, N$, and N (not necessarily distinct) positive eigenvalues ω_n^2:

$$\mathbf{M}^{-1/2}\mathbf{K}\mathbf{M}^{-1/2}\ \boldsymbol{\xi}^{(n)} = \omega_n^2 \boldsymbol{\xi}^{(n)} \tag{14}$$

Since $\boldsymbol{\xi}^{(n)}$ span R^N, we can write

$$y(t) = \sum_{n=1}^{N} \boldsymbol{\xi}^{(n)}\, z_n(t). \tag{15}$$

We now substitute (15) into (13) and make use of the orthonormality of $\boldsymbol{\xi}^{(n)}$ to obtain

$$\ddot{z}_n(t) + \omega_n^2\, z_n(t) = -\boldsymbol{\xi}^{(n)} \cdot \mathbf{M}^{-1/2}\kappa\,(t). \tag{16}$$

Further, causality requires

$$z_n(t) = 0 \qquad\qquad t < 0. \tag{17}$$

Solving (16) subject to the condition (17) yields

$$z_n(t) = -\frac{1}{\omega_n}\,\boldsymbol{\xi}^{(n)} \cdot \mathbf{M}^{-1/2}\boldsymbol{\kappa}\,\sin(\omega_n t) \qquad\qquad t \geq 0. \tag{18}$$

We obtain $g(t)$ by using (18) in (15) and (12) to find, for $t > 0$

$$g(t) = -\mathbf{M}^{-1/2}\sum_{n=1}^{N}\frac{1}{\omega_n}\boldsymbol{\xi}^{(n)}[\boldsymbol{\xi}^{(n)} \cdot \mathbf{M}^{-1/2}\boldsymbol{\kappa}]\,\sin(\omega_n t). \tag{19}$$

With $g(t)$ determined, the exact DtN condition follows directly using (11) and (8):

$$f_0(t) = m_o\ddot{x_0}(t) - \boldsymbol{\kappa}\cdot p x_0(t) - \int_{-\infty}^{t}\boldsymbol{\kappa}\cdot\mathbf{M}^{-1/2}\sum_{n=1}^{N}\frac{1}{\omega_n}\boldsymbol{\xi}^{(n)}[\boldsymbol{\xi}^{(n)}\cdot\mathbf{M}^{-1/2}\boldsymbol{\kappa}]\,\sin\omega_n(t-\tau)\,x_0(\tau)\,d\tau. \tag{20}$$

Equation (20) can be simplified by utilizing the concept of modal mass. O'Hara and Cunniff [14] define the modal mass as (see also Pierce [15], and generalizations in Cherukuri & Barbone [5]):

$$m_n = (p\cdot\mathbf{M}^{1/2}\boldsymbol{\xi}^{(n)})^2. \tag{21}$$

From the definition of $\boldsymbol{\xi}^{(n)}$, we note that

$$\mathbf{M}^{-1/2}\mathbf{K}\mathbf{M}^{-1/2}\boldsymbol{\xi}^{(n)} = \omega_n^2\boldsymbol{\xi}^{(n)}. \tag{22}$$

We left multiply (22) by $\boldsymbol{\kappa}\cdot\mathbf{K}^{-1}\mathbf{M}^{1/2}$, and use (4) to find

$$\boldsymbol{\kappa}\cdot\mathbf{M}^{-1/2}\boldsymbol{\xi}^{(n)} = -\omega_n^2 p\cdot\mathbf{M}^{1/2}\boldsymbol{\xi}^{(n)}. \tag{23}$$

We now use (23) and (21) to simplify (20) and obtain

$$f_0(t) = m_o\ddot{x_0}(t) + k_o x_0(t) - \int_{-\infty}^{t}\sum_{n=1}^{N} m_n\omega_n^3\,\sin\omega_n(t-\tau)\,x_0(\tau)\,d\tau. \tag{24}$$

4 Properties of DtN map

The exact DtN map (24) has many interesting properties which we now describe. These include relations among the various coefficients appearing in (24), as well as the behavior of the Laplace transform of the DtN in the complex plane.

4.1 The properties of the modal masses

O'Hara and Cunniff [14] show that the sum of the modal masses defined as in equation (21) is equal to the total mass of the substructure. i.e.

$$\sum_{n=1}^{N} m_n = M_T \tag{25}$$

For completeness of our presentation, we show a similar proof here. From (21) and the orthonormality of $\boldsymbol{\xi}^{(n)}$, we have:

$$\begin{aligned}
\sum_{n=1}^{N} m_n &= \sum_{n=1}^{N} (p \cdot \mathbf{M}^{1/2} \boldsymbol{\xi}^{(n)})^2 \\
&= \sum_{n=1}^{N} (p \cdot \mathbf{M}^{1/2} \boldsymbol{\xi}^{(n)})(p \cdot \mathbf{M}^{1/2} \boldsymbol{\xi}^{(n)}) \\
&= p \cdot \mathbf{M}^{1/2} \mathbf{M}^{1/2} p \\
&= p \cdot \mathbf{M} p \\
&= M_T.
\end{aligned} \tag{26}$$

A relation that is stated by neither O'Hara and Cunniff [14] nor Pierce [15] is that between the attachment stiffness k_o and the modal masses. To show this, we consider the sum:

$$\begin{aligned}
\sum_{n=1}^{N} \omega_n^2 m_n &= \sum_{n=1}^{N} \omega_n^2 (p \cdot \mathbf{M}^{1/2} \boldsymbol{\xi}^{(n)})^2 \\
&= \sum_{n=1}^{N} \omega_n^2 (p \cdot \mathbf{M}^{1/2} \boldsymbol{\xi}^{(n)})(p \cdot \mathbf{M}^{1/2} \boldsymbol{\xi}^{(n)}) \\
&= \sum_{n=1}^{N} \omega_n^2 (p \cdot (\frac{1}{\omega_n^2} \mathbf{K} \mathbf{M}^{-1/2} \boldsymbol{\xi}^{(n)}))(p \cdot \mathbf{M}^{1/2} \boldsymbol{\xi}^{(n)}) \qquad \text{by (22)} \\
&= p \cdot \mathbf{K} \mathbf{M}^{-1/2} \mathbf{M}^{1/2} p \\
&= k_o \qquad \text{by (4) and (5).}
\end{aligned} \tag{27}$$

Here, we again used the orthonormality of the $\boldsymbol{\xi}^{(n)}$.

The two parameters M_T and k_o can be used to define a "bulk" frequency scale for the subsystem. Thus we define Ω, the effective or bulk or gross frequency parameter of the subsystem as:

$$\Omega^2 = k_o/M_T. \tag{28}$$

4.2 The DtN in the Laplace domain

We now consider the Laplace transform of (24) and the resulting DtN in the transform domain. To that end, we first introduce the following definitions:

$$F_0(s) = \int_0^\infty f_0(t)\, e^{-st} dt \tag{29}$$

$$X_0(s) = \int_0^\infty x_0(t)\, e^{-st} dt \tag{30}$$

Multiplying (24) by e^{-st} and integrating with respect to t then yields:

$$F_0(s) = s^2 m_o X_0(s) + K(s) X_0(s) \tag{31}$$

Here we have introduced $K(s)$, the symbol of the DtN operator under Laplace transformation. It is given by the function:

$$K(s) = k_o - \int_0^\infty \sum_{n=1}^{N} m_n \omega_n^3 \sin(\omega_n t)\, e^{-st} dt. \tag{32}$$

In obtaining (31), we assumed that both $x_0(t) = 0$ and $f_0(t) = 0$ for all $t < 0$. Further, we assumed that

$$x_0(0) = 0 \quad ; \quad x_0'(0) = 0. \tag{33}$$

The transform of the DtN operator, $K(s)$ can be easily computed. Evaluating the integral indicated in (32) for $\mathcal{R}(s) > 0$ yields

$$K(s) = k_o - \sum_{n=1}^{N} m_n \frac{\omega_n^4}{s^2 + \omega_n^2} \tag{34}$$

We use (34) to continue the definition of $K(s)$ over the entire $s-$plane. We note by inspection that $K(s)$ has no singularities in the complex s plane except those at the points $s_n = \pm i\omega_n$.

4.2.1 Bounds on $K(s)$

Here we find it convenient to consider $K(s)$ as a function of s^2. That is, we consider the function:

$$K_2(s^2) \equiv K(s) = k_o - \sum_{n=1}^{N} m_n \frac{\omega_n^4}{s^2 + \omega_n^2} \tag{35}$$

We observe from (35) that $K_2(z)$ ($z = s^2$) is a rational function of z with singularities only at the points $z_n = -\omega_n^2 < 0$; i.e. only on the negative real axis.

Further, we note that the analytic continuation of $K_2(z)$ into the whole of the z plane is *Herglotz* [3]; i.e. $\mathcal{I}(K_2(z)) < 0 \iff \mathcal{I}(z) < 0, \mathcal{I}(K_2(z)) > 0 \iff \mathcal{I}(z) > 0$ and $\mathcal{I}(K_2(z)) = 0 \iff \mathcal{I}(z) = 0$. To show this, we let $z = x + iy$ (x and y are real), and obtain from (35)

$$K_2(z) = k_o - \sum_{n=1}^{N} m_n \frac{\omega_n^4}{(x+\omega_n^2)^2 + y^2}\Big[(x+\omega_n^2) - iy\Big]. \tag{36}$$

The fact that $K_2(z)$ is Herglotz thus follows by inspection, noting that $m_n > 0$ and ω_n is real. Finally, we note that $K_2(z) \to k_o$ as $z \to \infty$ for any $\arg z$. These properties together are sufficient to guarantee that $K_2(z)$ is bounded by its Pade' approximants [4].

Following the notation of Bender & Orszag (1978), an N-M Pade' approximation shall be denoted by $P_M^N(z)$. That is

$$K_2(z) \approx P_M^N(z) \equiv \frac{\sum_{n=0}^{N} a_n z^n}{\sum_{m=0}^{M} b_m z^m} \tag{37}$$

Without loss of generality, b_0 is chosen to be 1. Clearly, the fact that $K_2(z)$ is rational implies that the Pade' sequence will converge to $K_2(z)$ for N and M sufficiently large. Smaller values of N and M, however, provide upper and lower bounds on $K_2(z)$:

$$P_N^{N-1}(z) \le P_{N+1}^N(z) \le K_2(z) \le P_{N+1}^{N+1}(z) \le P_N^N(z) \qquad \forall N,\ z > 0 \tag{38}$$

Thus, each diagonal or nearly diagonal Pade' approximant provides a bound on $K_2(z)$: the higher order the approximant, the sharper the bound.

Pade' sequences can be developed from the Taylor expansion of $K_2(z)$ about any point. In particular, the values of $z = 0$ or $z = \infty$ correspond to the physical limits of low and high frequency response, respectively. Thus, if the low or high frequency limiting behavior of the system is known or can be accurately estimated, then a Pade' approximation can be formed there. Such estimates can be used to provide bounds on equipment models that will be presented later.

4.3 Low and High Frequency Approximate DtN Maps

Equation (24) represents the exact DtN for the dynamical subsystem under consideration. In general, $2N$ parameters are required to characterize the subsystem. When N is small, (24) can be conveniently used directly. In practice, however, N can be arbitrarily large. In such situations, it is often beneficial to consider approximations to (24) in which the DtN can be accurately represented by relatively few effective parameters. In this section, we discuss two limiting cases in which this is possible. These are the special cases when the excitation is either of very low frequency or very high frequency. These provide approximations valid not only at small and large s^2, but by the results of §4.2, also bounds on the behavior of $K(s)$ along the entire real $s-$line. The bounds thus found can be used to find bounds and interrelations between the the bulk or effective subsystem parameters, as we show below.

4.3.1 Low frequency limit

When the frequency of the excitation is much lower than the natural frequencies of the subsystem, then the inertia of the subsystem is negligible to a first approximation. To obtain an approximate DtN in this case, we rewrite (7) as

$$\mathbf{K}\,\mathbf{x}(t) = -\boldsymbol{\kappa}\, x_0(t) - \mathbf{M}\,\ddot{\mathbf{x}}. \tag{39}$$

Solving (39) by iteration yields

$$\mathbf{x}(t) = -\mathbf{K}^{-1}\boldsymbol{\kappa}\, x_0(t) + \mathbf{K}^{-1}\mathbf{M}\mathbf{K}^{-1}\boldsymbol{\kappa}\,\ddot{x_0}(t) - \mathbf{K}^{-1}\mathbf{M}\mathbf{K}^{-1}\mathbf{M}\mathbf{K}^{-1}\boldsymbol{\kappa}\,\frac{d^4x_0(t)}{dt^4} + \ldots. \tag{40}$$

We now substitute (40) into (8) and simplify using (5) to obtain

$$f_0(t) = m_o\,\ddot{x_0}(t) + M_T\,\ddot{x_0}(t) - p\cdot\mathbf{M}\mathbf{K}^{-1}\mathbf{M}p\,\frac{d^4x_0(t)}{dt^4} + \ldots. \tag{41}$$

Here, we have used the relation $M_T = p\cdot\mathbf{M}p$, which represents the total mass in the subsystem. We note that to leading order, the force is merely accelerating the subsystem as a rigid body.

Alternatively, we can derive a relation equivalent to (41) in the Laplace domain. Expanding (31) in a Taylor series about $s = 0$ yields

$$F_0(s) = \left[s^2m_o + K(0) + sK'(0) + \frac{1}{2}s^2K''(0) + \frac{1}{6}s^3K'''(0) + \frac{1}{24}s^4K''''(0) + \ldots\right]X_0(s). \tag{42}$$

The individual coefficients in the series can be evaluated from (34) and (27). Then (42) simplifies to:

$$F_0(s) = \left[s^2(m_o + M_T) - s^4\sum_{n=1}^{N}\frac{m_n}{\omega_n^2} + s^6\sum_{n=1}^{N}\frac{m_n}{\omega_n^4} - \ldots\right]X_0(s) \tag{43}$$

Inverse transforming (43), and using (21) yields (41).

It is interesting to consider a Pade' approximation of $K(s)$ obtained from this expansion. We can construct the P_1^1 and P_2^1 Pade' approximants (about $z = 0$) of $K_2(z) = K(s)$ by matching their asymptotic expansions about $z = 0$ to the coefficients in (43). This yields

$$P_2^1(s^2) \leq K(s) \leq P_1^1(s^2) \tag{44}$$

$$P_2^1(s^2) = \frac{s^2 {M_T}^2}{M_T + s^2 \sum_{n=1}^N (m_n/\omega_n^2) + s^4 \left[\left(\sum_{n=1}^N (m_n/\omega_n^2) \right)^2 - M_T \sum_{n=1}^N (m_n/\omega_n^4) \right] / M_T} \tag{45}$$

$$P_1^1(s^2) = \frac{s^2 {M_T}^2}{M_T + s^2 \sum_{n=1}^N (m_n/\omega_n^2)}. \tag{46}$$

Equation (44) provides not only approximations of $K(s)$, but also upper and lower bounds for all $s^2 > 0$.

Equation (44) can also be used to find relations between the different coefficients that appear in those equations. For example, evaluating (44) at $s = \infty$, and using (28) and (55) yields:

$$\Omega^2 \sum_{n=1}^N (m_n/\omega_n^2) \leq M_T. \tag{47}$$

Further, recognizing that $P_1^1 \geq P_2^1 \; \forall s^2$ gives us:

$$\left(\sum_{n=1}^N (m_n/\omega_n^2) \right)^2 \geq M_T \sum_{n=1}^N (m_n/\omega_n^4). \tag{48}$$

These results shall be used later.

4.3.2 High frequency limit

Alternatively, the time scale of the excitation may be much higher than any of the natural frequencies of the dynamical subsystem. In this case, the inertia term in equation (7) dominates. We rewrite (7), therefore, as

$$\mathbf{M}\ddot{\mathbf{x}}(t) = -\boldsymbol{\kappa} x_0(t) - \mathbf{K}\mathbf{x} \tag{49}$$

$$\mathbf{M}\ddot{\mathbf{x}}(t) \approx -\boldsymbol{\kappa} x_0(t) \tag{50}$$

Taking two time derivatives of (8) and simplifying using (50) yields

$$\ddot{f}_0(t) = m_o {x_0}^{(iv)}(t) + k_o \ddot{x}_0(t) - \boldsymbol{\kappa} \cdot \mathbf{M}^{-1} \boldsymbol{\kappa} x_0(t). \tag{51}$$

Carrying the process still further yields:

$${f_0}^{(iv)}(t) = m_o {x_0}^{(vi)}(t) + k_o {x_0}^{(iv)}(t) - \boldsymbol{\kappa} \cdot \mathbf{M}^{-1} \boldsymbol{\kappa} \ddot{x}_0(t) + \boldsymbol{\kappa} \cdot \mathbf{M}^{-1} k \mathbf{M}^{-1} \boldsymbol{\kappa} x_0(t). \tag{52}$$

At very high frequencies, the last term in (51) can be neglected yielding

$$\ddot{f}_0(t) = m_o x_0{}^{(iv)}(t) + k_o \ddot{x_0}(t). \tag{53}$$

From (53), we see that in this regime the force is resisted primarily by the mass at the attachment point and the elasticity in the equipment mount. Based on the interpretation of (53), we refer to the quantity k_o as the "high-frequency stiffness."

It is again interesting to consider the identical approximation in the Laplace domain. By doing so, we shall obtain further bounds on $K(s)$. Taking the Laplace transform of (52) and noting (31) yields

$$F_0(s) = s^2 m_o X_0(s) + K(s) X_0(s) \tag{54}$$

$$K(s) \sim k_o - \boldsymbol{\kappa} \cdot \mathbf{M}^{-1} \boldsymbol{\kappa}\, s^{-2} + \boldsymbol{\kappa} \cdot \mathbf{M}^{-1} k \mathbf{M}^{-1} \boldsymbol{\kappa}\, s^{-4} + o(s^{-6}) \qquad s \to \infty \tag{55}$$

From the expansion (55), we can form the P_1^1 and P_1^0 Pade' approximants, this time about the point $s = \infty$. Thus we obtain:

$$P_1^0(s^2) \le K(s) \le P_1^1(s^2) \tag{56}$$

$$P_1^0(s^2) = \frac{{k_o}^2}{k_o + \boldsymbol{\kappa} \cdot \mathbf{M}^{-1} \boldsymbol{\kappa}\, s^{-2}} \tag{57}$$

$$P_1^1(s^2) = \frac{k_o\, \boldsymbol{\kappa} \cdot \mathbf{M}^{-1} \boldsymbol{\kappa} + \left[(\boldsymbol{\kappa} \cdot \mathbf{M}^{-1} \boldsymbol{\kappa})^2 - k_o \boldsymbol{\kappa} \cdot \mathbf{M}^{-1} k \mathbf{M}^{-1} \boldsymbol{\kappa} \right] s^{-2}}{\boldsymbol{\kappa} \cdot \mathbf{M}^{-1} \boldsymbol{\kappa} + \boldsymbol{\kappa} \cdot \mathbf{M}^{-1} k \mathbf{M}^{-1} \boldsymbol{\kappa}\, s^{-2}} \tag{58}$$

Again, we have not only approximations of $K(s)$, but also bounds for all $s^2 \ge 0$. Equation (56) implies that (58) must be nonnegative at $s = 0$. This gives us:

$$(\boldsymbol{\kappa} \cdot \mathbf{M}^{-1} \boldsymbol{\kappa})^2 \ge k_o \boldsymbol{\kappa} \cdot \mathbf{M}^{-1} k \mathbf{M}^{-1} \boldsymbol{\kappa}. \tag{59}$$

Expanding (57) in the neighborhood of $s = 0$, and using (43) and (56) yields

$${k_o}^2 s^2 \le M_T\, \boldsymbol{\kappa} \cdot \mathbf{M}^{-1} \boldsymbol{\kappa} s^2. \tag{60}$$

Equations (59) and (60) can be rewritten in terms of the modal masses and natural frequencies. To do so, we use (4,21 & 22) to find:

$$\boldsymbol{\kappa} \cdot \mathbf{M}^{-1} \boldsymbol{\kappa} = \sum_{n=1}^{N} m_n \omega_n^4 \tag{61}$$

$$\boldsymbol{\kappa} \cdot \mathbf{M}^{-1} k \mathbf{M}^{-1} \boldsymbol{\kappa} = \sum_{n=1}^{N} m_n \omega_n^6. \tag{62}$$

Combining (59-62) (and using (28) as necessary) yields bounds on the modal sums:

$$M_T \Omega^4 \leq \sum_{n=1}^{N} m_n \omega_n^4 \tag{63}$$

$$\left[\sum_{n=1}^{N} m_n \omega_n^4 \right]^2 \geq k_o \sum_{n=1}^{N} m_n \omega_n^6 \tag{64}$$

Equation (64) shows that the behavior of the higher order moment ($\sum m_n \omega_n^6$) is determined by the behavior of lower order moments. Equation (63) shall be used in a later section.

5 High Modal Density

In the last section, we simplified the form of the exact DtN map (24) by making assumptions regarding the form of the excitation (i.e. high or low frequency.) In this section, we instead make an assumption regarding the complexity of the dynamical subsystem and thereby simplify the DtN map.

As noted earlier, the form of the DtN map in (24) is appropriate when the subsystem has few modes. In that case, the subsystem can be reasonably categorized as simple. On the other hand, when the subsystem has many modes in the frequency band of interest, i.e. is complicated, we seek an alternate representation that is more efficiently developed and evaluated.

Below we change the sum in (24) to an integral over frequency. We then approximate the kernel of the frequency integral and bound the resulting error. Making the error bound as small as possible identifies a sequence of parameters that govern the dynamics of the subsystem. Our analysis indicates that these parameters are fundamental in describing the dynamics of the subsystem. The identification of these parameters is one of the main contribution contained in this paper.

5.1 Replacing sum by integral

When the modes of the subsystem are closely spaced in frequency, the sum over modes in (24) can be accurately approximated by an integral. Such a substitution is the basis of the fuzzy structure representations of Pierce, Sparrow and Russel (1995). We shall also make use of Pierce et al.'s [15] notion of mass as a function of natural frequency.

Unlike Pierce et al., we *exactly* replace the sum over modes with an integral over a frequency parameter. To effect this replacement, we first introduce the generalized function, $m(\omega)$, defined by

$$\frac{dm}{d\omega}(\omega) = \sum_{n=1}^{N} m_n \delta(\omega - \omega_n) \tag{65}$$

$$m(0) = 0 \tag{66}$$

$$\tag{67}$$

Using equation (65) in the exact DtN condition (24), allows us to rewrite that exact relation as

$$f_0(t) = m_o \ddot{x_0}(t) + k_o x_0(t) - \int_{-\infty}^{t} \int_0^{\infty} \frac{dm(\omega)}{d\omega} \omega^3 \sin\omega(t-\tau)\, x_0(\tau)\, d\omega\, d\tau. \tag{68}$$

5.1.1 Properties of $m(\omega)$

The function $m(\omega)$ inherits its properties from the modal masses in terms of which it is defined. Using equation (65) in equations (26) and (27) yields directly

$$\int_0^\infty \frac{dm}{d\omega}(\omega)d\omega = M_T \tag{69}$$

$$\int_0^\infty \omega^2 \frac{dm}{d\omega}(\omega)d\omega = k_o \tag{70}$$

In addition, those inequalities derived in section §4.3 have counterparts in terms of $m(\omega)$.

5.2 High modal density approximation

When the modes of the subsystem are closely spaced in frequency, the kernel in the integral operator in (68) is rapidly varying. Under those conditions, the action of the operator can be simulated in terms of another integral operator with a smooth kernel. With this motivation in mind, we therefore consider splitting $m(\omega)$ into a "smooth" part and a rapidly varying part as follows:

$$m(\omega) = \bar{m}(\omega) + m_e\left(\frac{\omega}{\epsilon}\right). \tag{71}$$

Here, we have introduced the parameter ϵ defined by

$$\epsilon = \Delta\omega/\Omega \ll 1. \tag{72}$$

$\Delta\omega$ is taken to be a measure of the modal spacing, for example $\Delta\omega = \max_n(\omega_n - \omega_{n-1})$, or the average over all n of $(\omega_n - \omega_{n-1})$. Thus ϵ is a nondimensional measure of the modal spacing. An approximate DtN map (or *fuzzy structure* approximation) is obtained by neglecting the $m_e(\omega)$ term in (71) and replacing $m(\omega)$ by $\bar{m}(\omega)$ in (68). The key to obtaining an *accurate* approximate DtN lies in choosing $\bar{m}(\omega)$ appropriately.

We note that (71) leaves $\bar{m}(\omega)$ unspecified in its relation to $m(\omega)$. Thus we are considering the action of any continuous $\bar{m}(\omega)$ as an approximation for the action of $m(\omega)$. This notion is in contrast to the presentation of Cherukuri & Barbone (1996), who require $\bar{m}(\omega)$ to be the limit of $m(\omega)$ as $\epsilon \to 0$. Obviously, some choices of $\bar{m}(\omega)$ will lead to better approximations of the DtN map than others. In order to yield an accurate DtN map, some properties of the exact $m(\omega)$ must be duplicated in $\bar{m}(\omega)$. Precisely what aspects of $m(\omega)$ must be duplicated in $\bar{m}(\omega)$ in order to accurately represent the dynamics of the subsystem is determined below, in an error analysis.

5.3 Error Bounds

5.3.1 Error Analysis

To obtain an approximate DtN, we substitute (71) into (68) to write:

$$f_0(t) = m_o\ddot{x_0}(t) + k_o x_0(t) - \int_0^t \int_0^\infty \frac{d\bar{m}}{d\omega}(\omega)\omega^3 \sin\omega(t-\tau)\, x_0(\tau)\, d\omega\, d\tau + \text{error}(t), \quad (73)$$

$$\text{error}(t) = -\int_0^t \int_0^\infty \frac{d}{d\omega}\left[m_e(\frac{\omega}{\epsilon})\right] \omega^3 \sin\omega(t-\tau)\, x_0(\tau)\, d\omega\, d\tau. \quad (74)$$

Here we have made the assumption that

$$x_0(t) \equiv 0 \qquad \forall\, t < 0 \quad (75)$$

We shall now analyze the error in the force, error(t). In what follows, we shall assume that all functions are regular enough to carry out our calculations, and that all integrals and limits are defined. Integrating (74) by parts three times with respect to t and using (75) yields:

$$\text{error}(t) = -\int_0^\infty \frac{d}{d\omega}\left[m_e(\frac{\omega}{\epsilon})\right] \left\{\omega^2 x_0(t) - x_0''(t) + \int_0^t \cos\omega(t-\tau)\, x_0'''(\tau)\, d\tau\right\} d\omega. \quad (76)$$

In terms of a new integration variable $\nu = \omega/\epsilon$, equation (76) can be rewritten as

$$\begin{aligned}\text{error}(t) = &\int_0^\infty \frac{dm_e}{d\nu}(\nu)\, d\nu\; x_0''(t) \\ &-\epsilon^2 \int_0^\infty \nu^2 \frac{dm_e}{d\nu}(\nu)\, d\nu\; x_0(t) \\ &-\int_0^t \left\{\int_0^\infty \frac{dm_e}{d\nu}(\nu)\, \cos\epsilon\nu(t-\tau)\, d\nu\right\} x_0'''(\tau)\, d\tau. \end{aligned} \quad (77)$$

We now introduce the following integrals of $m_e(\omega)$:

$$m_1(\nu) = \int_0^\nu m_e(\nu')d\nu' \quad (78)$$

$$m_n(\nu) = \int_0^\nu m_{n-1}(\nu')d\nu' \quad (79)$$

Integration by parts with respect to ν allows us to write:

$$\begin{aligned}\int_0^\infty \frac{dm_e}{d\nu}(\nu)\, \cos\epsilon\nu t\, d\nu = &\; m_e(\nu)\cos\epsilon\nu t\big|_{\nu=\infty} \\ &+\epsilon t\, m_1(\nu)\sin\epsilon\nu t\big|_{\nu=\infty} \\ &+ \ldots \\ &+(-1)^n\epsilon^{2n}t^{2n}\, m_{2n}(\nu)\cos\epsilon\nu t\big|_{\nu=\infty} \\ &+(-1)^n\epsilon^{2n+1}t^{2n+1}\int_0^\infty m_{2n+1}(\nu)\, \sin\epsilon\nu t\, d\nu \end{aligned} \quad (80)$$

Here we have integrated by parts an odd number of times. One can, of course, integrate by parts an even number of times to obtain a similar result. The expansion indicated in (80) can be continued indefinitely, provided that the integrals at each stage converge. This convergence can be guaranteed for any $m(\omega)$ by an appropriate choice of $\bar{m}(\omega)$. In order for the limits (at $\nu = \infty$) indicated in (80) to exist, we require:

$$\lim_{\nu\to\infty} m_e(\nu) = 0 \tag{81}$$

$$\lim_{\nu\to\infty} m_j(\nu) = 0 \qquad j = 1,\ldots,2n \tag{82}$$

Substituting (80–82) (with $n \geq 2$) into (77) now allows us to write error(t) as

$$\text{error}(t) = (-1)^{n+1}\epsilon^{2n+1}\int_0^t\int_0^\infty m_{2n+1}(\nu)\,\sin\epsilon\nu(t-\tau)\,d\nu\;(t-\tau)^{2n+1}\,x_0'''(\tau)\;d\tau. \tag{83}$$

5.3.2 Error Bound

We now seek to bound error(t). To that end, we note

$$\begin{aligned}
\text{error}(t) &\leq \left|(-1)^{n+1}\epsilon^{2n+1}\int_0^t\int_0^\infty m_{2n+1}(\nu)\,\sin\epsilon\nu(t-\tau)\,d\nu\;(t-\tau)^{2n+1}\,x_0'''(\tau)\;d\tau\right| \\
&\leq \epsilon^{2n+1}t^{2n+1}\left|\int_0^\infty m_{2n+1}(\nu)\int_0^t \sin\epsilon\nu(t-\tau)\,x_0'''(\tau)\;d\tau\;d\nu\;\right| \\
&\leq \epsilon^{2n+2}t^{2n+1}\left|\int_0^\infty \nu\,m_{2n+1}(\nu)\int_0^t \cos\epsilon\nu(t-\tau)\,x_0''(\tau)\;d\tau\;d\nu\;\right| \\
&\leq \epsilon^{2n+2}t^{2n+1}\int_0^\infty |\nu\,m_{2n+1}(\nu)|\int_0^t |\cos\epsilon\nu(t-\tau)\,x_0''(\tau)\;|\,d\tau\;d\nu \\
&\leq \epsilon^{2n+2}t^{2n+1}\int_0^\infty |\nu\,m_{2n+1}(\nu)|\,d\nu\int_0^t |x_0''(\tau)\;|\,d\tau \\
&\leq \epsilon^{2n+2}t^{2n+1}\int_0^\infty |\nu\,m_{2n+1}(\nu)|\,d\nu\int_0^t d\tau\;|x_0''(\max)| \\
&= \epsilon^{2n+2}(t)^{2n+2}C_{2n+1}\;|x_0''(\max)|
\end{aligned} \tag{84}$$

Here, we have introduced the constant C_{2n+1} which is defined as

$$C_{2n+1} = \int_0^\infty |\nu\,m_{2n+1}(\nu)|\,d\nu \tag{85}$$

We note that for any $m(\omega)$, $\bar{m}(\omega)$ can always be chosen in such a way that C_{2n+1} exists. Further, the error grows with time as t^{2n+2}. Thus, no matter how small ϵ may be, the error becomes significant at a time $t = O(\epsilon^{-1})$. We note, however, that up to this point in the derivation we have neglected all forms of dissipation. If the subsystem under consideration has a small amount of dissipation (as shown in reference [5]) then the error will remain bounded for all time. In essence, this requires that all transient motion of $x_0(t)$ has stopped before the error has had a chance to accumulate.

The source of the error The accumulation of error in this approximation is due to approximations of the phase of the individual modes. Replacing the exact DtN (24) by the approximation (73) can be thought of as replacing the individual term in (24) by the following integral:

$$m_n\omega_n^3 \sin\omega_n(t-\tau) \approx \frac{1}{\omega_n\epsilon}\int_{\omega_n(1-\epsilon)/2}^{\omega_n(1+\epsilon)/2} \bar{m}(w)\omega^3 \sin\omega(t-\tau)\,d\omega \tag{86}$$

This approximation is valid only as long as the sine terms in the integral remain in phase with each other. To show this, we approximate the integral on the right of (86) in the following manner:

$$\frac{1}{\omega_n\epsilon}\int_{\omega_n(1-\epsilon)/2}^{\omega_n(1+\epsilon)/2} \bar{m}(w) \quad \omega^3 \quad \sin\omega(t-\tau)\,d\omega \approx \bar{m}(w_n)\omega_n^3\frac{1}{\omega_n\epsilon}\int_{\omega_n(1-\epsilon)/2}^{\omega_n(1+\epsilon)/2} \sin\omega(t-\tau)\,d\omega \tag{87}$$

$$\approx \frac{-\bar{m}(w_n)\omega_n^3}{\omega_n\epsilon(t-\tau)}\cos\omega(t-\tau)\Big|_{\omega_n(1-\epsilon)/2}^{\omega_n(1+\epsilon)/2} \tag{88}$$

$$\approx \frac{\bar{m}(w_n)\omega_n^3}{\omega_n\epsilon(t-\tau)}2\sin\omega_n(t-\tau)\ \sin\big(\omega_n\epsilon(t-\tau)/2\big) \tag{89}$$

$$\approx \frac{\bar{m}(w_n)\omega_n^3}{\omega_n\epsilon(t-\tau)}\big(\omega_n\epsilon(t-\tau)/2 - \omega_n^3\epsilon^3(t-\tau)^3/12\big)\ 2\sin\omega_n(t-\tau) \tag{90}$$

$$\approx \bar{m}(w_n)\omega_n^3\sin\omega_n(t-\tau)\big(1-\omega_n^2\epsilon^2(t-\tau)^2/6\big) \tag{91}$$

Therefore, we see that the error is due to accumulation of frequency approximations in the substitution of the sum for the integral. Thus, there is no need to appeal to any argument based on limiting dissipation [20].

5.4 Effective Dynamical Parameters

Equations (81) and (82) state the conditions under which the error in the DtN map is bounded (see equation (84).) Through equation (71) these conditions specify certain restrictions on $\bar{m}(\omega)$ in its relation to $m(\omega)$. In satisfying these conditions, we shall identify several effective dynamical parameters which characterize a given dynamical subsystem.

To do so, we first consider the nth moment of the mass-frequency distribution $\frac{dm_e}{d\nu}(\nu)$

$$I_n = \int_0^\infty \nu^n \frac{dm_e}{d\nu}(\nu)\, d\nu. \tag{92}$$

We now integrate (92) by parts to obtain

$$I_n = \sum_{j=0}^{n} (-1)^j \nu^{n-j} m_j(\nu). \tag{93}$$

Thus we conclude that conditions (81) and (82) are equivalent to

$$\int_0^\infty \nu^j \frac{dm_e}{d\nu}(\nu)\, d\nu = 0, \qquad j = 0, \ldots, 2n. \tag{94}$$

From the definition of $m_e(\omega/\epsilon)$ in equation (71), we obtain

$$\int_0^\infty \nu^j \frac{dm_e}{d\nu}(\nu)\, d\nu = 0 \iff \int_0^\infty \omega^j \left(\frac{dm}{d\omega}(\omega) - \frac{d\bar{m}}{d\omega}(\omega)\right) d\omega = 0. \tag{95}$$

Using the definition of $m(\omega)$, equation (65), in (95) yields

$$\int_0^\infty \omega^j \frac{d\bar{m}}{d\omega}(\omega) d\omega = \sum_{n=1}^{N} \omega_n^j m_n. \tag{96}$$

Equation (96) shows that in order to accurately represent a dynamical subsystem in a simulation, one must choose the moments of $\bar{m}(\omega)$ to agree with those of the subsystem itself. These parameters, the frequency moments of the modal masses, are in this way fundamental in describing a system's dynamical response. We call them the "effective dynamical parameters."

5.4.1 Physical interpretation of effective parameters

For this section, and through the rest of this paper, we shall consider the special case of $n = 1$ (c.f. equation (82)). That is, we shall require that

$$\int_0^\infty \frac{d\bar{m}}{d\omega}(\omega) d\omega \;=\; \sum_{n=1}^{N} m_n \;= M_T \tag{97}$$

$$\int_0^\infty \omega \frac{d\bar{m}}{d\omega}(\omega)d\omega = \sum_{n=1}^{N} \omega_n m_n = \eta_o \tag{98}$$

$$\int_0^\infty \omega^2 \frac{d\bar{m}}{d\omega}(\omega)d\omega = \sum_{n=1}^{N} \omega_n^2 m_n = k_o. \tag{99}$$

Here we have used the results of equations (25) and (27). We recall that M_T is the total mass of the subsystem, while k_o is the "high frequency stiffness." In (98) we have introduced the quantity η_o, which we shall call the "effective dissipation" of the subsystem.

Equation (84) with $n = 1$ shows that if one chooses $\bar{m}(\omega)$ to correctly represent the total mass M_T, high frequency stiffness k_o, and the effective dissipation η_o of a subsystem, then the error incurred in a dynamical simulation will be bounded by

$$\text{error}(t) \leq (\epsilon t)^4 C_5 \left| x_0''(\max) \right|. \tag{100}$$

From equations (97-99) we can see that with each dynamical subsystem, we can associate a total mass and two frequencies. In what follows, we shall find it convenient to represent a subsystem in terms of its "frequency" parameter Ω, (c.f. equation (28)) and "damping" parameter α_0, which is defined by

$$\alpha_0 = \eta_o / M_T \Omega. \tag{101}$$

In Appendix A, we show that $\alpha_0 \leq 1$ for all discrete dynamical systems.

6 Modeling Dynamical Subsystems: Canonical Representations

6.1 Canonical Representations

In the last section, we determined those parameters of a dynamical subsystem that are important to describe the dynamics of that subsystem. That is, we determined which features of $m(\omega)$ must be duplicated in $\bar{m}(\omega)$ in order to accurately reproduce the force at the attachment point. Beyond the specification of the effective parameters just described, however, $\bar{m}(\omega)$ remains unspecified up to now.

In this section, we consider several canonical representations of dynamical subsystems that are based on different modeling perspectives. By "representation," we mean a function $\bar{m}(\omega)$ which is used in the approximate DtN (73). In the rest of this section we consider different choices for $\bar{m}(\omega)$

which have prescribed values of M_T, η_o, and k_o. Each choice differs in its functional dependence on ω, but nevertheless satisfies the conditions (97) - (99) above. Therefore, each choice will yield accurate results in a dynamical simulation as specified in (100). Thus the specific choice of $\bar{m}(\omega)$ as described here is more a matter of taste or ease of application than of accuracy.

The three canonical functions we shall describe are derived from different perspectives. In the first, we shall derive an optimal representation based on information theory. The calculation presented below is motivated by and is similar in both spirit and detail to that presented by Pierce in [17]. We include it as one perspective to obtain a canonical $\bar{m}(\omega)$. In the second approach, we consider the form of $\bar{m}(\omega)$ to be a self-similar function of frequency. This leads to a nonlinear functional equation which we solve for the function $\bar{m}(\omega)$. The third approach, the rational function representation, is motivated by the resulting simplicity of the approximate DtN map. It leads to a very satisfying physical analogy, which is presented in §6.4.3.

In what follows, we shall find it convenient to work in terms of a nondimensional mass distribution function. Thus we introduce the nondimensional frequency ν and nondimensional mass distribution $\mu(\nu)$ as follows:

$$\nu = \omega/\Omega \tag{102}$$

$$\mu(\nu) = \frac{\Omega}{M_T}\frac{d\bar{m}}{d\omega}(\omega). \tag{103}$$

In terms of (102) and (103), the three conditions (97) - (99) take the form:

$$\int_0^\infty \mu(\nu)d\nu = 1 \tag{104}$$

$$\int_0^\infty \nu\mu(\nu)d\nu = \alpha_0 \tag{105}$$

$$\int_0^\infty \nu^2\mu(\nu)d\nu = 1. \tag{106}$$

6.2 Maximum Entropy Formulation

6.2.1 Derivation of $\mu(\nu)$

Because of the normalization property (104) of $\mu(\nu)$, we may think of this function in the abstract sense as a probability distribution. Following up on this line of thinking, we may also consider the conditions (105) and (106) as constraints on $\mu(\nu)$. Thus we seek to find a $\mu(\nu)$ that maximizes the "entropy" or "uncertainty" subject to the constraints that (105) and (106) are satisfied. The uncertainty or entropy function for $\mu(\nu)$ can be written as [17]:

$$H[\mu] = -\int_0^\infty \mu(\nu)\,\log(\mu(\nu))\,d\nu. \tag{107}$$

We wish to find $\mu(\nu)$ such that H is stationary subject to the conditions (104 –106). Therefore, we introduce the functional $\Pi[\bar{m}]$ defined by

$$\Pi[\mu] = H[\mu] - \lambda_0\Big(\int_0^\infty \mu d\nu - 1\Big) - \lambda_1\Big(\int_0^\infty \nu\frac{d\bar{m}}{d\omega}(\omega)d\nu - \alpha_0\Big) - \lambda_2\Big(\int_0^\infty \nu^2\frac{d\bar{m}}{d\omega}(\omega)d\nu - 1\Big). \tag{108}$$

Here, $\lambda_0 - \lambda_2$ are Lagrange multipliers enforcing the constraints.

Making Π stationary with respect to μ, λ_0, λ_1, and λ_2 leads to equations (104-106) and:

$$\int_0^\infty \delta\mu\left[\log\mu - 1 + \lambda_0 + \lambda_1\nu + \lambda_2\nu^2\right]\,d\nu = 0 \tag{109}$$

Equation (109) leads directly to the result

$$\mu(\nu) = \exp\left(1 - \lambda_0 - \lambda_1\nu - \lambda_2\nu^2\right). \tag{110}$$

6.2.2 Evaluating the coefficients, λ_0, λ_1, λ_2

Substituting (110) into equations (104), (105) and (106) and rearranging yields the following equations for λ_0, λ_1 and λ_2:

$$1 = Ae^{\lambda_1^2/4\lambda_2}\,\frac{1}{2}\sqrt{\frac{\pi}{\lambda_2}}\mathrm{erfc}\Big(\frac{\lambda_1}{2\sqrt{\lambda_2}}\Big) \tag{111}$$

$$\alpha_0 = \frac{A - \lambda_1}{2\sqrt{\lambda_2}} \tag{112}$$

$$1 = \sqrt{\frac{1}{\lambda_2}}\left[\frac{1}{2} + \frac{\lambda_1^2}{4\lambda_2} - \frac{A\lambda_1}{2\lambda_2}\right] \tag{113}$$

$$A = e^{1-\lambda_0} \tag{114}$$

Given α_0, equations (111) - (113) are to be solved for λ_0 - λ_2. These values are then to be substituted into (110) to obtain $\mu(\nu)$. In order to solve (111) - (113), we combine them to write a single equation

for the variable $c = \lambda_1/2\sqrt{\lambda_2}$:

$$(\alpha_0 + c)\sqrt{\pi}\,\exp(c^2)\,\mathrm{erfc}(c) = 1. \tag{115}$$

Once c is determined from (115), $A/\sqrt{\lambda_2}$ can be found from (112). Finally, λ_2 is obtained from (113). We note that it is easy to verify that for any value of $0 < \alpha_0 \leq 1$, equation (115) has a solution.

6.2.3 Implementation of Maximum Entropy Representation

In order to get the DtN map associated with the Maximum Entropy Representation of $\frac{d\bar{m}}{d\omega}(\omega)$, we substitute (110) (in dimensional form) into (73) to write

$$f_0(t) = k_o x_0(t) - \int_0^t \kappa(t-\tau)\, x_0(\tau)\, d\tau, \tag{116}$$

$$\kappa(t) = M_T A \int_0^\infty \omega^3 \exp(-\lambda_1\omega/\Omega - \lambda_2\omega^2/\Omega^2)\, \sin\omega(t)\, d\omega. \tag{117}$$

We note that λ_1 may be positive or negative, but λ_2 is strictly positive. We now evaluate the integral in (117) by writing $\sin(\omega t)$ as $\mathcal{I}\{e^{i\omega t}\}$ and integrating three times by parts to obtain

$$\begin{aligned}\kappa(t) = &-\frac{\Omega^4\lambda_1}{4\lambda_2^3}\Omega t + \frac{\Omega^4}{8\lambda_2}\sqrt{\frac{\pi}{\lambda_2}}e^{(\lambda_1^2-\Omega^2t^2)/4\lambda_2} \\ &\times\mathcal{I}\left\{(i\Omega t-\lambda_1)\left[3+\frac{1}{2\lambda_2}(i\Omega t-\lambda_1)^2\right]\left[\mathrm{erfc}\left((i\Omega t-\lambda_1)/2\sqrt{\lambda_2}\right)\right]e^{-2i\lambda_2\Omega t}\right\}.\end{aligned} \tag{118}$$

The error function is defined by $\mathrm{erfc}(z) = \frac{2}{\sqrt{\pi}}\int_z^\infty e^{-t^2}dt$ [1].

In the form (118), $\kappa(t)$ is difficult to use since the error function must be evaluated for complex argument. Of course, given the values of λ_1 and λ_2, this calculation could be done as a preprocess and the result tabulated. For more complicated functions of $\kappa(t)$, this would be recommended. For the special case of $\lambda_1 = 0$, the error function drops out of the formulation.

6.3 Self-similar Formulation

Here we formulate and solve the problem of determining the "limiting" $\bar{m}'(\omega)$ in a complicated subsystem. The subsystem is imagined to be made up a collection of smaller "minor" subsystems, each of which, in turn, is made up of a collection of still smaller minor subsystems, and so on. As the subsystems become more and more complicated, we hope to find a limiting form of the $\frac{d\bar{m}}{d\omega}(\omega)$ function.

To each minor subsystem, we shall prescribe three parameters: M_j, η_j, and k_j. Further, we define a "frequency" and "damping factor" for each minor subsystem defined as $\Omega_j = \sqrt{k_j/M_j}$, and $\alpha_{0j} = \eta_j/M_j\Omega_j$, respectively. In the Laplace domain, the DtN for each subsystem can be written as:

$$F_j(s) = M_j\Omega_j^2 K(s/\Omega_j, \alpha_{0j})\, X(s). \tag{119}$$

If the minor subsystems are sufficiently complicated that their representation has reached its limiting form, then the function K will be *the same function for all the subsystems comprising the whole.* This is the essential assumption on which the following is based.

We now consider a subsystem comprised of many smaller subsystems as depicted in figure 1. The sum of the forces in springs j must balance the force f_0, thus

$$f_0 = \sum_{j=1} f_j. \tag{120}$$

Also, the dispacements of each of the subsystems are identical

$$x_0 = x_j \qquad j = 1, 2, \ldots \tag{121}$$

Combining equations (119) - (121) allows us to write

$$M_0\Omega_0^2 K(s/\Omega_0, \alpha_0)\, X_0(s) = \sum_{j=1} M_j\Omega_j^2 K(s/\Omega_j, \alpha_0)\, X_0(s) \tag{122}$$

We require (122) to hold for arbitrary $X_0(s)$, which we can therefore cancel from both sides.

We now pass to the limit in which the number of subsystems becomes infinite. For convenience, we nondimensionalize all frequencies with respect to Ω_0, and all masses with respect to M_0. Therefore we make the following replacements in (122):

$$\sigma = s/\Omega_0 \tag{123}$$

$$\Omega_j = \omega_j\Omega_0 \tag{124}$$

$$M_j = M_0 \left.\frac{d\bar{m}}{d\omega}(\omega)\right|_{\omega=\omega_j} d\omega \tag{125}$$

$$\sum_{j=1} = \int_0^\infty \tag{126}$$

Thus we obtain an integral equation for $\frac{d\bar{m}}{d\omega}(\omega)$:

$$K(\sigma, \alpha_0) = \int_0^\infty \frac{d\bar{m}}{d\omega}(\omega) K(\sigma/\omega, \alpha_0)\, d\omega \tag{127}$$

In order to close (127), we must specify the relation between $K(\sigma)$ and $\frac{d\bar{m}}{d\omega}(\omega)$. If we assume that the relation between $K(\sigma)$ and $\frac{dm}{d\omega}(\omega)$ is the same here as it is in the case of simple oscillators, then such a closure relation can be obtained from equations (35) and (65). This yields, (for $\frac{d\bar{m}}{d\omega}(\omega)$ analytic in the upper half $\omega-$plane)

$$K(\sigma) = -\frac{\pi}{2}\sigma^3 \left.\frac{d\bar{m}}{d\omega}(\omega)\right|_{\omega=i\sigma}. \tag{128}$$

We combine equations (127) and (128) to find the following homogeneous nonlinear integral equation for $\frac{d\bar{m}}{d\omega}(\omega)$:

$$\frac{d\bar{m}}{d\omega}(i\sigma) = \int_0^\infty \frac{d\bar{m}}{d\omega}(\omega) \frac{d\bar{m}}{d\omega}\left(\frac{i\sigma}{\omega}\right) \frac{d\omega}{\omega}. \tag{129}$$

To solve (129), we replace $z = \log(i\sigma)$, $\nu = \log\omega$ and $\mu(z) = \frac{d\bar{m}}{d\omega}(e^z)$ to write:

$$\mu(z) = \int_{-\infty}^\infty \mu(\nu)\mu(\nu - z)\, d\nu. \tag{130}$$

Equation (130) may be solved by Fourier transform. We denote by $\bar{\mu}$ the transform of μ. Taking the transform of (130) leads to

$$\bar{\mu} = \bar{\mu}^2 \tag{131}$$

$$\bar{\mu} = 1 \tag{132}$$

Thus, we conclude that

$$\frac{d\bar{m}}{d\omega}(\omega) = \delta(\omega - \omega_0) \tag{133}$$

Equation (133) describes the mass-frequency distribution of a single oscillator with arbitrary natural frequency ω_0. The implication of (133) is that only *identical oscillators* can be connected together (in the manner that we have assumed) such that the behavior of whole is the same as the behavior of the individual parts.

Clearly the mass-frequency distribution in (133) is not representative of whole classes of complicated subsystems. While this result is not of practical interest, it is of interest to see where the assumption of self-similarity has lead. We note, however, that self-similarity was not the only assumption made in this section, and that perhaps the concept of self-similarity might still lead to valuable subsystem models.

6.4 Rational Function Approximation

Here we consider representing $\mu(\nu)$ by a rational function of ν. This representation has considerable benefits in terms of both ease of application and in terms of physical interpretation.

To obtain a rational function representation of $\mu(\nu)$, we must first choose a desirable form. We shall choose $\mu(\nu)$ to be an even function of ν. In order that the integral in (106) be well defined, we require that $\mu(\nu)$ be $o(\nu^{-3})$ $\nu \to \infty$. These requirements lead us to choose the following form for $\mu(\nu)$:

$$\mu(\nu) = \frac{c}{(\nu^4 - 2(a^2 - b^2)\nu^2 + (a^2 + b^2)^2)}. \tag{134}$$

We note that more elaborate choices of $\mu(\nu)$ can lead to higher order models with (presumably) greater accuracy than that chosen here, however (134) shall suffice to satisfy our three conditions (104) - (106).

6.4.1 Evaluating the coefficients a, b and c.

The three coefficients in (134) are to be determined by requiring (134) to satisfy equations (104) - (106). This leads to the equations [12]

$$1 = \frac{\pi c}{4b(a^2 + b^2)} \tag{135}$$

$$\alpha_0 = \frac{c}{4ab}[\pi - 2\theta] \tag{136}$$

$$1 = \frac{\pi c}{4b}. \tag{137}$$

In (136), θ is defined so that $\tan\theta = b/a$. Solving equations (135) and (137) in terms of θ yields

$$a = \cos\theta \tag{138}$$

$$b = \sin\theta \tag{139}$$

$$c = 4/\pi \sin\theta. \tag{140}$$

The value of θ is determined from equation (136) which simplifies using (138-140) to

$$\frac{\pi - 2\theta}{\pi \cos\theta} = \alpha_0. \tag{141}$$

Thus, given α_0 for a particular subsystem, we determine θ by solving (141). Then we obtain a, b and c from equations (138-140). We note that (141) has real solutions for θ only for $\alpha_0 > 2/\pi$. Smaller values of α_0 can be obtained by allowing $\theta = \pi/2 + i\gamma$, as we shall discuss later.

6.4.2 Implementation of Rational Function Approximation

The rational function approximation can be implemented in either convolution form, or in a form local in time. To obtain the convolution form, we merely substitute $\mu(\nu)$ into (24). Since the kernel is a rational function of ν, however, the resulting DtN can be written alternatively in a form that is local in time.

To show this, we consider the non-dimensional DtN in the Laplace domain. Therefore we introduce $\bar{K}(\sigma)$ which is non-dimensional Laplace transform of the approximate DtN resulting from $\bar{m}(\omega)$ (c.f. equations (31, 32, 68).)

$$\begin{aligned} \bar{K}(\sigma) &= 1 - \int_0^\infty \int_0^\infty \nu^3 \mu(\nu) \sin(\nu\tau) d\nu \, e^{-\sigma\tau} d\tau \\ &= 1 - \int_0^\infty \mu(\nu) \frac{\nu^4}{\sigma^2 + \nu^2} d\nu \end{aligned} \tag{142}$$

Here, $\bar{K}$ is nondimensionalized with respect to k_o, and σ is nondimensionalized with respect to Ω. Thus with the definition (142), (31) becomes:

$$F_0(s) = s^2 m_o X_0(s) + k_o \bar{K}(s/\Omega) X_0(s). \tag{143}$$

When $\mu(\nu)$ is a rational even function, as here, the integral (142) is easily evaluated by residues. The result is a rational function of σ of the form [12]:

$$\bar{K}(\sigma) = 1 - N(\sigma)/D(\sigma) \tag{144}$$

$$N(\sigma) = (1 + 2b\sigma) \tag{145}$$

$$D(\sigma) = (\sigma^2 + 2b\sigma + 1). \tag{146}$$

We now substitute (144) into (143), multiply both sides by $D(\sigma)$, and inverse Laplace transform to obtain:

$$\mathcal{D} f_0(t) = m_o \frac{d^2}{dt^2} \mathcal{D} x_0(t) + k_o \frac{d^2}{dt^2} x_0(t). \tag{147}$$

The operator $\mathcal{D}$ is given by:

$$\mathcal{D} = \frac{d^2}{dt^2} + 2b\Omega \frac{d}{dt} + \Omega^2 \tag{148}$$

The form of the DtN (147) is much more convenient in implementation than the convolution form. For one, it does not require the full displacement history at the attachment point. Further, the evaluation of the force $f_0(t)$ at each time step is relatively efficient compared to a long time convolution. We shall show below an equivalent formulation which is not only local in time, but has an appealing physical analogy.

Before closing this section, we note that the form (147) with the coefficients as given is subject to the restriction of homogeneous initial conditions on $f(t)$ and $x_0(t)$:

$$\begin{aligned} f_0(0) &= 0 \qquad \dot{f}_0(0) = 0. \\ x_0(0) &= 0 \end{aligned} \tag{149}$$

6.4.3 A physical analogy.

In this section, we describe a simple model which corresponds to the local (in time) DtN (147). To start with, we rewrite (147) as

$$f_0(t) = m_o \frac{d^2}{dt^2} x_0(t) + f_2(t), \tag{150}$$

$$\mathcal{D} f_2(t) = k_o \frac{d^2}{dt^2} x_0(t). \tag{151}$$

We now introduce a "dummy" displacement-type variable, $y(t)$, defined by

$$f_2(t) = M_T \ddot{y}(t); \qquad y(0) = \dot{y}(0) = 0. \tag{152}$$

Substituting (152) into (151) and integrating twice with zero initial conditions yields:

$$M_T \ddot{y}(t) + 2b M_T \Omega \dot{y}(t) + k_o y(t) = k_o x(t). \tag{153}$$

Equation (153) is the equation of motion for a spring-dashpot-mass system in series. The parameters M_T and k_o are the mass and spring constants of mass-spring system, respectively. The coefficient b defined in equation (139) has the physical interpretation of the fraction of critical damping. This implies that the dashpot constant C in the analogy is given by

$$C = M_T \Omega / 2b = k_o / 2b\Omega \tag{154}$$

We emphasize that the physical analogy is exactly equivalent to the local DtN resulting from the rational function representation of $\bar{m}(\omega)$.

In terms of the "dummy" displacement variable $y(t)$, the local DtN (150-151) can now be rewritten as:

$$f_0(t) = m_o \frac{d^2}{dt^2} x_0(t) + M_T \ddot{y}(t), \tag{155}$$

$$k_o x(t) = M_T \ddot{y}(t) + 2b M_T \Omega \dot{y}(t) + k_o y(t). \tag{156}$$

Equations (155) and (156) are in the most convenient form for practical implementation.

6.4.4 Relation between critical damping parameter and effective dissipation parameter

It is interesting to examine the relation between the critical damping parameter b from the physical analogy and the effective dissipation parameter α_0 that results from the high modal density approximation. These two can be related through equations (139) and (141).

Underdamped case: Provided $b \leq 1$, α_0 and b are related by:

$$\alpha_0 = \frac{\pi - 2\sin^{-1} b}{\pi\sqrt{1-b^2}}. \tag{157}$$

Overdamped case: When $b \geq 1$, (157) is still valid, but can be rewritten to a much more convenient form. We shall use the identity

$$\sin^{-1} x = \pi/2 + i\cosh^{-1} x. \tag{158}$$

Thus (157) simplifies to

$$\alpha_0 = \frac{2\cosh^{-1} b}{\pi\sqrt{b^2-1}}. \tag{159}$$

The two relations (157) and (159) are summarized in the plot in figure 2.

6.4.5 Estimated bounds on critical damping parameter

In section §4.2 we showed that $K(s)$ is bounded by its Pade' approximants. We have no such bounds on $\bar{K}(\sigma)$, however. It is interesting, nevertheless, to assume that those bounds derived in §4.2 hold for $\bar{K}(\sigma)$, and thus derive estimated bounds for the critical damping factor, b. Therefore, based on equation (38) we shall assume:

$$P_1^0(s^2) \leq k_o\bar{K}(s/\Omega) \leq P_1^1(s^2). \tag{160}$$

We use the high frequency derivation of P_1^0 given by (57) and the low frequency expression for P_1^1 given by (46) in equation (160) to write

$$\frac{{k_o}^2}{k_o + s^{-2}\sum_{n=1}^{N} m_n\omega_n^4} \leq k_o\bar{K}(s/\Omega) \leq \frac{s^2{M_T}^2}{M_T + s^2\sum_{n=1}^{N}(m_n/\omega_n^2)}. \tag{161}$$

We gain some confidence in our assumption of (160) by the fact that (161) is satisfied in both the $s = 0$ and $s = \infty$ limits.

To obtain bounds on b, we substitute (144-146) into (161) and evaluate the result at $s = \Omega$ to obtain:

$$\frac{{k_o}^2}{k_o + \Omega^{-2}\sum_{n=1}^{N} m_n\omega_n^4} \leq \frac{k_o}{2+2b} \leq \frac{{M_T}^2\Omega^2}{M_T + \Omega^2\sum_{n=1}^{N}(m_n/\omega_n^2)}. \tag{162}$$

Simplifying leads to

$$\frac{\sum_{n=1}^{N}(m_n/\omega_n^2)}{M_T/\Omega^2} - 1 \leq 2b \leq \frac{\sum_{n=1}^{N} m_n\omega_n^4}{M_T\Omega^4} - 1. \tag{163}$$

The inequality (47), however, shows the left hand side of (163) to be non-positive. The inequality in (63), on the other hand, shows the right hand side of (163) to be always non-negative. Thus we obtain the estimated bound on the critical damping coefficient, b:

$$0 \leq 2b \leq \frac{\sum_{n=1}^{N} m_n\omega_n^4}{M_T\Omega^4} - 1. \tag{164}$$

7 Examples

In the examples that follow, we shall remove a large portion of the computational problem and replace it with a DtN boundary condition as we have described earlier. The DtN shall be computed either exactly (as indicated) or with a high-modal density approximation. The results of using the DtN shall be compared to results obtained by simulating the full dynamical system.

7.1 Large oscillator connected to complicated substructure.

The first system that we shall consider is that studied by Weaver in [19, 20]. It consists of a "large" mass-spring oscillator which is attached to a complicated substructure, as shown in figure 3. The equations of motion for the system are

$$M\ddot{x_0}(t) + Kx_0(t) = \sum_{n=1}^{N} \kappa_n(x_n(t) - x_0) \tag{165}$$

$$m_n\ddot{x}_n(t) + \kappa_n x_n(t) = \kappa_n x_0(t) \tag{166}$$

$$k_o = \sum_{n=1}^{N} \kappa_n. \tag{167}$$

7.1.1 Exact DtN Formulation

In order to apply the DtN concept, we rewrite (165-167) as follows:

$$M\ddot{x_0}(t) + Kx_0(t) = -f_0(t) \tag{168}$$

$$f_0(t) = \sum_{n=1}^{N} \kappa_n(x_n(t) - x_0) \tag{169}$$

To make the connection to our original formulation, we note that (166) is identical to (7), (167) is a special case of (5), and (169) is a special case of (8).

In this example, $m_o = 0$, $\omega_n^2 = \kappa_n/m_n$, $M_T = \sum_n m_n$, $\Omega^2 = k_o/M_T$. Thus, (24) gives us the force as:

$$f_0(t) = k_o x_0(t) - \int_{-\infty}^{t} \sum_{n=1}^{N} m_n\omega_n^3 \sin\omega_n(t-\tau)\, x_0(\tau)\, d\tau. \tag{170}$$

Therefore, in order to determine the dynamic response of the mass, we must solve (168) with (170), subject to initial conditions

$$x_0(0) = A \quad ; \quad \dot{x_0}(0) = B. \tag{171}$$

7.1.2 Approximate DtN Formulation

Alternatively, we can use the approximate DtN (155-156). For this example, (155-156) simplify to

$$f_0(t) = k_o x_0(t) - 2bM_T\Omega\dot{y}(t) - k_o y(t), \tag{172}$$

$$k_o x_0(t) = M_T\ddot{y}(t) + 2bM_T\Omega\dot{y}(t) + k_o y(t). \tag{173}$$

Combining (172) with (168) yields

$$M\ddot{x_0}(t) + (K + k_o)x_0(t) = 2bM_T\Omega\dot{y}(t) + k_o y(t). \tag{174}$$

Therefore, in order to determine the approximate dynamic response of the mass, we must solve (174) with (173), subject to initial conditions (171) and

$$y(0) = 0 \quad ; \quad \dot{y}(0) = 0. \tag{175}$$

The differential equations (174) with (173) exactly represent the system depicted in figure 4.

To evaluate the constant b, we must first evaluate η_o which is given by (98) as

$$\eta_o = \sum_{n=1}^{N} \omega_n m_n. \tag{176}$$

Then, $\alpha_0 = \eta_o / M_T\Omega$ (by 101) and b can be evaluated by solving either (157) or (159), as appropriate.

7.1.3 Example results

Here we compare the results for a subsystem of $N = 1000$ masses attached to a single large mass. We compare the results of the approximate DtN, (174) with (173), to the results obtained by directly simulating the full system of equations (165-167).

The large mass is $M = 2$, while its spring has spring constant $K = 2$. The values of ω_n were chosen randomly between 0 and $\Omega_{max} = 10$. The values of m_n were chosen according to a selected distribution, as

$$m_n = p(\omega)\Omega_{max}/N. \tag{177}$$

In all the examples, $p(\omega)$ is chosen to be $p(\omega) = M_T \exp(-\lambda\omega)/\lambda$, with $\lambda = 2.0$. For the dynamical simulations, the initial conditions are given by (171) and (175), with $A = 0$ and $B = 1$.

We consider two different subsystems with very different masses. In one case, the subsystem has mass $M_T \approx 0.25$, while in the other case $M_T \approx 10$. The two results are shown in figures 5 and 6, respectively. We note that remarkably different physical behavior results in the two cases. In

each case, however, we see that the approximate solution, obtained from integrating just two second order equations, closely approximates the reference solution for times below about 50 units. Above those times, the approximation breaks down as predicted by the error analysis in section 5.3.1.

7.2 Elastic rod connected to complicated substructure.

We now consider the interaction between two elastic structures: a homogeneous elastic rod connected to a "complicated," randomly inhomogeneous elastic rod. See figure 7. We shall represent the inhomogeneous rod using a high-modal density DtN as we did in the last example. Indeed, to model the inhomogeneous rod, we follow similar steps as those outlined above.

In figure 8, we plot the displacement profiles on the homogeneous portion of the rod at even time intervals. We plot the displacement predicted by the approximate DtN and compare that to the displacement predicted in the reference structure. The input is a Gaussian shaped pulse which propagates to the right. The right traveling wave is represented at 25 time-unit intervals by the large peaks centered at $x = 10,\ 35,\ 60,\ 85$. (The wave speed in the homogeneous rod is unity.) The right traveling pulse is reflected at the right end of the homogeneous rod. The reflected left traveling pulse is of lower amplitude.

We see that the approximate and reference solutions agree exactly up to the reflection from the complicated substructure. The subsequent reflected pulses agree closely in shape and amplitude. The main difference between them is represented in the slow decay of the tail in the approximate solution. The elapsed time shown in the figures is not sufficient to show the pulse reflected from the far end of the complicated rod. The approximate solution does *not* predict this pulse, though it is present in the reference solution, of course.

8 Conclusions

We have proposed the use of a time-domain DtN map to represent complicated subsystems in dynamical simulations. We derived an exact DtN map for a general linear-elastic system which is attached to the outside world at one point. We studied the properties of this map and found many interesting results including interrelations between bulk dynamical coefficients, and bounds on the symbol of the map in the Laplace domain. We also studied the high modal density or infinitely complicated limit, and derived the "effective dynamical parameters" governing the dynamics of a subsystem. These were used to construct various subsystem representations which are accurate in the high modal density limit. The most intriguing of these is the rational function representation. From this representation we were lead to conclude that a sufficiently complicated subsystem is asymptotically equivalent (as $\epsilon \to 0$) to a simple single spring-dashpot-mass system, (for $t = o(\epsilon^{-1})$.) Several examples of our high modal density approximation were studied. The agreement between model and reference solutions was initially very good, but gradually deteriorated in agreement with the predictions of §5.3.1.

The results presented here show that a sufficiently complicated subsystem can be accurately represented by a subsystem of much smaller dimensionality. The model system is dissipative, even though the original system is not. The dissipation models vibratory energy being transferred from the master structure to the slave subsystem [16, 18]. This analogy provides an interesting dynamical interpretation of the origin of damping in physical systems.

Though our analysis is presented in the context of structural dynamics, it generally applies to any large system of oscillators. We emphasize, however, that the high modal density approximation presented here is valid only for simulation time $= o(\epsilon^{-1})$. Further work is required to obtain a similar approximation valid beyond that time.

9 Acknowledgments

The authors acknowledge helpful discussions with Ofer Michael, Karl Grosh, Jeffrey L. Cipolla, Donald Cox, Charles Milligan, Geoffrey Main, and Allan D. Pierce. The financial support of the Office of Naval Research is also gratefully acknowledged.

References

[1] M. Abramowitz and I. A. Stegun. *Handbook of Mathematical Functions.* Dover Publications, New York, 1972. General reference.

[2] Paul E. Barbone. Equipment representations for shock calculations: Time domain Dirichlet to Neumann maps. In *Acoustics, Vibrations, and Rotating Machines*, volume 3, Part B, pages 223–228, Boston, MA., September 1995. Proceedings of 1995 Design Engineering Technical Conferences, ASME Press, New York.

[3] Carl M. Bender and Steven A. Orszag. *Advanced Mathematical Methods for Scientists and Engineers.* McGraw-Hill, Singapore, international edition, 1987. pg. 358.

[4] Carl M. Bender and Steven A. Orszag. *Advanced Mathematical Methods for Scientists and Engineers.* McGraw-Hill, Singapore, international edition, 1987. pg. 406.

[5] Aravind Cherukuri and Paul E. Barbone. High modal density approximations for equipment in the time domain. *J. Acoust. Soc. Am.*, accepted, 1998.

[6] R.R. Craig. Substructure methods in vibration. *Trans. ASME J. Vib. Acoust.*, 117(3):207–213, 1995.

[7] D. Givoli. *Numerical Methods for Problems on Infinite Domains.* Elsevier, Amsterdam, first edition, 1992.

[8] Dan Goldman and Paul E. Barbone. Dirichlet to neumann maps for the representation of equipment with weak nonlinearities. In *Proc. ASME Noise Control and Acoustics Division, 1996 International Mechanical Engineering Congress*, volume NCA22, pages 71–76, Atlanta, GA, November 1996. ASME Press, New York.

[9] R.J. Guyan. Reduction of stiffness and mass matrices. *AIAA Journal*, 3(2):380, 1965.

[10] W.C. Hurty. Dynamic analysis of structural systems using component modes. *AIAA Journal*, 3(4):678–685, 1965.

[11] C. Lanczos. *The Variational Principles of Mechanics.* Dover, reprint of fourth (1970) edition, 1986.

[12] Mathematica. A system for doing mathematics by computer. Mathematica 3.0, Wolfram Research, Inc., 1988-97.

[13] R.J. Nagem, I. Veljkovic, and G.v.H. Sandri. Vibration damping by a continuous distribution of undamped oscillators. *J. Sound Vib.*, 207(3):429–434, 1997.

[14] G.J. O'Hara and P.F. Cunniff. Elements of normal mode theory. *Naval Research Laboratory Report*, 6002, 1963.

[15] A.D. Pierce. Resonant-frequency-distribution of internal mass inferred from mechanical impedance matrices, with application to fuzzy structure theory. In *Proceedings of the ASME Symposium on Acoustics of Submerged Structures and Transduction Systems.* ASME Press, New York, September 17–21 1995.

[16] A.D. Pierce, V.W. Sparrow, and D.A. Russel. Fundamental structural-acoustic idealizations for structures with fuzzy internals. *ASME Transactions*, Paper No. 93-WA/NCA-17(ASME Winter Annual Meeting, New Orleans), November 1993.

[17] Allan D. Pierce. Fuzzy elements, their coupling rules, and the Jaynes-Shannon maximum entropy principle. Technical Report AM-95-032, Department of Aerospace and Mechanical Engineering, Boston University, November 1995.

[18] M. Strasberg and D. Feit. Vibration damping of large structures induced by attached small resonant structures. *J. Acoust. Soc. Am.*, 99(1):335–344, 1996.

[19] R.L. Weaver. The effect of an undamped finite degree of freedom "fuzzy" substructure: Numerical solutions and theoretical discussion. *J. Acoust. Soc. Am.*, 100(5):3159–3164, 1996.

[20] R.L. Weaver. Mean and mean-square responses of a prototypical master/fuzzy structure. *J. Acoust. Soc. Am.*, 101(3):1441–1449, 1997.

A Proof that $\alpha_0 \leq 1$ for all subsystems

In this appendix, we prove that $\alpha_0 \leq 1$ for all subsystems. The proof proceeds by induction. We first show that for a system with a single mode, $\alpha_0 = 1$. Then we show if $\alpha_0 \leq 1$ for a system with N modes of vibration, then $\alpha_0 \leq 1$ with the addition of another mode of vibration.

We recall the definition α_0 given in (101)

$$\alpha_0 = \eta_o / M_T \Omega > 0. \tag{178}$$

Here, $\Omega^2 = k_o/M_T$, and M_T, η_o, k_o are the "effective dynamical parameters" defined in equations (97-99).

Here we consider the values of M_T, η_o, k_o as functions of N. To that end, we define:

$$M_N = \sum_{n=1}^{N} m_n \tag{179}$$

$$\eta_N = \sum_{n=1}^{N} m_n \omega_n \tag{180}$$

$$k_N = \sum_{n=1}^{N} m_n \omega_n^2 \tag{181}$$

$$\Omega_N^2 = k_N / M_N \tag{182}$$

$$\alpha_N = \eta_N / M_N \Omega_N \tag{183}$$

To begin, we let $N = 1$ in (179-183) to find

$$\alpha_1 = 1. \tag{184}$$

From (179-181), we now note

$$M_{N+1} = M_N + m_{N+1} \tag{185}$$

$$\eta_{N+1} = \eta_N + m_{N+1}\omega_{N+1} \tag{186}$$

$$k_{N+1} = k_N + m_{N+1}\omega_{N+1}^2. \tag{187}$$

Thus we can write the following equation for α_{N+1}^2:

$$\alpha_{N+1}^2 = \frac{\eta_{N+1}^2}{M_{N+1} k_{N+1}} \tag{188}$$

$$= \frac{\alpha_N^2 + 2\alpha_N \frac{m_{N+1}}{M_N}\frac{\omega_{N+1}}{\Omega_N} + \frac{m_{N+1}^2}{M_N^2}\frac{\omega_{N+1}^2}{\Omega_N^2}}{(1 + \frac{m_{N+1}}{M_N})(1 + \frac{m_{N+1}}{M_N}\frac{\omega_{N+1}^2}{\Omega_N^2})}. \tag{189}$$

For convenience, we are motivated to introduce the following variables:

$$\mu = m_{N+1}/M_N \qquad \nu = \omega_{N+1}/\Omega_N. \tag{190}$$

We note that these definitions hold in this appendix only, and are not to be confused with the definitions of μ and ν given in the main text of the paper.

In terms of μ and ν, (189) can be rewritten as

$$\alpha_{N+1}^2 = \frac{\alpha_N^2 + 2\alpha_N\mu\nu + \mu^2\nu^2}{(1+\mu)(1+\mu\nu^2)}. \tag{191}$$

From (191), we conclude:

$$\alpha_{N+1}^2 > 1 \quad \Longleftrightarrow \quad \alpha_N^2 + 2\alpha_N\mu\nu + \mu^2\nu^2 > (1+\mu)(1+\mu\nu^2). \tag{192}$$

Simplifying the right hand side of (192) yields:

$$\alpha_{N+1}^2 > 1 \quad \Longleftrightarrow \quad \alpha_N^2 + 2\mu\nu\alpha_N - (1+\mu(1+\nu^2)) > 0. \tag{193}$$

We shall now show that $\alpha_N^2 + 2\mu\nu\alpha_N - (1+\mu(1+\nu^2)) > 0$ is not satisfied for any $0 < \alpha_N \leq 1$. We let α^* be the positive root of

$$\alpha^{*2} + 2\mu\nu\alpha^* - (1+\mu(1+\nu^2)) = 0. \tag{194}$$

It is easy to show that the second root of (194) is negative. α^* is given by:

$$\begin{aligned} \alpha^* &= \sqrt{(1+\mu\nu)^2 + \mu(1-\nu)^2} - \mu\nu \\ &\geq \sqrt{(1+\mu\nu)^2} - \mu\nu = 1. \end{aligned} \tag{195}$$

Finally, we note that $\alpha_N = 0$ leads to the right hand side of (193) being false.

We conclude that

$$\alpha_{N+1}^2 > 1 \quad \Longleftrightarrow \quad \alpha_N > \alpha^* \geq 1. \tag{196}$$

Thus, $\alpha_{N+1} > 1$ if and only if $\alpha_N > 1$. Since $\alpha_1 = 1$, α_2 and all subsequent $\alpha_n's$ will be equal to or less than unity.

It is worth noting before we close this section that the equality in (195) is achieved only for $\nu = 1$.

B Figures

Figure captions

Fig. 1 A subsystem composed of many smaller subsystems. Each subsystem is connected at its attachment point to a light rigid rod. The rigid rod defines the attachment point of the new "composite" subsystem. The attachment point displacement of the composite subsystem is $x_0(t)$, and the force required to specify that motion is $f_0(t)$.

Fig. 2 Relation between critical damping factor, b, and "effective" damping constant, α_0. The relation is described quantitatively in equations (152) and (154).

Fig. 3 A large mass-spring oscillator connected to a complicated substructure. The substructure is represented by the collection of small oscillators.

Fig. 4 The asymptotically equivalent system. The response of the master structure in this system is approximately the same as that depicted in figure 3. The substructure has been replaced by a spring-dashpot-mass structure.

Fig. 5 Example 1a: "Large" mass-spring oscillator interacting with light but complicated substructure.

Fig. 6 Example 1b: "Large" mass-spring oscillator interacting with heavier complicated substructure.

Fig. 7 A homogeneous elastic rod connected to an inhomogeneous elastic rod. The homogeneous rod is the main structure of interest. The effect of the "complicated" inhomogeneous rod on the dynamics of the other shall be represented by an approximate DtN map.

Fig. 8 Example 2: Reflection from elastic bar with random mass density.

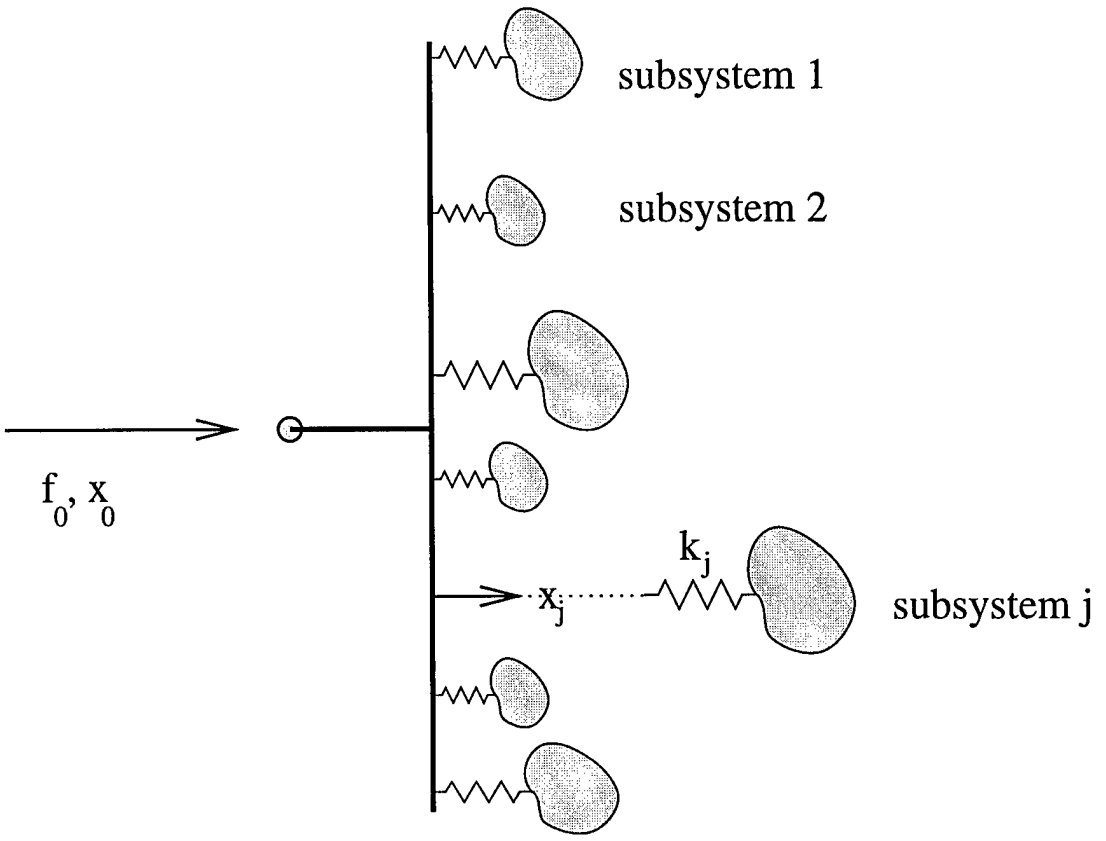

Figure 1: A subsystem composed of many smaller subsystems. Each subsystem is connected at its attachment point to a light rigid rod. The rigid rod defines the attachment point of the new "composite" subsystem. The attachment point displacement of the composite subsystem is $x_0(t)$, and the force required to specify that motion is $f_0(t)$.

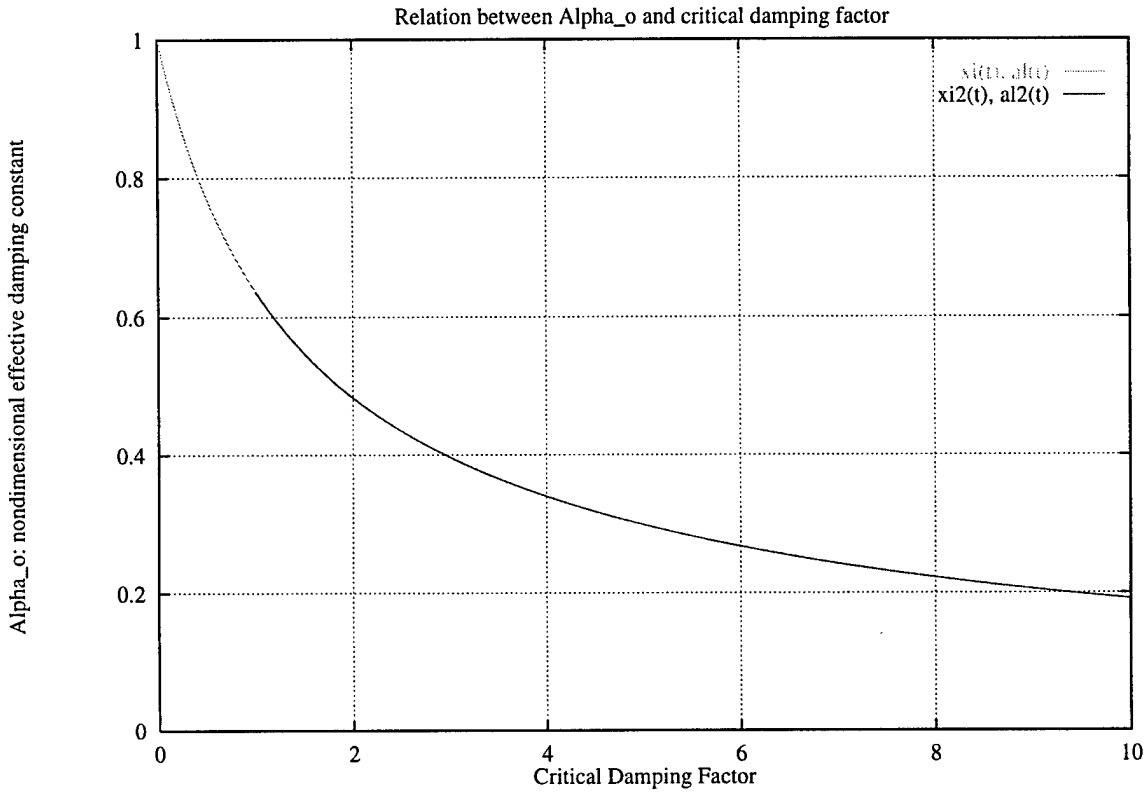

Figure 2: Relation between critical damping factor, b, and "effective" damping constant, α_0. The relation is described quantitatively in equations (152) and (154).

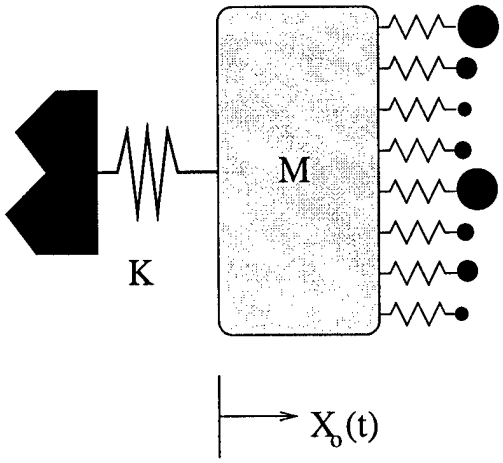

Figure 3: A large mass-spring oscillator connected to a complicated substructure. The substructure is represented by the collection of small oscillators.

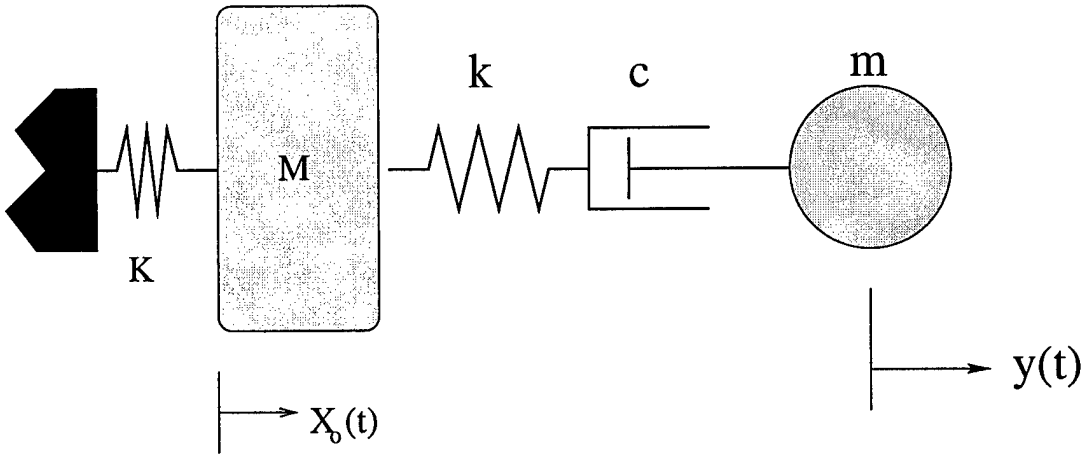

Figure 4: The asymptotically equivalent system. The response of the master structure in this system is approximately the same as that depicted in figure 3. The substructure has been replaced by a spring-dashpot-mass structure.

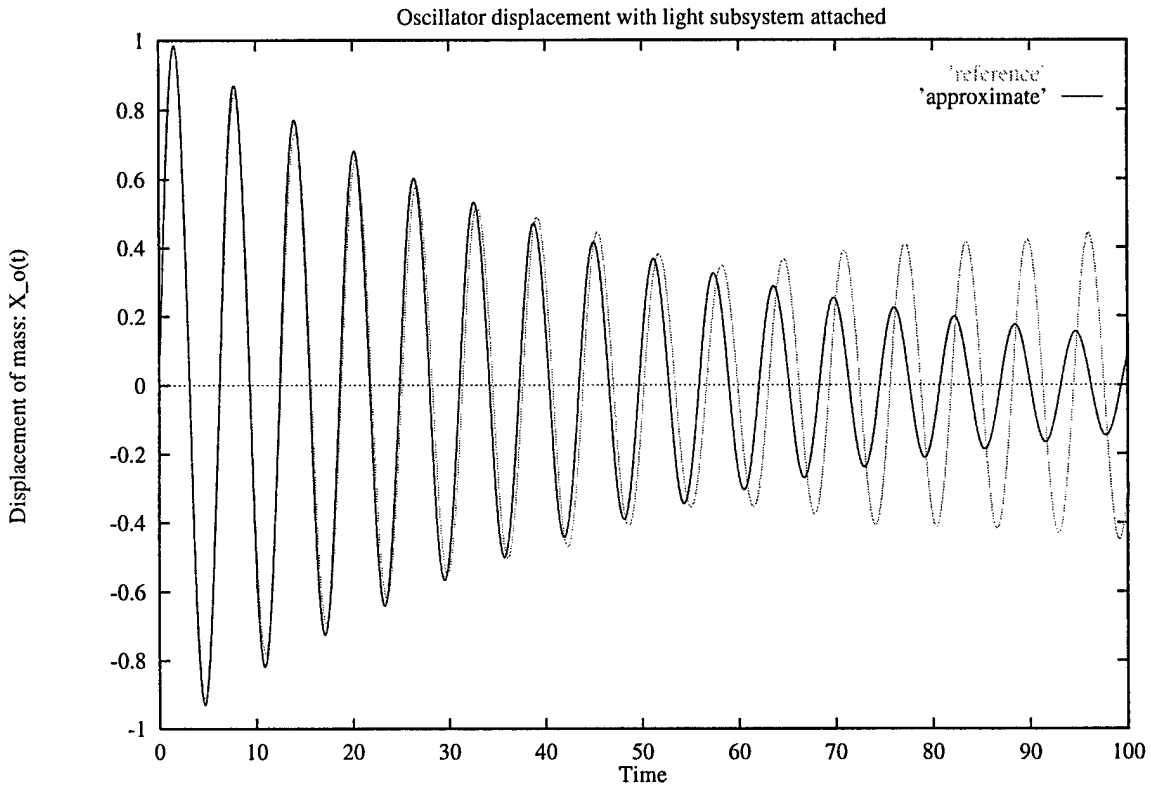

Figure 5: Example 1a: "Large" mass-spring oscillator interacting with light but complicated substructure.

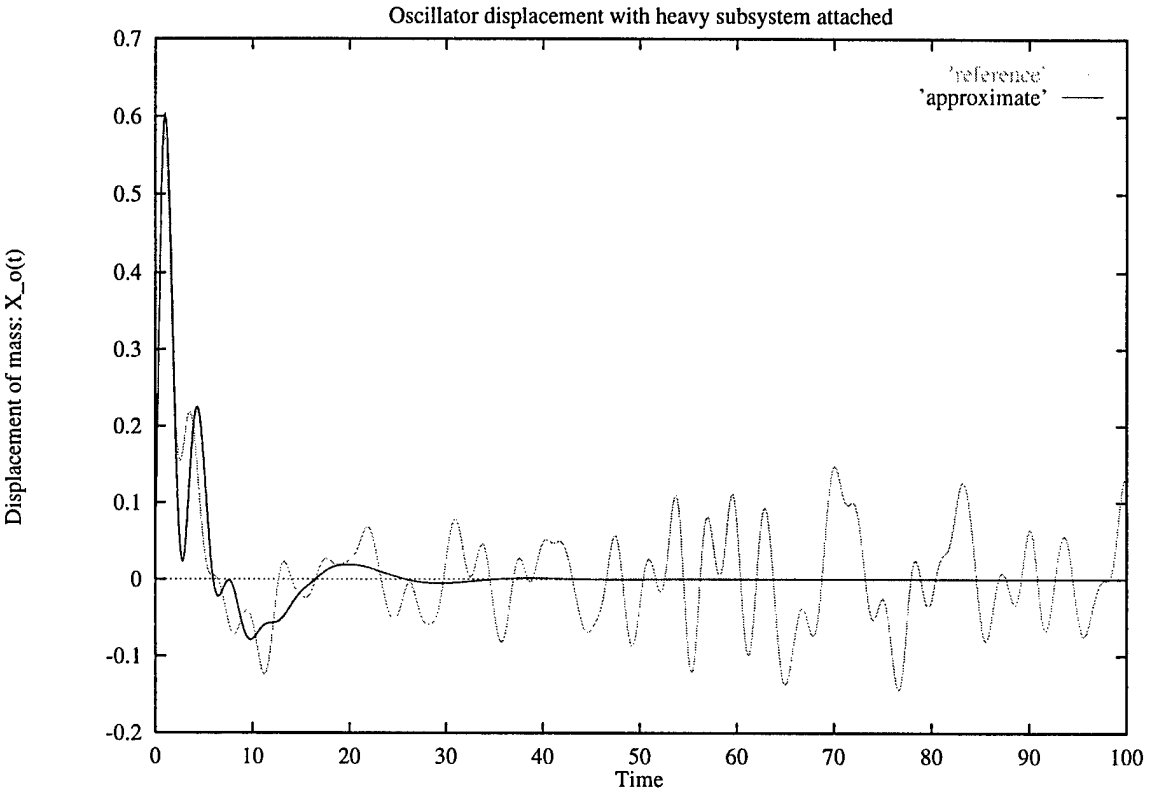

Figure 6: Example 1b: "Large" mass-spring oscillator interacting with heavier complicated substructure.

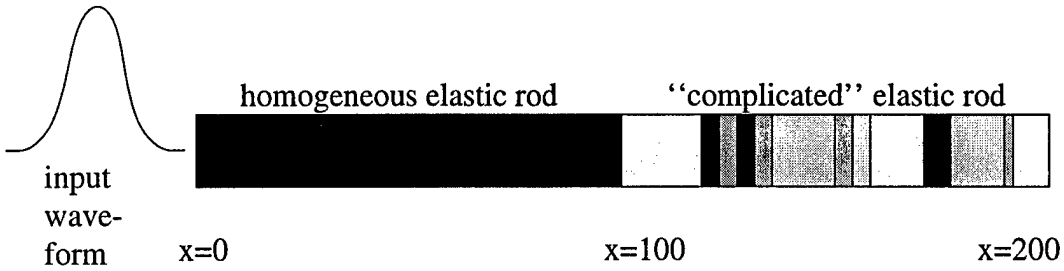

Figure 7: A homogeneous elastic rod connected to an inhomogeneous elastic rod. The homogeneous rod is the main structure of interest. The effect of the "complicated" inhomogeneous rod on the dynamics of the other shall be represented by an approximate DtN map.

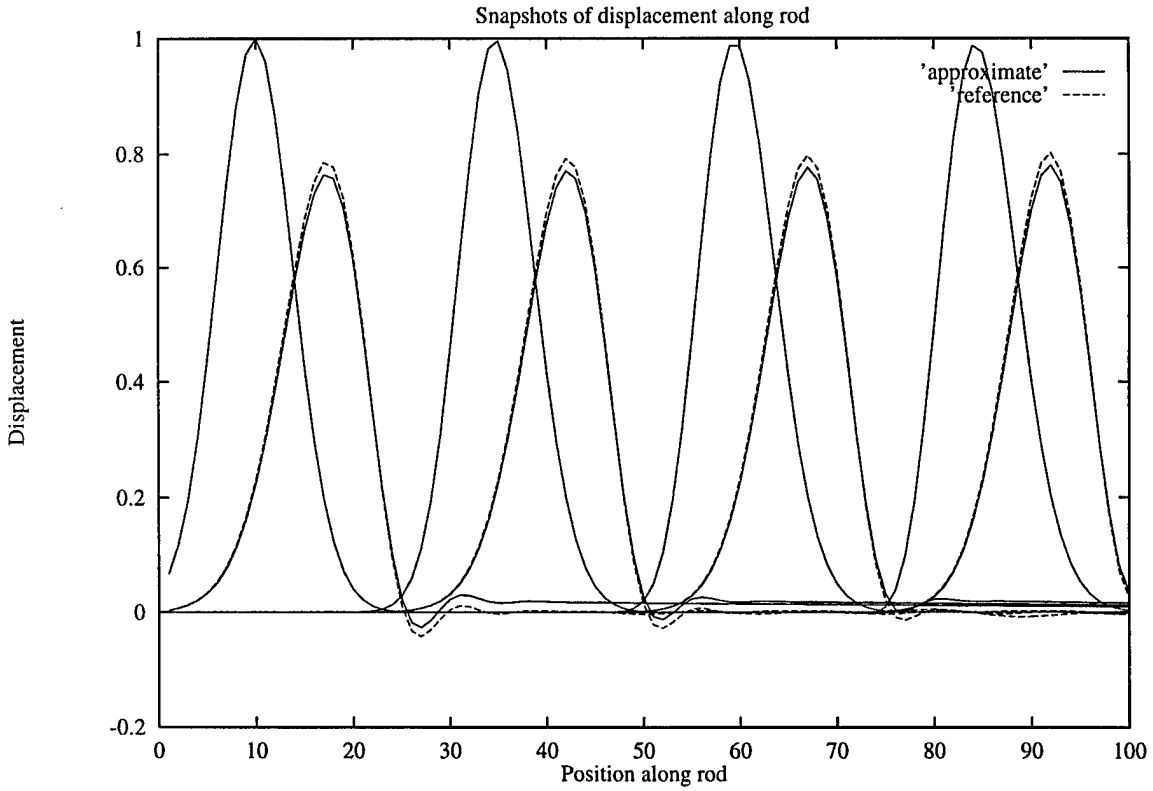

Figure 8: Example 2: Reflection from elastic bar with random mass density.

C.3 High Modal Density Approximations for Equipment in the Time Domain

A. Cherukuri and P. E. Barbone. "High Modal Density Approximations for Equipment in the Time Domain," *J. Acoust. Soc. Am.*, Vol 104, No 4, pp. 2048-2053, October 1998.

High modal density approximations for equipment in the time domain

Aravind Cherukuri[a] and Paul E. Barbone
Department of Aerospace and Mechanical Engineering, Boston University, Boston, Massachusetts 02215

(Received 19 May 1997; revised 12 January 1998; accepted 8 June 1998)

This article considers modeling the effect of complex subsystems on the dynamics of the main structure to which they are attached. It is proposed that the substructure (say a piece of equipment) be replaced by an equivalent set of forces which react back on the main structure. These forces are given as time convolutions of the displacements at the equipment attachment points. The convolution integral, which represents a time domain DtN (Dirichlet-to-Neumann) map, is approximated in the high modal density limit with determined error bounds. This approximation leads to a family of equipment representations. The simplest requires few measured equipment properties, though more information can lead to greater accuracy. Our approximate DtNs are demonstrated numerically in finite element simulations. © *1998 Acoustical Society of America.* [S0001-4966(98)04709-2]

PACS numbers: 43.20.Tb, 43.40.At [ANN]

INTRODUCTION

Analysis of problems involving simulations over large/infinite domains can often be simplified by replacing a portion of the domain by a Dirichlet to Neumann, or DtN map.[1] Here we utilize the concepts of Dirichlet to Neumann mapping to replace a dynamical subsystem by a set of forces $\mathbf{f}(t)$. We consider the subsystem to interact with the main structure through a finite number of degrees of freedom which we refer to as attachment points. The forces $\mathbf{f}(t)$ that the dynamical subsystem exerts on the main structure depend on the displacement histories of the attachment points. Thus a Dirichlet to Neumann map in this context is a map that takes displacement histories into current forces. Once the DtN map characterizing a dynamical subsystem is known, its effect on the main structure is completely determined.

Approximate representations of dynamical subsystems (equipment) have two important advantages over exact representations or models. First, the approximate DtNs often provide enough accuracy while reducing computational costs. Second, approximate DtNs require relatively little effort to formulate. Here we formulate an approximate DtN map based on a few gross parameters of the subsystem.

Many methods have been proposed to model the effects of complicated substructures on the dynamics of the main structure. Soize[2] has attempted to do so by treating the substructures as random structural elements, the parameters of which are imprecisely known. Because of the uncertainty in their structure, he has referred to them as "fuzzy structures." Given a master (main) structure with random attachments, Soize sets out to find the ensemble average of the response of the main structure. Following Soize's example, many other authors have used different closure approximations in an attempt to achieve the same goal.[3–7] Statistical energy analysis is also concerned with finding the ensemble average response of a random system.

Pierce *et al.*,[8] on the other hand, found the "typical response" of a plate with a densely packed collection of oscillators. Crighton[9] has noted that in order to make predictions about an individual realization of a system, one must seek a "typical response" of a complicated system, rather than an average response. Any introductory statistics text makes the point that knowledge of the average response alone is insufficient to make judgments about the behavior of the individual. This has recently been emphasized in regard to fuzzy structures in Ref. 10.

Our approach is to examine a complicated *deterministic* system. We obtain a model for the system which can be exact if sufficient information about the system is given. We consider approximations for the response of the system which exploit the one thing that we have assumed from the outset: the subsystem is complicated. Therefore, the number of modes in the frequency range of interest in the system is large. Thus we obtain an approximation that is valid for any individual subsystem, and not only for an ensemble.

We conduct our analysis in the time domain (rather than the frequency domain) for two reasons. First, for dynamical simulations, this is the domain of interest. Second, the analysis of the causal limit of zero damping and high modal density in the frequency domain can be subtle. On the other hand, in the time domain we can more easily obtain results for zero damping than with damping, as we will show.

In the next section we formulate the problem for constructing the time domain DtN map for a general linear elastic subsystem. The exact equations are derived for the case of zero damping. We then solve the equations of motion to derive the exact DtN map for the subsystem. The effects of small damping are then incorporated approximately. We use a modal representation similar to that used by Pierce[6] and develop an approximate DtN map for the subsystem in the high modal density limit. We derive error bounds on the approximate DtN map based on the choice of parameters.

[a]Currently affiliated with Parametric Technologies Corporation, Waltham, MA.

 0001-4966/98/104(4)/2048/6/$15.00

Finally we compare the results of using an exact DtN map to those from an approximate DtN map in a dynamical simulation. The simulation is performed for the special case of a single attachment point subsystem whose components move unidirectionally.

I. FORMULATION

We consider a linear dynamical subsystem whose configuration is specified by $N+M$ generalized coordinates, ξ_i with $i=1,\ldots,N+M$. These generalized coordinates may be thought of as being the generalized displacements of the components of the subsystem from their equilibrium positions. This subsystem interacts with the outside world through the first N of the $N+M$ generalized coordinates ξ_β with $\beta=1,\ldots,N$. Henceforth we shall refer to these generalized degrees of freedom as the degrees of freedom of the attachment points. We denote the generalized forces that are applied to the system through the first N generalized coordinates by f_γ where $\gamma=1,2,\ldots,N$.

The equations of motion for the subsystem are:

$$\begin{pmatrix}\mathbf{M}_{11} & \mathbf{M}_{12}\\ \mathbf{M}_{21} & \mathbf{M}_{22}\end{pmatrix}\begin{pmatrix}\ddot{\xi}_1\\ \ddot{\xi}_2\end{pmatrix}+\begin{pmatrix}\mathbf{C}_{11} & \mathbf{C}_{12}\\ \mathbf{C}_{21} & \mathbf{C}_{22}\end{pmatrix}\begin{pmatrix}\dot{\xi}_1\\ \dot{\xi}_2\end{pmatrix}$$
$$+\begin{pmatrix}\mathbf{K}_{11} & \boldsymbol{\kappa}_{12}\\ \boldsymbol{\kappa}_{21} & \mathbf{K}_{22}\end{pmatrix}\begin{pmatrix}\xi_1\\ \xi_2\end{pmatrix}=\begin{pmatrix}\mathbf{f}_1\\ 0\end{pmatrix}. \tag{1}$$

Here, ξ_1 represents the generalized coordinates of the attachment points and ξ_2 represents the generalized coordinates of the internal degrees of freedom. The $\mathbf{K}$'s represent the stiffness parameters coupling the attachment degrees of freedom or the internal degrees of freedom to one another. The $\boldsymbol{\kappa}$'s represent the stiffness parameters coupling the attachment degrees of freedom to the internal degrees of freedom. The $\mathbf{M}$'s represent mass elements, while the $\mathbf{C}$'s are damping coefficients.

In the derivations that follow, we shall consider only the special case in which $\mathbf{C}_{11}=\mathbf{0}$ and $\mathbf{C}_{12}=\mathbf{C}_{21}^T=\mathbf{0}$. We shall also usually consider the case of zero damping, in which $\mathbf{C}_{22}=\mathbf{0}$. We shall, however, allow for the situations in which $\mathbf{M}_{11}=0$ and/or $\mathbf{M}_{12}=\mathbf{M}_{21}^T=\mathbf{0}$. The matrices $\mathbf{M}_{22}$, $\mathbf{K}_{11}$, $\mathbf{K}_{22}$ are all assumed to be positive definite.

In order to distinguish between the various blocks that appear in the matrices in (1), we shall adopt a summation convention where repeated subscripts are summed through their range. Since we require different ranges to distinguish between attachment points and internal degrees of freedom, we adopt the convention

$$\begin{aligned}&\alpha,\beta,\gamma,\ldots=1,2,\ldots,N,\\ &p,q,r,s,\ldots=N+1,\ldots,N+M.\end{aligned} \tag{2}$$

Thus $\mathbf{M}_{11}\rightarrow M_{\alpha\beta}$, $\mathbf{M}_{12}\rightarrow M_{\alpha p}$, $\mathbf{M}_{22}\rightarrow M_{pq}$, etc. Using this convention (2) allows us to rewrite (1) as

$$M_{\alpha\beta}\ddot{\xi}_\beta+M_{\alpha p}\ddot{\xi}_p+K_{\alpha\beta}\xi_\beta+\kappa_{\alpha p}\xi_p=f_\alpha \tag{3}$$

and

$$M_{pq}\ddot{\xi}_q+C_{pq}\dot{\xi}_q+K_{pq}\xi_q=-M_{p\alpha}\ddot{\xi}_\alpha-\kappa_{p\alpha}\xi_\alpha. \tag{4}$$

In Eq. (4) we see that the internal degrees of freedom are forced by the motions of the attachment points. Equations (3) and (4) are the equations of motion of the subsystem. We can now solve (4) for the unknown generalized coordinates, ξ_p, and use the result in (3) to formulate a Dirichlet to Neumann Map or DtN.[1] The DtN map can be written as

$$\mathbf{f}=\tilde{\mathbf{F}}(\xi_\alpha). \tag{5}$$

Here, $\tilde{\mathbf{F}}$ is the Dirichlet to Neumann map; the forces f_α represent the Neumann data and the displacements of the attachment points ξ_α represent the Dirichlet data. Thus the DtN describes the forces exerted by the subsystem on its environment in terms of the displacements of its attachment points. We note that in the case of linear systems, as are treated here, the Fourier transform of the time-domain DtN map (5) is directly proportional to the impedance of the subsystem.

II. EXACT SOLUTION FOR THE INTERNAL DEGREES OF FREEDOM

We now consider the special case of $\mathbf{C}_{22}=\mathbf{0}$. On that basis, we obtain an exact solution of (4) for the generalized displacements of the internal degrees of freedom ξ_p in terms of the displacements of the attachment points ξ_β. The solution may be obtained in terms of a normal mode expansion using the eigenvectors of the matrix $\mathbf{M}_{22}^{-1/2}\mathbf{K}_{22}\mathbf{M}_{22}^{-1/2}$. For details of this derivation we refer the reader to Ref. 11. Here we need not compute $\mathbf{M}_{22}^{-1/2}$ explicitly. We only need to note that $\mathbf{M}_{22}^{1/2}$ is the unique positive definite matrix that satisfies $\mathbf{M}_{22}^{1/2}\mathbf{M}_{22}^{1/2}=\mathbf{M}_{22}$.

The matrix $M_{sp}^{-1/2}K_{pq}M_{qr}^{-1/2}$ is symmetric because $\mathbf{K}_{22}$ is symmetric. We assume that $M_{sp}^{-1/2}K_{pq}M_{qr}^{-1/2}$ is positive definite; i.e.,

$$\mathbf{x}^T(\mathbf{M}^{-1/2}\mathbf{K}\mathbf{M}^{-1/2})\mathbf{x}>0,\quad \forall\mathbf{x}\neq 0\in\mathbf{R}^M. \tag{6}$$

Since $M_{sp}^{-1/2}K_{pq}M_{qr}^{-1/2}$ is symmetric and positive definite, it has M positive eigenvalues, $(\omega^{(P)})^2$, $P=1,\ldots,M$, and M distinct orthonormal eigenvectors, $\boldsymbol{\gamma}^{(P)}$, $P=1,\ldots,M$.

In what follows summation is implied on repeated subscripts, but superscripts are not summed unless explicitly specified. We solve Eq. (4) subject to the conditions $\xi_\alpha(t)=0$, $\xi_p(t)=0$, $\forall t\leq 0$, and use the properties of $(M_{sp}^{-1/2}K_{pq}M_{qr}^{-1/2})$ to get

$$\xi_s(t)=-\int_0^t\sum_{Q=1}^{M}\frac{A_{sp}^{(Q)}}{\omega^{(Q)}}\sin(\omega^{(Q)}(t-\tau))$$
$$\times\{\kappa_{p\alpha}\xi_\alpha(\tau)+M_{p\alpha}\ddot{\xi}_\alpha(\tau)\}\,d\tau. \tag{7}$$

We note that the time integration starts at $t=0$ because the subsystem has no displacement history prior to this. In (7), we have denoted the outer product $\mathbf{M}^{-1/2}\boldsymbol{\gamma}\otimes\boldsymbol{\gamma}\mathbf{M}^{-1/2}$ by $\mathbf{A}$:

$$A_{ps}^{(P)}=M_{pq}^{-1/2}\gamma_q^{(P)}\gamma_r^{(P)}M_{rs}^{-1/2}. \tag{8}$$

A. Exact Dirichlet to Neumann map

We now obtain an exact DtN map by substituting Eq. (7) into Eq. (3). This yields

$$f_\alpha = M_{\alpha\beta}\ddot{\xi}_\beta + K_{\alpha\beta}\xi_\beta - \left(\kappa_{\alpha p} + M_{\alpha p}\frac{d^2}{dt^2}\right)\int_0^t \sum_{P=1}^{M} \frac{A_{ps}^{(P)}}{\omega^{(P)}} \sin(\omega^{(P)}(t-\tau)) \times\{M_{s\beta}\ddot{\xi}_\beta(\tau) + \kappa_{s\beta}\xi_\beta(\tau)\}\, d\tau. \quad (9)$$

Various expressions for the exact DtN map may be constructed by rearranging the terms of Eq. (9).[11] It is, perhaps, most illustrative to conduct integration by parts on terms containing ξ and simplify the result to write

$$f_\alpha = [M_{\alpha\beta} - M_{\alpha i}M_{ij}^{-1}M_{j\beta}]\ddot{\xi}_\beta + [K_{\alpha\beta} - \kappa_{\alpha p}K_{ps}^{-1}\kappa_{s\beta}]\xi_\beta(t) + \int_0^t \sum_{P=1}^{M} \omega^{(P)} m_{\alpha\beta}^{(P)} \sin(\omega^{(P)}(t-\tau))\ddot{\xi}_\beta(\tau)\, d\tau. \quad (10)$$

Here we have used the relation[11]

$$K_{pq}^{-1} = \sum_{P=1}^{M} \frac{A_{pq}^{(P)}}{(\omega^{(P)})^2}. \quad (11)$$

In Eq. (10) we have introduced the modal mass tensor $m_{\alpha\beta}^{(P)}$. We define the modal mass tensor to be

$$m_{\alpha\beta}^{(P)} = \frac{1}{(\omega^{(P)})^4}(M_{\alpha p}(\omega^{(P)})^2 - \kappa_{\alpha q})\begin{pmatrix} A_{pr}^{(P)} & A_{ps}^{(P)} \\ A_{qr}^{(P)} & A_{qs}^{(P)} \end{pmatrix} \times \begin{pmatrix} M_{r\beta}(\omega^{(P)})^2 \\ -\kappa_{s\beta} \end{pmatrix}. \quad (12)$$

This modal mass tensor is a generalization of the modal mass definition of Pierce[6] and O'Hara and Cunniff.[12]

B. Properties of the modal mass tensor

The modal mass tensors have the property that their sum over all modes, $P=1,\ldots,M$, yields the total mass of the subsystem.[11] This may be written as

$$\zeta_\alpha^i[M_{\alpha\beta} - M_{\alpha i}M_{ij}^{-1}M_{j\beta}]\zeta_\beta^j + \sum_{P=1}^{M} \zeta_\alpha^i m_{\alpha\beta}^{(P)}\zeta_\beta^j = M_{(T)}\delta^{ij}. \quad (13)$$

Here ζ_α^i represents a unit displacement of the attachment points in the ith Cartesian direction and δ^{ij} is the Kronecker delta function. Further, the modal mass tensors can also be shown to satisfy the relationship[11]

$$\sum_{P=1}^{M} (\omega^{(P)})^2 m_{\alpha\beta}^{(P)} = M_{\alpha p}M_{pq}^{-1}K_{qr}M_{rs}^{-1}M_{s\beta} - M_{\alpha p}M_{pq}^{-1}\kappa_{q\beta} - \kappa_{\alpha p}M_{pq}^{-1}M_{q\beta} + \kappa_{\alpha p}K_{pq}^{-1}\kappa_{q\beta}. \quad (14)$$

C. The role of damping

We now briefly reconsider Eq. (4) with $\mathbf{C}_{22} \neq 0$. We shall assume, however, that $\mathbf{C}_{22}$ can be diagonalized by the eigenvectors γ. Thus, we write

$$M_{rp}^{-1/2}C_{pq}M_{qs}^{-1/2}\gamma_s^{(Q)} = 2\eta^{(Q)}\omega^{(Q)}\gamma_s^{(Q)} \quad \text{(no sum on } Q\text{)}. \quad (15)$$

Here, $\eta^{(Q)}$ is the fraction of critical damping of the Qth mode of the clamped subsystem. Assuming $\eta^{(Q)} \ll 1$ leads to the following solution of (4):

$$\xi_s = -\int_0^t \sum_{Q=1}^{M} \frac{A_{sp}^{(Q)}}{\omega^{(Q)}} \sin(\omega^{(Q)}(t-\tau)) \times \exp(-\eta^{(Q)}\omega^{(Q)}(t-\tau))\{\kappa_{p\alpha}\xi_\alpha(\tau) + M_{p\alpha}\ddot{\xi}_\alpha(\tau)\}d\tau. \quad (16)$$

Following the same steps as those leading to Eq. (10), gives an approximate DtN that includes the effects of small damping on the internal degrees of freedom:

$$f_\alpha = [M_{\alpha\beta} - M_{\alpha i}M_{ij}^{-1}M_{j\beta}]\ddot{\xi}_\beta + [K_{\alpha\beta} - \kappa_{\alpha p}K_{ps}^{-1}\kappa_{s\beta}]\xi_\beta(t) + \int_0^t \sum_{P=1}^{M} \omega^{(P)} m_{\alpha\beta}^{(P)} \times \sin(\omega^{(P)}(t-\tau))e^{-\eta^{(P)}\omega^{(P)}(t-\tau)}\ddot{\xi}_\beta(\tau)\, d\tau. \quad (17)$$

We emphasize here that (17) is exact for $\eta^{(P)} = 0$, but is only approximately valid for $\eta^{(P)} \neq 0$. We shall refer to results derived consistently from (17) as "exact" in the rest of the paper, with the understanding that they are exact for $\eta^{(P)} = 0$.

III. APPROXIMATE DTN MAP AND ERROR BOUNDS

We begin this section by introducing the modal mass function:

$$\mathbf{m}(\omega) = \sum_{P=1}^{M} \mathbf{m}^{(P)} H(\omega - \omega^{(P)}). \quad (18)$$

In (18), $H(\omega)$ is the Heaviside unit step function. This definition is similar although not identical to that of Pierce.[6] We note that the function $\mathbf{m}(\omega)$ is discontinuous. Therefore its derivatives are to be interpreted as delta functions. We also introduce a continuous damping function $\eta(\omega)$ such that $\eta(\omega^{(Q)}) = \eta^{(Q)}$, and that

$$\min_{\omega} \eta(\omega) = \min_{Q=1,\ldots,M} \eta^{(Q)}. \quad (19)$$

When the subsystem has many internal degrees of freedom and therefore many modes, we expect that the modal mass function $\mathbf{m}(\omega)$ is well approximated by a smooth function $\bar{\mathbf{m}}(\omega)$. We now show that the error in $\mathbf{f}(t)$ resulting from approximating the modal mass function is bounded for all time, subject to some conditions. We do this by rewriting our discrete DtN in (17) using (18) and (19):

$$f_\alpha = [M_{\alpha\beta} - M_{\alpha i}M_{ij}^{-1}M_{j\beta}]\ddot{\xi}_\beta + [K_{\alpha\beta} - \kappa_{\alpha p}K_{ps}^{-1}\kappa_{s\beta}]\xi_\beta(t) + \int_0^t \int_0^\infty \omega \frac{dm_{\alpha\beta}(\omega)}{d\omega} \times \sin\omega(t-\tau)e^{-\eta(t-\tau)}\ddot{\xi}_\beta(\tau)\, d\omega\, d\tau. \quad (20)$$

Here we emphasize that Eq. (20) is exact for the case of zero damping, and no "fuzzy" approximations have as yet been made. That (20) is indeed exact can be easily verified by substituting (18) into (20) and integrating the resulting sum of delta functions.

We now consider approximating $\mathbf{m}(\omega)$ by $\bar{\mathbf{m}}(\omega)$. Thus we introduce the difference function $\mathbf{m}^e(\nu)$ with $\nu=\omega/\epsilon$ such that

$$\mathbf{m}(\omega)=\bar{\mathbf{m}}(\omega)+\epsilon\mathbf{m}^e\left(\frac{\omega}{\epsilon}\right), \quad \epsilon\ll 1. \tag{21}$$

Here, $\epsilon\mathbf{m}^e(\omega/\epsilon)$ is a small but rapidly varying function which represents the error in approximating $\mathbf{m}(\omega)$ by $\bar{\mathbf{m}}(\omega)$. The fact that it is rapidly varying is accounted for explicitly through its dependence on the argument (ω/ϵ). The nondimensional parameter ϵ is a measure of the modal spacing. We now substitute Eq. (21) into (20) to get

$$\begin{aligned} f_\alpha=&[M_{\alpha\beta}-M_{\alpha i}M_{ij}^{-1}M_{j\beta}]\ddot{\xi}_\beta \\ &+[K_{\alpha\beta}-\kappa_{\alpha p}K_{ps}^{-1}\kappa_{s\beta}]\xi_\beta(t)+\int_0^t\int_0^\infty \omega\,\frac{d\bar{m}_{\alpha\beta}(\omega)}{d\omega} \\ &\times\sin\,\omega(t-\tau)e^{-\eta(t-\tau)}\ddot{\xi}_\beta(\tau)\,d\omega\,d\tau+\mathrm{error}_\alpha(t). \end{aligned} \tag{22}$$

The error term in Eq. (22) is given by

$$\begin{aligned} \mathbf{error}(t)=&\int_0^t\int_0^\infty \omega\frac{d\mathbf{m}^e}{d\nu}(\nu)\bigg|_{\nu=\omega/\epsilon}\sin\,\omega(t-\tau) \\ &\times e^{-\eta(t-\tau)}\ddot{\xi}(\tau)\,d\omega\,d\tau. \end{aligned} \tag{23}$$

Here, $m^{e'}_{\alpha\beta}(\nu)$ is the derivative with respect to its argument. We now show that the error is bounded. We integrate (23) by parts once in time and twice in frequency to obtain:

$$\begin{aligned} \mathbf{error}(t)=&\epsilon^2\int_0^t\int_0^\infty \mathbf{m}^e_{-1}\left(\frac{\omega}{\epsilon}\right)(t-\tau)^2\cos\,\omega(t-\tau) \\ &\times e^{-\eta(t-\tau)}\xi'''(\tau)\,d\omega\,d\tau. \end{aligned} \tag{24}$$

Here $\mathbf{m}^e_{-1}(\nu)$ is the integral of $\mathbf{m}^e(\nu)$ with respect to its argument. In deriving Eq. (24) the following assumptions were made regarding the choice of $\bar{\mathbf{m}}(\omega)$:

$$\begin{aligned} &\bar{\mathbf{m}}(0)=\mathbf{0}, \quad \bar{\mathbf{m}}(\infty)=\sum_{P=1}^{M}\mathbf{m}^{(P)}, \\ &\mathbf{m}^e_{-1}(0)=\mathbf{0}, \quad C\equiv\int_0^\infty ||\mathbf{m}^e_{-1}(\nu)||\,d\nu<\infty. \end{aligned} \tag{25}$$

In Eq. (24) we observe

$$\begin{aligned} &\int_0^\infty\left\|\mathbf{m}^e_{-1}\left(\frac{\omega}{\epsilon}\right)\right\|d\omega=\epsilon C<\infty, \\ &|\cos\,\omega(t-\tau)|\leqslant 1, \\ &(t-\tau)^3e^{-\eta(t-\tau)}\leqslant\left(\frac{3}{\eta_{\min}}\right)^3e^{-3}. \end{aligned} \tag{26}$$

Substituting (26) into (24) yields

$$\begin{aligned} &||\mathbf{error}(t)|| \\ &\leqslant\begin{cases}\dfrac{\epsilon^3}{\eta^3}27e^{-3}C|\xi'''(t)|_{\max}, & \eta\neq 0,\eta\ll 1,\forall t, \\ \epsilon^3t^3C|\xi'''(t)|_{\max}, & \eta=0,\forall t.\end{cases} \end{aligned} \tag{27}$$

Equation (27) shows that the error incurred in replacing $\mathbf{m}(\omega)$ by a smooth $\bar{\mathbf{m}}(\omega)$ is bounded for all time in the presence of damping. When there is no damping, the error is small for simulation time less than $O(1/\epsilon)$.

IV. EXAMPLE APPLICATION OF DTNs

In this section we illustrate the application of our formulation and DtNs to a particular problem. We consider an elastic rod (main structure) that we model discretely using ten elastic finite elements. At one end of the rod we prescribe a unit step displacement at $t=0$. At the other end of the rod we attach a dynamical subsystem whose components are allowed unidirectional motion only. We represent the effect of the subsystem on the dynamics of the elastic rod through a DtN map. We use this special case to compare the results of the exact DtN map to an approximate (fuzzy) DtN map. The basis of our comparison is the force $\mathbf{f}(t)$ that the substructure exerts on the rod in each case.

The exact DtN for such a subsystem may be derived from Eq. (20) to be

$$\begin{aligned} f_0(t)=&K_0\xi_0(t)-\int_0^t\int_0^\infty \omega^3\frac{dm(\omega)}{d\omega}\sin\,\omega(t-\tau) \\ &\times e^{-\eta(\omega)(t-\tau)}\xi_0(\tau)\,d\omega\,d\tau. \end{aligned} \tag{28}$$

Here ξ_0 is the displacement of the attachment point between the rod and the subsystem (equipment), f_0 is the force exerted by the subsystem on the elastic rod, and K_0 is the high-frequency attachment point stiffness. For details of the formulation and derivation of Eq. (28) we refer the reader to Ref. 13. We consider exact and approximate modal mass functions of the form

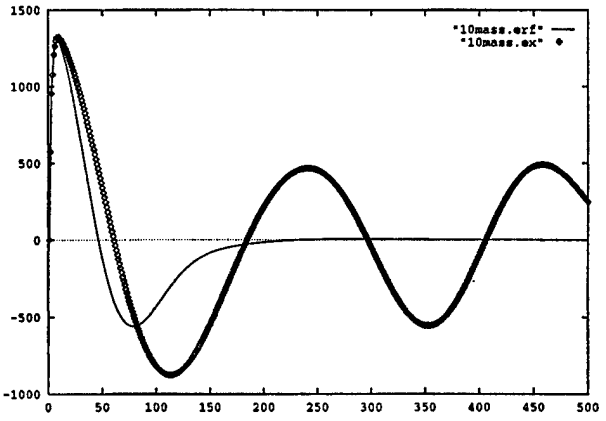

FIG. 1. Force at the attachment point plotted as a function of time. The full time scale is one unit. The parameters of the rod and subsystem are such that $\Omega\approx\omega_0\approx 10$. 10 internal d.o.f. subsystem.

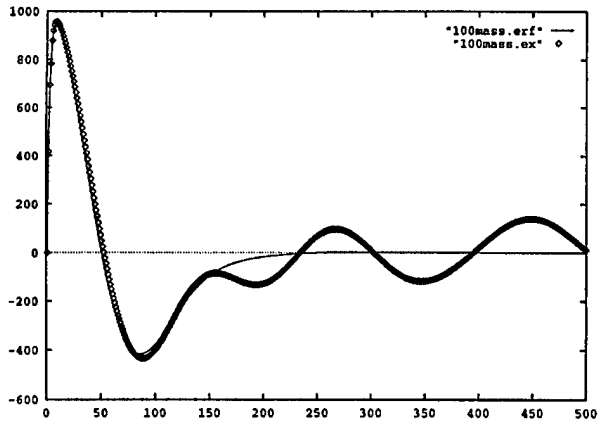

FIG. 2. The 100 internal d.o.f subsystem.

$$m(\omega)=\sum_{P=1}^{M} m^{(P)}H(\omega-\omega^{(P)}),$$

$$\bar{m}(\omega)=M_T \operatorname{erf}\left(\frac{\omega}{\sqrt{2}\Omega}\right). \tag{29}$$

Here erf (z) is the error function as defined in Ref. 14, M_T is the total mass of the subsystem, and Ω is a characteristic frequency scale of the subsystem. The frequencies $\omega^{(P)}$ are chosen randomly between 0 and $3\times\Omega$. The modal masses $m^{(P)}$ are chosen to approximate the continuous distribution $\bar{m}(\omega)$ in (29), thus satisfying the assumption (21).

We note further that the modal mass functions $m(\omega)$ and $\bar{m}(\omega)$ satisfy[13]

$$m(0)=0, \quad m(\infty)=M_T=\sum_{P=1}^{M} m^{(P)},$$

$$\frac{dm}{d\omega}\geqslant 0, \quad \int_0^{\infty}\omega^2\frac{dm(\omega)}{d\omega}\,d\omega=K_0. \tag{30}$$

From condition (30) we obtain $\Omega=\sqrt{K_0/M_T}$ in the approximate modal mass function. We use the modal mass functions from (29) in the DtN (28) to obtain our exact and approximate (fuzzy) DtN as[13]

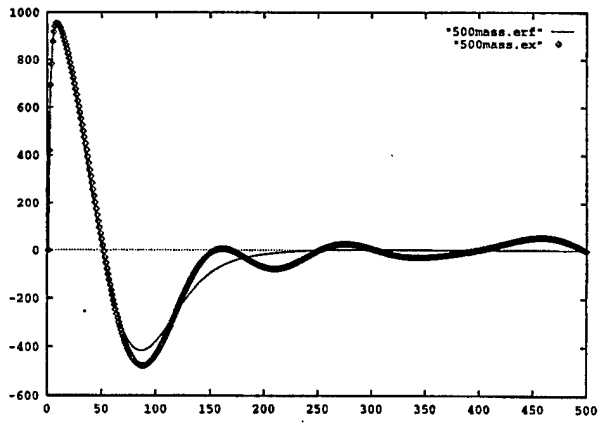

FIG. 3. The 500 internal d.o.f subsystem.

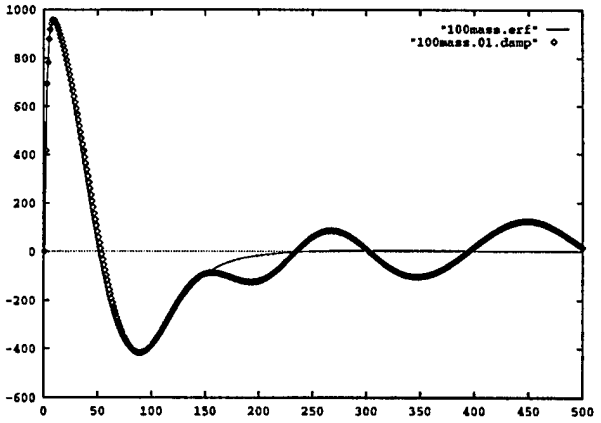

FIG. 4. The 100 internal d.o.f with 1% damping.

$$f_0(t)=K_0\xi_0(t)-\int_0^t\sum_{P=1}^{M}(\omega^{(P)})^3m^{(P)}$$

$$\times\sin(\omega^{(P)}(t-\tau))e^{-\eta^{(P)}(t-\tau)}\xi_0(\tau)\,d\tau, \tag{31}$$

$$\bar{f}_0(t)=K_0\xi_0(t)-M_T\Omega^4\int_0^t[3-\Omega^2(t-\tau)^2]$$

$$\times(t-\tau)e^{-(t-\tau)^2\Omega^2/2}\xi_0(\tau)\,d\tau. \tag{32}$$

We note that other choices of $\bar{m}(\omega)$ lead to different results.

A. Implementation and numerical results

We analyze the elastic rod described above using finite elements. The rod is discretized and represented by ten finite elements. The DtN boundary condition given by Eq. (31) or (32) is applied at the end of the rod at $x=L$. We apply a unit Heaviside step in displacement at the end $x=0$. We integrate the equations of motion explicitly to update the displacements in the rod and the force at the attachment point. The force at the attachment point at any time t depends on the value of ξ_0 at all *earlier* times. Therefore, we maintain a time history of the displacement of the node at $x=L$ and use this in (32) to evaluate the force f_0 at each time step. This allows us to compute the displacement of the rod at the next time step, and so on. Below we compare the forces between

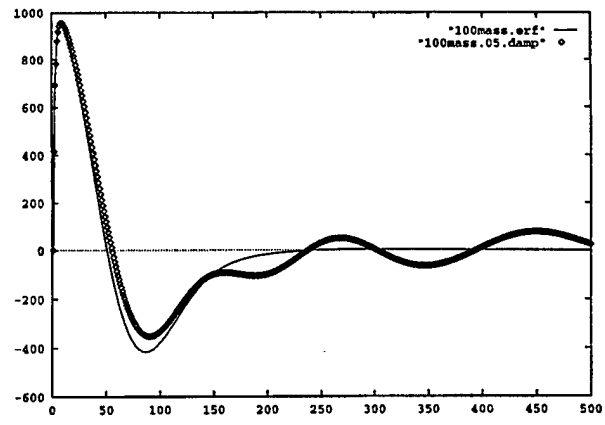

FIG. 5. The 100 internal d.o.f with 5% damping.

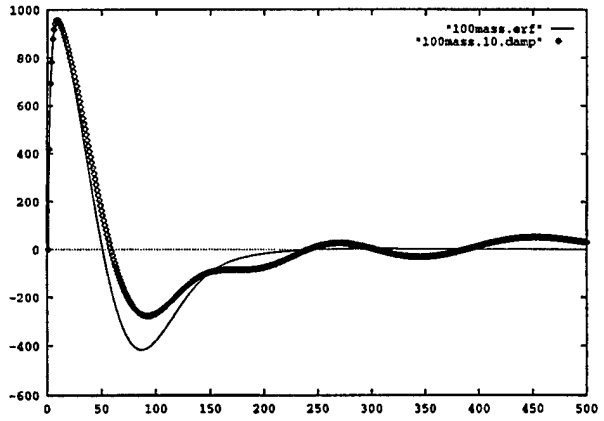

FIG. 6. The 100 internal d.o.f with 10% damping.

the rod and the equipment predicted by the exact DtN and the approximate DtN for various modal densities and modal damping.

The properties of the rod and the subsystem are chosen so that $\Omega \approx \omega_0 \approx 10$, where ω_0 is the lowest natural frequency of the rod. Further, the mass of the rod is approximately the same as the mass of the attachment. The rod has high ($\approx 10\%$) damping, which is the same throughout the simulations, and tends to make the travel time slightly faster than would be indicated by ω_0. The equipment has either zero dissipation or a value as stated in the figure captions. The full time range for the simulations is one time unit.

In Figs. 1–3 we see the effect of the number of internal degrees of freedom M (modes) on the exact and approximate DtNs (31) and (32), respectively. The number of modes is related inversely to the small parameter ϵ introduced in Eq. (21). Specifically, $\epsilon = O(1/M)$. Thus, as M increases, we expect the results from the approximate DtN (32) to better approximate the exact DtN results. From these figures we can see that the approximate DtN map in Eq. (32) indeed provides a more accurate representation of the subsystem as the number of internal degrees of freedom increase from 10 to 500.

In Figs. 4–6 we study the effect of subsystem damping on the validity of the DtN approximation. Based on the results from Sec. IV, we should expect that increasing damping (with M fixed) would control the long time error in the simulations. In Figs. 4–6, we see precisely this behavior as η increases from 1% to 10% of critical damping. We note that in all these figures the approximate DtN has zero added damping. We conjecture that better agreement in the "over shoot" region (near $t = 100$) would be realized by using an approximate DtN that included damping.

V. CONCLUSIONS

In Sec. III A we have shown that a general dynamical subsystem can be represented by an exact DtN map. The map can be used to replace the subsystem in a dynamical simulation. In Sec. IV we provided approximate representations for the dynamical subsystem. We showed that the error can be bounded. In the final section we studied an example problem and performed a dynamical simulation using both our exact and approximate DtNs. The simulation demonstrates the validity of our results when the number of modes is high. It also shows that the model improves with the presence of a small amount of damping.

The approximate structure model presented here requires knowledge of "the limiting structure." That is, we need to know

$$\lim_{\epsilon \to 0} m(\omega) = \bar{m}(\omega). \tag{33}$$

Equation (33) is very restrictive in terms of developing approximations for real structures. In a future contribution,[15] we shall show that a given structure can be accurately modeled without full knowledge of the limit in (33). That is, we can construct an $\bar{m}(\omega)$ with knowledge of only a few relatively simple parameters that describe the system.

ACKNOWLEDGMENTS

The authors would like to thank Allan D. Pierce, Isaac Harari, Dan Givoli, Daniel Goldman, Raymond Nagem, Josh Montgomery and Brian Rush for many helpful discussions and ideas. They also thank the anonymous reviewers for their helpful comments. This work was supported by the Office of Naval Research.

[1] D. Givoli, *Numerical Methods for Problems on Infinite Domains* (Elsevier, Amsterdam, 1992), 1st ed.
[2] C. Soize, "A model and numerical method in the medium frequency range for vibroacoustic predictions using the theory of structural fuzzy, J. Acoust. Soc. Am. **94**, 849–865 (1993).
[3] R. L. Weaver, "The effect of an undamped finite degree of freedom fuzzy substructure: numerical solutions and theoretical discussion," J. Acoust. Soc. Am. **100**, 3159–3164 (1996).
[4] R. L. Weaver, "Mean and mean-square responses of a prototypical master/fuzzy structure," J. Acoust. Soc. Am. **101**, 1441–1449 (1997).
[5] R. H. Lyon, "Statistical energy analysis and structural fuzzy," J. Acoust. Soc. Am. **97**, 2878–2881 (1995).
[6] A. D. Pierce, "Resonant-frequency-distribution of internal mass inferred from mechanical impedance matrices, with application to fuzzy structure theory," *Proceedings of ASME Symposium on Acoustics of Submerged Structures and Transduction Systems*, September 17–21, 1995 (ASME, New York, 1996).
[7] M. Strasberg, "Continuous structures as fuzzy substructures," J. Acoust. Soc. Am. **100**, 3456–3459 (1996).
[8] A. D. Pierce, V. W. Sparrow, and D. A. Russel, "Fundamental structural-acoustic idealizations for structures with fuzzy internals," ASME Transactions, Paper No. 93-WA/NCA-17, ASME Winter Annual Meeting, New Orleans, November 1993.
[9] D. G. Crighton, private communication.
[10] Y. K. Lin, "On the standard deviation of change-in-impedance due to fuzzy subsystems," J. Acoust. Soc. Am. **101**, 616–618 (1997).
[11] A. Cherukuri and P. E. Barbone, "Time Domain Dirichlet to Neumann Maps For Representing Complex Dynamical Subsystems," Boston University, Department of Aerospace & Mechanical Eng. Technical Report, No. AM-96-017, 1996.
[12] G. J. O'Hara and P. F. Cunniff, "Elements of Normal Mode Theory," Naval Research Laboratory Report, 6002 (1963).
[13] P. E. Barbone, "Equipment Representations for Shock Calculations: Time Domain Dirichlet to Neumann Maps," in *Acoustics, Vibrations, and Rotating Machines*, Proceedings of the 1995 Design Engineering Technical Conferences, Sept. 17–20, 1995 (ASME Press, New York, 1996), Vol. 3, Part B, pp. 223–228.
[14] M. Abramowitz and I. A. Stegun, *Handbook of Mathematical Functions* (Dover, New York, 1972).
[15] P. E. Barbone, A. Cherukuri, and D. Goldman, "Canonical representations of complex vibratory subsystems, Part I: Single attachment point," Boston University Aerospace and Mechanical Engineering Technical Report No. AM-98-027, June 1998.

C.4 Dirichlet to Neumann Maps for the Representation of Equipment with Weak Nonlinearities

Daniel Goldman and Paul E. Barbone. "Dirichlet to Neumann Maps for the Representation of Equipment with Weak Nonlinearities," Proc. ASME Noise Control and Acoustics Division, Vol. NCA22, pp. 71–76, Proceedings of the 1996 International Mechanical Engineering Congress, Atlanta, GA, November 17–22, 1996.

NCA-Vol. 22, Proceedings of the ASME
Noise Control and Acoustics Divsion
ASME 1996

Dirichlet to Neumann Maps for the Representation of Equipment with Weak Nonlinearities

Daniel Goldman and Paul E. Barbone
Department of Aerospace and Mechanical Engineering
Boston University
Boston, Massachusetts

ABSTRACT

We consider modeling the presence of a substructure in a dynamical simulation in terms of the force the substructure exerts on the main structure of interest. The reaction force is given in terms of the displacement of the attachment points. We call the map between the displacement of the attachment points and the force at the attachment a *Dirichlet to Neumann*, or DtN, map. We use a regular perturbation expansion to derive an approximate DtN for the case when the substructure exhibits weakly nonlinear behavior. The representation is accurate to $O(\epsilon^2 t^2) + O(t^2/N^2)$, where ϵ is a measure of the strength of the nonlinearity, N is the number of modes of the subsystem and t is the simulation time. We note that the representation is particularly suited to the situation when $\epsilon = O(N^{-1})$.

INTRODUCTION

Calculations of the mechanical response of complex structures can often be simplified by first determining the response characteristics of the internal components. Barbone (1995, henceforth (I)) proposed doing this in terms of a Dirichlet to Neumann map (DtN), which converted displacements of equipment attachment points to forces. An exact DtN was derived for a general subsystem consisting of masses and linear springs, and it was shown that in several cases of interest it is possible to obtain much simpler, approximate DtN's. In particular, when the density of eigenstates of the internal subsystem is very high, the application of "fuzzy structures" techniques (Pierce, Sparrow & Russel, 1993; Pierce, 1995) produces an approximation which involves a few easily estimated physical parameters. In this paper, we discuss the extension of the results in (I) to the case of a subsystem with weakly nonlinear internal interactions. We first derive an approximate DtN for an arbitrary but weak nonlinearity, and discuss the resulting error of the approximation. We then describe two specific models of nonlinearities. Finally, we discuss the derivation of higher-order approximate DtN's for weakly nonlinear subsystems, and demonstrate the validity of our first-order result through a numerical example.

FIRST-ORDER DTN FOR WEAK NONLINEARITY

As in (I) we shall assume that the subsystem is attached to the main structure at a single point and that all motion is purely unidirectional. In this case, the displacements of the attachment point and the N subsystem components can be described by the scalar $x_0(t)$ and the N-dimensional vector $\boldsymbol{x}(t)$. The force exerted on the equipment by the structure is denoted $f_0(t)$. The goal in deriving a DtN for the subsystem is to obtain an expression for $f_0(t)$ which depends only on $x_0(t)$.

The movement of the equipment and the resulting force on the main structure are assumed to obey the

following equations:

$$\begin{aligned} M\ddot{x}(t) + Kx(t) + \epsilon v[x(t)] &= -\kappa x_0(t) \quad (1) \\ \kappa \cdot (x(t) - px_0(t)) &= f_0(t), \quad (2) \end{aligned}$$

Here the $N \times N$ positive definite matrix M and the $N \times N$ symmetric matrix K describe the masses and spring constants of the subsystem. κ is an N-dimensional vector of coupling spring constants, and p is an N-dimensional vector with each component equal to unity, which represents uniform rigid translation of the subsystem. In (1)–(2), x_0 is the displacement of the attachment point, x is the vector of displacements of subsystem internal degrees of freedom, and f_0 is the force exerted on the subsystem by the main structure. We assume $\epsilon \ll 1$ and take v to be a given nonlinear function of x. For $\epsilon = 0$, equations (1) and (2) reduce to the equations used in (I).

In order to obtain a relation involving $f_0(t)$ and $x_0(t)$ only, equation (1) must be solved for $x(t)$, treating $x_0(t)$ as arbitrary. Though there are many advanced asymptotic techniques to treat equations like (1), they require specific forms of excitation (c.f. Nayfeh, 1981.) To treat an arbitrary excitation, however, the best procedure is to employ a straightforward regular perturbation expansion. Thus we assume that $x(t)$ can be expanded in a regular perturbation series:

$$x(t) = x^{(0)}(t) + \epsilon x^{(1)}(t) + \epsilon^2 x^{(2)}(t) + O(\epsilon^3). \quad (3)$$

Therefore,

$$\begin{aligned} f_0(t) &= k_0 x_0(t) \quad (4) \\ &+ \kappa \cdot \left(x^{(0)}(t) + \epsilon x^{(1)}(t) + \epsilon^2 x^{(2)}(t) + O(\epsilon^3) \right). \end{aligned}$$

Here, $k_0 = -p \cdot \kappa = p \cdot Kp$. The zeroth-order solution of (1) is that obtained in (I) for the linear case:

$$\begin{aligned} x^{(0)}(t) &= -\int_{-\infty}^{t} M^{-1/2} \sum_{n=1}^{N} \xi^{(n)} \left[\xi^{(n)} \cdot M^{-1/2} \kappa \right] \\ &\quad \times \frac{1}{\omega_n} \sin \omega_n (t - \tau) x_0(\tau) d\tau. \quad (5) \end{aligned}$$

The mode shapes and natural frequencies are defined by the equation

$$M^{-1/2} K M^{-1/2} \xi^{(n)} = \omega_n^2 \xi^{(n)}. \quad (6)$$

The first-order equation given by (1) and (3) is

$$M\ddot{x}^{(1)}(t) + Kx^{(1)}(t) = -v[x^{(0)}(t)] \equiv -\tilde{v}(t). \quad (7)$$

This can be solved exactly in terms of $x^{(0)}(t)$. Letting $x^{(1)}(t) = M^{-1/2} y(t)$ in equation (7) yields

$$\ddot{y}(t) + M^{-1/2} K M^{-1/2} y(t) = -M^{-1/2} \tilde{v}(t). \quad (8)$$

Since $M^{-1/2} K M^{-1/2}$ is symmetric and positive definite, we can write

$$y(t) = \sum_{n=1}^{N} \xi^{(n)} z_n(t). \quad (9)$$

Substituting (9) into (8) and using the orthonormality of the eigenvectors yields

$$\ddot{z}_n + \omega_n^2 z_n(t) = -\xi^{(n)} \cdot M^{-1/2} \tilde{v}(t). \quad (10)$$

The above scalar equation is easily solved using a Green's function $g_n(t)$ which satisfies

$$\begin{aligned} \ddot{g}_n(t) + \omega_n^2 g_n(t) &= -\delta(t) \quad (11) \\ g_n(t) &= 0 \quad t < 0. \quad (12) \end{aligned}$$

The solution $g_n(t) = -\frac{1}{\omega_n} \sin \omega_n t$ gives

$$z_n(t) = -\int_{-\infty}^{t} \frac{1}{\omega_n} \sin \omega_n (t - \tau) \xi^{(n)} \cdot M^{-1/2} \tilde{v}(\tau) d\tau. \quad (13)$$

We now subsitute (13) into (9) and use the definitions of $y(t)$ and $\tilde{v}(t)$ to obtain the following solution to (7):

$$\begin{aligned} x^{(1)}(t) &= -M^{-1/2} \sum_{n=1}^{N} \xi^{(n)} \int_{-\infty}^{t} \frac{1}{\omega_n} \sin \omega_n (t - \tau) \\ &\quad \times \xi^{(n)} \cdot M^{-1/2} v[x^{(0)}(\tau)] d\tau. \quad (14) \end{aligned}$$

The first-order approximation of the DtN map for the weakly nonlinear system (1)–(2) can now be written as

$$\begin{aligned} f_0(t) &= k_0 x_0(t) \quad (15) \\ &- \kappa \cdot \textstyle\int_{-\infty}^{t} M^{-1/2} \sum_{n=1}^{N} \xi^{(n)} \frac{1}{\omega_n} \sin \omega_n (t - \tau) \\ &\quad \times \left[\xi^{(n)} \cdot M^{-1/2} \kappa \right] x_0(\tau) d\tau \\ &- \epsilon \kappa \cdot \textstyle\int_{-\infty}^{t} M^{-1/2} \sum_{n=1}^{N} \xi^{(n)} \frac{1}{\omega_n} \sin \omega_n (t - \tau) \\ &\quad \times \left\{ \xi^{(n)} \cdot M^{-1/2} v[x^{(0)}(\tau)] \right\} d\tau + O(\epsilon^2 t^2), \end{aligned}$$

where $x^{(0)}(t)$ is given by (5).

The parameter which controls the error in (15) is ϵ. In our derivation of the general first-order DtN (15), we gave no special treatment to the secular terms in $\boldsymbol{x}^{(0)}$ and $\boldsymbol{x}^{(1)}$. Therefore, we expect that the $O(\epsilon^2)$ error terms can experience unbounded growth proportional to t^2. (c.f. Nayfeh 1981.) Therefore, we have denoted the error in equation (15) as $O(\epsilon^2 t^2)$. Thus, we can expect (15) to be an accurate approximation to the exact nonlinear DtN when $t \ll \epsilon^{-1}$ and $\epsilon \ll 1$.

TWO NONLINEAR FUNCTIONS WITH FUZZY-STRUCTURE APPROXIMATIONS

We now discuss two specific forms of the nonlinear function $v[x]$ in (1). In each case, we first describe $v[x]$ and the resulting DtN (15), and then make a high modal density (fuzzy) approximation. Following these two examples, we discuss the errors which can be expected from our fuzzy-structure approximations and compare these with the error due to our weakly nonlinear treatment.

Unidirectional Quadratic Nonlinearity

Here, as a simple example, we assume that

$$v[x] = \kappa \sum_{n=1}^{N} \left[\xi^{(n)} \cdot M^{1/2} x\right]^2. \tag{16}$$

We now substitute (16) into (15), to obtain

$$\kappa \cdot x^{(1)} = -\int_{-\infty}^{t} \sum_{n=1}^{N} \frac{1}{\omega_n} \sin\omega_n(t-\tau)\kappa \cdot M^{-1/2}\xi^{(n)}$$

$$\times \xi^{(n)} \cdot M^{-1/2}\kappa \sum_{l=1}^{N} \left[\xi^{(l)} \cdot M^{1/2} x^{(0)}(\tau)\right]^2 d\tau. \tag{17}$$

By using (5), we get the following expression for the term in square brackets in (17):

$$\xi^{(l)} \cdot M^{1/2} x^{(0)}(\tau) = \tag{18}$$

$$-\xi^{(l)} \cdot M^{-1/2}\kappa \int_{-\infty}^{\tau} \frac{1}{\omega_l} \sin\omega_l(\tau-\tau')x_0(\tau')d\tau'$$

We now simplify (17) using the "modal mass" (O'Hara & Cunniff, 1963; see also Pierce, 1995 and (I)), defined as

$$m_n = \left(p \cdot M^{1/2}\xi^{(n)}\right)^2. \tag{19}$$

It can be shown that

$$\kappa \cdot M^{-1/2}\xi^{(n)} = -\omega_n^2\sqrt{m_n}, \tag{20}$$

hence (17) becomes

$$\kappa \cdot x^{(1)}(t) = -\int_{-\infty}^{t} \sum_{n=1}^{N} m_n\omega_n^3 \sin\omega_n(t-\tau) \tag{21}$$

$$\times \sum_{l=1}^{N} m_l\omega_l^2 \left[\int_{-\infty}^{\tau} \sin\omega_l(\tau-\tau')x_0(\tau')d\tau'\right]^2 d\tau.$$

Similary, one has

$$\kappa \cdot x^{(0)}(t) = -\int_{-\infty}^{t} \sum_{n=1}^{N} m_n\omega_n^3 \sin\omega_n(t-\tau)x_0(\tau)d\tau. \tag{22}$$

Substituting the preceding two expressions into (4) gives a DtN for the quadratically nonlinear subsystem under consideration which has an error of order $\epsilon^2 t^2$.

High Modal Density. We now prepare to make the approximation of assuming that the modes are closely spaced in frequency. In this case, the modal mass can be represented by a function of frequency, $m(\omega)$, which is defined by (Cherukuri 1996, Cherukuri & Barbone 1996):

$$\frac{dm(\omega)}{d\omega} = \sum_{n=1}^{N} m_n\,\delta(\omega-\omega_n). \tag{23}$$

We can now exactly replace the sums over N modes in (21) and (22) by integrals over all frequencies. The $O(\epsilon)$ DtN for (1)–(2) with the nonlinear function (16) then becomes

$$f_0(t) = k_0 x_0(t) \tag{24}$$

$$-\int_{-\infty}^{t}\int_{0}^{\infty} \frac{dm(\omega)}{d\omega}\omega^3 \sin\omega(t-\tau)d\omega\, x_0(\tau)d\tau$$

$$-\epsilon\int_{-\infty}^{t}\int_{0}^{\infty} \frac{dm(\omega)}{d\omega}\omega^3 \sin\omega(t-\tau)d\omega$$

$$\times \int_{0}^{\infty} \frac{dm(\omega')}{d\omega'}\omega'^2 \left[\int_{-\infty}^{\tau} \sin\omega'(\tau-\tau')x_0(\tau')d\tau'\right]^2$$

$$\times d\omega' d\tau + O(\epsilon^2 t^2).$$

We note that when the modal density is high, the exact discontinuous $\frac{dm(\omega)}{d\omega}$ (23) can be replaced with a smooth approximation. The error so introduced in $f_0(t)$ is discussed below.

Quartic Potential Energy

Here we make the physically reasonable assumption that $v[x]$ is the gradient of a quartic potential energy function. Specifically, we let

$$v_p[x] = \frac{\partial}{\partial x_p} \sum_{i,j,k,l=1}^{N} \frac{1}{4}\Gamma_{ijkl}\, x_i x_j x_k x_l, \tag{25}$$

where $\mathbf{\Gamma}$ is a constant, rank 4 tensor which is symmetric with respect to all pairs of indices. Applying the above definition,

$$v_p[x] = \sum_{j,k,l=1}^{N} \Gamma_{pjkl}\, x_j x_k x_l. \tag{26}$$

We now assume that $\mathbf{\Gamma}$ can be expressed in terms of symmetric $N \times N$ stiffness matrices $\boldsymbol{K}$ as follows:

$$\Gamma_{ijkl} = \frac{1}{3}\left[K_{ij}K_{kl} + K_{il}K_{kj} + K_{ik}K_{jl}\right]. \tag{27}$$

Using (27), we obtain

$$\boldsymbol{x}^{(1)}(t) = -\int_{-\infty}^{t} \boldsymbol{M}^{-1/2} \sum_{n=1}^{N} \boldsymbol{\xi}^{(n)} \frac{1}{\omega_n} \sin\omega_n(t-\tau)$$
$$\times \boldsymbol{\xi}^{(n)} \cdot \boldsymbol{M}^{-1/2}\boldsymbol{K}\boldsymbol{x}^{(0)}(\tau)\left(\boldsymbol{x}^{(0)}(\tau)\cdot \boldsymbol{K}\boldsymbol{x}^{(0)}(\tau)\right) d\tau \tag{28}$$

Writing $\boldsymbol{x}^{(0)}$ as

$$\boldsymbol{x}^{(0)}(t) = \sum_{l=1}^{N} a_l(t)\boldsymbol{M}^{-1/2}\boldsymbol{\xi}^{(l)} \tag{29}$$

and noting that $\boldsymbol{M}^{-1/2}$ is symmetric allows us to write (28) as

$$\boldsymbol{x}^{(1)}(t) = -\int_{-\infty}^{t} \boldsymbol{M}^{-1/2} \sum_{n=1}^{N} \boldsymbol{\xi}^{(n)} \frac{1}{\omega_n} \sin\omega_n(t-\tau)$$
$$\times \left\{ a_n(\tau)\omega_n^2 \sum_{l=1}^{N} a_l^2(\tau)\omega_l^2 \right\} d\tau. \tag{30}$$

We can now explicitly write down the order ϵ term in the DtN for the cubic nonlinearity given by (26)–(27). Substituting the full expression for $a_n(t)$ from (5) and using the modal mass m_n gives us

$$\boldsymbol{\kappa}\cdot\boldsymbol{x}^{(1)}(t) = \int_{-\infty}^{t} \sum_{n=1}^{N} \omega_n^4 m_n \sin\omega_n(t-\tau) \tag{31}$$
$$\times \int_{-\infty}^{\tau} \sin\omega_n(\tau-\tau')x_0(\tau')d\tau'$$
$$\times \sum_{l=1}^{N} \omega_l^4 m_l \left(\int_{-\infty}^{\tau} \sin\omega_l(\tau-\tau')x_0(\tau')d\tau'\right)^2 d\tau.$$

High Modal Density. We now assume that the modal density of the subsystem under consideration is very high, and let the modal mass be a continuous function of frequency $m(\omega)$, as was done above. In this case, the $O(\epsilon^2)$ DtN corresponding to (31) becomes

$$f_0(t) = k_0 x_0(t) \tag{32}$$
$$- \int_{-\infty}^{t}\int_{0}^{\infty} \frac{dm(\omega)}{d\omega}\omega^3 \sin\omega(t-\tau)d\omega\, x_0(\tau)d\tau$$
$$+\epsilon \int_{-\infty}^{t}\int_{0}^{\infty} \omega^4 \frac{dm(\omega)}{d\omega} \sin\omega(t-\tau)$$
$$\times \int_{-\infty}^{\tau} \sin\omega(\tau-\tau')d\omega\, x_0(\tau')d\tau'$$
$$\times \int_{0}^{\infty} \omega'^4 \frac{dm(\omega')}{d\omega'}$$
$$\times \left(\int_{-\infty}^{\tau} \sin\omega'(\tau-\tau')x_0(\tau')d\tau'\right)^2 d\omega'\, d\tau.$$

Error Due To Fuzzy-Structure Approximation

The DtN's (24) and (32) involve approximations based on two explicit assumptions: weak nonlinearity and high modal density. The function $m(\omega)$ introduced in equation (23) can be chosen to represent the subsystem exactly. Frequently, however, an approximation to $m(\omega)$, say $\bar{m}(\omega)$, will be used for any of various reasons. Such an approximation naturally leads to error in the DtN. Cherukuri and Barbone (1996) point out that $\bar{m}(\omega)$ should be chosen so that for $n = 0, 1, 2$:

$$\int_0^\infty \omega^n \frac{d\bar{m}}{d\omega}\, d\omega = \int_0^\infty \omega^n \frac{dm}{d\omega}\, d\omega. \tag{33}$$

In this case, the error due to the approximation of $m(\omega)$ with $\bar{m}(\omega)$ is $O(t^2/N^2)$ (Cherukuri & Barbone, 1996). Here, N is the number of components in the internal subsystem.

Both the weakly nonlinear and fuzzy-structure approximations cause the error in $f_0(t)$ to grow as simulation times advance. If there is significant dissipation in the system, however, we can expect that the long time response will vanish before significant error can accumulate. In particular, if the dissipation time scale is $O(\tau)$, then we conjecture that for $m(\omega) = \bar{m}(\omega)$ (as defined in (33)) the DtN's (24) and (32) will be valid for all time when $\tau = o(\epsilon^{-1})$ and $\tau = o(N)$.

HIGHER-ORDER DTN's

We now describe a method for obtaining approximate DtN's for the weakly nonlinear system (1)–(2) which are accurate to second-order or higher in ϵ. We concentrate on solving (1), since it is straightforward to obtain the $O(\epsilon^n)$ DtN from (5) once $\boldsymbol{x}^{(n)}(t)$ has been found.

Assuming an arbitrary function $v[\boldsymbol{x}]$, we expand about $\boldsymbol{x}^{(0)}(t)$:

$$v[\boldsymbol{x}^{(0)} + \epsilon\boldsymbol{x}^{(1)} + \epsilon^2\boldsymbol{x}^{(2)} + \ldots] = \tag{34}$$

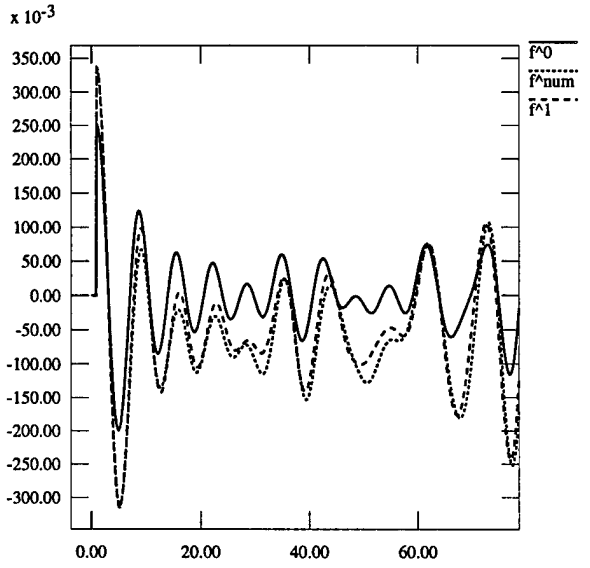

Figure 1: Comparison of attachment point forces given by the linear DtN ($f^{(0)}$), the first-order weakly nonlinear DtN ($f^{(1)}$), and the fully nonlinear numerical integration ($f^{(num)}$). The forces are plotted as functions of simulation time for the case $N = 10$, $\epsilon = 0.1$, described in the text.

$$v_0 + \left(\epsilon x^{(1)} + \epsilon^2 x^{(2)} + \ldots\right) v_0' + \tfrac{1}{2}\left(\epsilon x^{(1)} + \epsilon^2 x^{(2)} + \ldots\right)^2 v_0'' + \ldots,$$

where $v_0 \equiv v[x^{(0)}(t)]$ and $' = \partial/\partial x$. From (1), it can be seen that the $O(\epsilon^{m-1})$ terms on the r.h.s. of (34) give an equation for $x^{(m)}(t)$. We write this as

$$M\ddot{x}^{(m)} + Kx^{(m)} = \mathcal{L}^{(m-1)}(\nabla, t)v[x^{(0)}], \qquad (35)$$

where $\mathcal{L}$ is a scalar linear differential operator on $v[x]$ which depends on $\{x^{(1)} \cdot \nabla, x^{(2)} \cdot \nabla, \ldots, x^{(m-1)} \cdot \nabla\}$. To solve (35), we can use an expansion in the eigenvectors $\xi^{(n)}$ and then use Green's functions to find the time-dependent coefficients, as was done above. This yields the general solution for $x^{(m)}(t)$, given $\{x^{(0)}, x^{(1)}, \ldots, x^{(m-1)}\}$:

$$x^{(m)}(t) = -\int_{-\infty}^{t} \sum_{n=1}^{N} \frac{1}{\omega_n} \sin\omega_n(t-\tau) \times \left[M^{-1/2}\xi^{(n)}\xi^{(n)} \cdot M^{-1/2}\right] \times \left\{\mathcal{L}^{(m-1)}(\nabla, \tau)v[x^{(0)}(\tau)]\right\} d\tau. \qquad (36)$$

To obtain an explicit solution for $x^{(m)}(t)$, and hence an mth-order approximate DtN, one must calculate $\{\mathcal{L}^{(0)}, \mathcal{L}^{(1)}, \ldots, \mathcal{L}^{(m-1)}\}$. The general solution obtained above for $x^{(1)}(t)$ shows that $\mathcal{L}^{(0)} = 1$. For concreteness, we now write $\mathcal{L}^{(m)}$ for $m = 1, 2, 3$:

$$\mathcal{L}^{(1)}(\nabla, t) = x^{(1)}(t) \cdot \nabla \qquad (37)$$

$$\mathcal{L}^{(2)}(\nabla, t) = x^{(2)}(t) \cdot \nabla + \frac{1}{2}\left(x^{(1)}(t) \cdot \nabla\right)^2 \qquad (38)$$

$$\mathcal{L}^{(3)}(\nabla, t) = x^{(3)}(t) \cdot \nabla + \left(x^{(1)}(t) \cdot \nabla\right) \times \left(x^{(2)}(t) \cdot \nabla\right) + \frac{1}{6}\left(x^{(1)}(t) \cdot \nabla\right)^3. \qquad (39)$$

A NUMERICAL EXAMPLE

To demonstrate the usefulness of our first-order DtN (15), we now compute $f_0(t)$ for a given weakly nonlinear subsystem. We will compare the result given by (15) to both the purely linear result ($\epsilon = 0$) and to the fully nonlinear result, which we obtain by direct numerical integration.

We choose the quadratic nonlinearity (16), hence the first-order DtN is given by (21)–(22) and (4). We now must select a forcing function $x_0(t)$ and the following parameters: N, $\{\omega_n, m_n : n = 1, 2, \ldots N\}$, and ϵ. Once we do this, the approximate DtN provides zeroth- and first-order results for $f_0(t)$, denoted $f_0^{(0)}(t)$ and $f_0^{(1)}(t)$. To obtain the fully nonlinear solution numerically, we integrate the equations

$$\ddot{z}_n(t) + \omega_n^2 z_n(t) + \epsilon\omega_n^2\sqrt{m_n}\sum_{l=1}^{N} z_l^2(t) = -\omega_n^2\sqrt{m_n}x_0(t) \qquad (40)$$

where $n = 1, 2, \ldots N$, and thus obtain

$$f_0(t) \simeq f_0^{(num)}(t) = k_0 x_0(t) + \sum_{l=1}^{N} \omega_l^2\sqrt{m_l}z_l(t). \qquad (41)$$

We note the fact that $k_0 = \sum_{n=1}^{N} m_n\omega_n^2$.

For this example, we let $N = 10$ and $\epsilon = 0.1$. We chose a realization characterized by modal masses $m_n = 0.1(1 + r_n)$, $n = 1, 2, \ldots, 10$. Similarly, we chose nominally evenly spaced frequencies between 0 and 1: $\omega_n = 0.1\,n(1 + r_n')$, $n = 1, 2, \ldots, 10$. Here, r_n and r_n' are random numbers drawn from a uniform distribution between -0.125 and 0.125. The results, obtained using the forcing function $x_0(t) = H(t-1)$, where $H(t)$ is the Heaviside step function, are shown in Fig.1. Comparing $f^{(0)}(t)$ and $f^{(num)}(t)$, it can be seen that a small amount of nonlinearity significantly changes the response of the system. However, $f^{(1)}(t)$, given by our first-order DtN, captures a large part of the nonlinear behavior, especially at

short times. In particular, it accurately predicts the first large positive and negative peaks in the force at the attachment point. Even for larger values of ϵ, our first-order DtN has been found to give short-time results which compare favorably with the fully nonlinear case. Thus we have demonstrated the applicability of the DtN concept to structures which exhibit nonlinearity. We note that for the special classes of nonlinearities treated above, the substructure is entirely described by the function $m(\omega)$.

ACKNOWLEDGMENTS

The authors gratefully acknowledge the financial support of the Office of Naval Research.

REFERENCES

Barbone, Paul E., 1995, "Equipment representations for shock calculations: time domain Dirichlet to Neumann maps," In *Proceedings of the ASME Symposium on Acoustics of Submerged Structures and Transduction Systems*, ASME Press, New York, September 17–21, 1995.

Cherukuri, A., 1996, "Time domain Dirichlet to Neumann maps for representing complex dynamical subsystems," *M.Sc. thesis*, Boston University Department of Aerospace & Mechanical Engineering, 1996.

Cherukuri, A. and Barbone, Paul E., 1996, "High modal density approximations for equipment in the time domain," *Boston University Department of Aerospace & Mechanical Engineering Report*, No. AM-95-012, July, 1996.

Nayfeh, A.H., 1981, *Introduction to Perturbation Techniques*, John Wiley & Sons.

O'Hara, G.J. and Cunniff P.F., 1963, "Elements of normal mode theory," *Naval Research Laboratory Report*, 6002.

Pierce, A.D., 1995, "Resonant-frequency distribution of internal mass inferred from mechanical impedance matrices, with application to fuzzy structure theory," In *Proceedings of the ASME Symposium on Acoustics of Submerged Structures and Transduction Systems*, ASME Press, New York, September 17–21, 1995.

Pierce, A.D., Sparrow, V.W., and Russel D.A., 1993, "Fundamental structural-acoustic idealizations for structures with fuzzy internals," *ASME Transactions*, Paper No. 93-WA/NCA-17 (ASME Winter Annual Meeting, New Orleans), November 1993.

C.5 Time Domain Dirichlet to Neumann Maps for Representing Complex Dynamical Subsystems

Aravind Cherukuri and Paul E. Barbone, "Time Domain Dirichlet to Neumann Maps for Representing Complex Dynamical Subsystems," BU Dept. Aerospace & Mechanical Engineering Technical Report No. AM-96-018, 1996.

TIME DOMAIN DIRICHLET TO NEUMANN MAPS FOR REPRESENTING COMPLEX DYNAMICAL SUBSYSTEMS

Aravind Cherukuri
Paul E. Barbone

Technical Report No. AM-96-018

May 1996

Acknowledgments

The author would like to thank Paul E. Barbone for his guidance on this work. The author would also like to thank Allan D. Pierce, Isaac Harari, Dan Givoli, Daniel Goldman, Raymond Nagem, Josh Montgomery, Brian Rush and Keerthi Sadananda for many helpful discussions and ideas. This work was supported by the Office of Naval Research.

TIME DOMAIN DIRICHLET TO NEUMANN MAPS FOR REPRESENTING COMPLEX DYNAMICAL SUBSYSTEMS

ARAVIND CHERUKURI

Boston University, College of Engineering, 1996

Major Professor: Paul E. Barbone Assistant Professor of: Mechanical Engineering

Abstract

The presence of complex subsystems can dramatically affect the dynamics of the main structure to which they are attached. Exactly modeling these subsystems, however, is often impossible. Here we propose replacing the substructure (say a piece of equipment) in a simulation by an equivalent set of forces which react back on the main structure. These forces are given as time convolutions of the displacements at the equipment attachment points. The convolution integral, which represents a time domain DtN (Dirichlet-to-Neumann) map, is approximated in the high modal density limit with determined error bounds. Bounding the error serves to determine those properties of the dynamical subsystem that must be accurately reproduced by approximate models. We propose a hierarchy of equipment approximations based on this error analysis. We then analyze a special type of subsystem that interacts with the outside world through a single degree of freedom. We propose implementation schemes of approximate DtN maps for such subsystems based on the natural frequency scales of the subsystem and its known resonant frequencies. Finally our approximate DtN's are validated numerically in finite element simulations.

Contents

Chapter 1

Introduction

Analysis of problems involving simulations of complex dynamical subsystems often pose difficulties. Exact representations of complex dynamical subsystems are hard to formulate for two main reasons. First, exact representations are computationally expensive and require a large amount of man power to generate. Second, it is often impossible to determine all the relevant properties and natural modes of vibration of a complex dynamical subsystem.

Here we address two important goals that make simulation of complex dynamical subsystems possible. These are:

- To find computationally efficient representations of complex dynamical subsystems.
- To determine the relevant information for accurately representing a complex subsystem.

We formulate accurate yet computationally efficient representations for general dynamical subsystems by addressing these issues.

Approximate representations of dynamical subsystems (equipment) have two important advantages over exact models or representations. First, the approximate representations can provide sufficient accuracy while reducing computational costs. Second, approximate representations require relatively little effort and information to formulate.

Dynamical simulations of field problems defined on a large or infinite domain can often be simplified by replacing a portion of the domain by a Dirichlet to Neumann map [4]. In this thesis we utilize the concept of a Dirichlet to Neumann map to represent a complex dynamical subsystem. Thus we propose representing a complex dynamical subsystem in a simulation by an equivalent set of forces acting through the attachment degrees of freedom. The set of forces is given by a DtN map that may be expressed as:

$$\mathbf{f}(t) = \tilde{\mathbf{F}}(\boldsymbol{\xi}). \tag{1.1}$$

Here $\tilde{\mathbf{F}}$ is the Dirichlet to Neumann map. It takes the time history of displacements of the attachment degrees of freedom, $\boldsymbol{\xi}$, to the current forces $\mathbf{f}(t)$. In the context of this problem Dirichlet data refers to displacements and Neumann data refers to forces. Once the DtN map characterizing a given subsystem is known, its effect on the main structure is completely determined. Thus, we can replace the subsystem by its DtN map in a dynamical simulation.

In this setting, the DtN map is related to the time domain impedance operator of the subsystem. The idea of breaking a structure up into smaller components and analyzing each component separately is, of course, central in all substructuring approaches ([9], [10] and [11]). In existing substructuring strategies, some form of a truncated modal sum is used to represent each subsystem (c.f. Craig and Bampton (1968) [10] and papers referencing them). One exception is that of Hale and Meirovitch (1980) [11] who consider any admissible functions within a variational method to represent a subsystem.

Here we formulate an approximate DtN map for a general dynamic subsystem by replacing the modal sum with a modal integral. We determine the information that is necessary to formulate an approximate DtN map. Further, we compute the error made in approximating the exact DtN map of a general dynamic subsystem. We then bound the error in the approximation by imposing conditions on the choice of parameters used to represent the subsystem. Finally we show implementation methods for our approximate DtN maps and validate them in numerical simulations.

In chapter 2 we formulate the problem that allows us to construct the exact time domain Dirichlet to Neumann map for a general dynamical subsystem. We develop and introduce the notation used to describe a general dynamical subsystem. Following the work of Pierce [2], we impose conditions of translational invariance on the quadratic potential energy function (of

generalized displacements) of the subsystem. In addition we apply the condition of rotational invariance of the potential energy quadratic for small displacements. Thus we derive important physical properties of the subsystem that manifest themselves in the structure of the symmetric positive semidefinite stiffness matrix $\mathbf{K}$ of the dynamical subsystem.

In chapter 3 we solve the equations of motion of the subsystem to obtain the generalized displacements of the internal degrees of freedom in terms of the generalized displacements of the attachment degrees of freedom. We write this solution as a decomposition into normal modes. We then use this solution to construct the exact DtN map of the dynamical subsystem. We simplify the exact DtN map of the subsystem by introducing a generalization of the modal mass tensor (Cunniff and O'Hara [3], Pierce [2]). We also introduce a *modal stiffness* tensor. We derive properties of the modal mass and the modal stiffness of the subsystem using the results of translational invariance from chapter 2.

In chapter 4 we use the properties of the modal mass and the modal stiffness of the dynamical subsystem to develop approximate DtN maps for the subsystem. We recognize the system parameters that are needed to approximate a dynamical subsystem. We derive strict error bounds for the approximate DtN's both in the presence and in the absence of small subsystem damping. We emphasize that these are strict error bounds, rather than asymptotic error estimates. We show that the error is small when the number of modes in the subsystem is high. We then discuss three different levels at which one may approximate the modal mass of a subsystem and the physical implications of these approximations.

In chapter 5 we discuss methods of efficiently implementing our approximate DtN's in numerical simulations. For this purpose we consider the special case of a single attachment point subsystem whose components move unidirectionally. We derive the exact DtN map of this sub-

system based on the results of the previous chapters. In this discussion we use the approximate DtN for this subsystem proposed by Barbone [5]. We address the problem of implementing these DtN's in numerical simulations. We develop implementation methods for these DtN's for the cases when the natural frequencies of the subsystem are small compared to the time scales of the excitations and when a few resonant modes of the subsystem are known.

In chapter 6 present a numerical simulation of a problem utilizing the results of the previous chapters. We discuss the problem and the method by which the problem is modeled. We show the time marching scheme used for analyzing the dynamics of the super structure and the subsystem in the numerical code. Finally we provide two sets of results to validate the DtN's developed in the previous chapters. One set of results shows the effects of the number of internal degrees of freedom (modes) of the subsystem on the errors in the approximations. The other set of results show the dependence of the error in approximating the exact DtN on the amount of subsystem damping.

Chapter 2

Problem Formulation

In this chapter we formulate and discuss the equations of motion representing the dynamics of a subsystem. We derive the equations of motion using Lagrange's Principle [1]. We discuss the structure of the stiffness matrix that shows up in the Lagrange's equations of motions: The quadratic potential energy function of the generalized displacements must satisfy translational and rotational invariance. We shall solve the resulting equations of motion in the subsequent chapters.

2.1 Equations of Motion

We consider a dynamical subsystem that has $N+M$ degrees of freedom and a quadratic potential energy function, $V(\xi_1, \xi_2, ..., \xi_{N+M})$, of $N + M$ generalized coordinates, $\xi_i; i = 1, ..., N + M$. These generalized coordinates may be thought of as being the generalized displacements of the components of the subsystem from their equilibrium positions. This subsystem interacts with the outside world through the first N of the $N + M$ generalized coordinates $\xi_j; j = 1, ..., N$. We denote the generalized forces that are applied to the system through the first N generalized coordinates by f_k where $k = 1, 2, ...N$.

We will now derive a system of equations to describe the dynamics of the subsystem by constructing the Lagrangian function of the subsystem and setting its variation equal to zero. The Lagrangian function is $\mathcal{L} = \mathcal{T} - \mathcal{V}$. Here T is the kinetic energy and is a function of the generalized velocities, $\dot{\xi}_j$ while V, the potential energy, is a function of ξ_j.

The kinetic energy $T\left(\dot{\xi}\right)$ may be written as:

$$T(\dot{\xi}) = \frac{1}{2} \sum_{i,j=1}^{N+M} \dot{\xi}_i M_{ij} \dot{\xi}_j. \tag{2.1}$$

The potential energy $V(\xi)$ is:

$$V(\xi) = \frac{1}{2} \sum_{i,j=1}^{N+M} \xi_i K_{ij} \xi_j. \tag{2.2}$$

Here M is the positive semidefinite mass matrix of the subsystem and K is the symmetric positive semidefinite stiffness matrix of the subsystem. Equations (2.1) and (2.2) give the Lagrangian as:

$$\mathcal{L} = T - V = \frac{1}{2} \sum_{i,j=1}^{N+M} \dot{\xi}_i M_{ij} \dot{\xi}_j - \frac{1}{2} \sum_{i,j=1}^{N+M} \xi_i K_{ij} \xi_j. \tag{2.3}$$

The equations of motion which follow from Lagrange's Principle [1] are:

$$\frac{d}{dt}\left(\frac{\partial \mathcal{L}}{\partial \dot{\xi}_j}\right) + \frac{\partial \mathcal{L}}{\partial \xi_j} = f_j. \tag{2.4}$$

We substitute equation (2.3) into equation (2.4) to get the equations of motion of the subsystem in terms of the generalized coordinates-ordinates ξ_j:

$$\sum_{j=1}^{N+M} (M_{ij} \ddot{\xi}_j + K_{ij} \xi_j) = f_i. \tag{2.5}$$

We now split equation (2.5) into two parts as follows:

$$\begin{pmatrix} M_{ij} & M_{iq} \\ M_{pj} & M_{pq} \end{pmatrix} \begin{pmatrix} \ddot{\xi}_j \\ \ddot{\xi}_q \end{pmatrix} + \begin{pmatrix} K_{ij} & \kappa_{iq} \\ \kappa_{pj} & K_{pq} \end{pmatrix} \begin{pmatrix} \xi_j \\ \xi_q \end{pmatrix} = \begin{pmatrix} f_i \\ 0 \end{pmatrix} \tag{2.6}$$

Here we arrange the generalized coordinates such that the first N generalized coordinates correspond to the attachment degrees of freedom and the next M generalized coordinates correspond to the internal degrees of freedom of the subsystem. Once again we note that the system interacts with the outside world only through the attachment degrees of freedom. Henceforth we shall refer to the attachment degrees of freedom as the degrees of freedom of the attachment points. In equation (2.6) we use the following index representation:

$$\left.\begin{aligned} &i, j = 1, 2, ..., N \\ &p, q = N+1, .., N+M \end{aligned}\right\} \tag{2.7}$$

In all that follows we adopt a summation convention where repeated indices are summed through their range. Since we require different ranges to distinguish between attachment points and internal degrees of freedom we adopt the convention defined by (2.7). We now write the symmetric stiffness matrix, K, in the form:

$$\begin{pmatrix} K_{11} & \cdots & K_{1N} & \kappa_{1N+1} & \cdots & \kappa_{1N+M} \\ \vdots & \ddots & \vdots & \vdots & \ddots & \vdots \\ K_{N1} & \cdots & K_{NN} & \kappa_{NN+1} & \cdots & \kappa_{NN+M} \\ \kappa^T_{N+11} & \cdots & \kappa^T_{N+1N} & K_{N+1N+1} & \cdots & K_{N+1N+M} \\ \vdots & \ddots & \vdots & \vdots & \ddots & \vdots \\ \kappa^T_{N+M1} & \cdots & \kappa^T_{N+MN} & K_{N+MN+1} & \cdots & K_{N+MN+M} \end{pmatrix} \tag{2.8}$$

Here the K's represent the stiffness parameters between the attachment degrees of freedom or the internal degrees of freedom. The κ's and their transposes, κ^T represent the stiffness parameters between the attachment degrees of freedom and the internal degrees of freedom.

We now drop the summation symbol and write equation (2.6) as follows:

$$M_{ij}\ddot{\xi}_j + M_{ip}\ddot{\xi}_p + K_{ij}\xi_j + \kappa_{ip}\xi_p = f_i \tag{2.9}$$

and

$$M_{pq}\ddot{\xi}_q + K_{pq}\xi_q = -M_{pi}\ddot{\xi}_i - \kappa_{pi}\xi_i. \tag{2.10}$$

Equations (2.9) and (2.10) are the equations of motion of the subsystem. We can now solve (2.10) for the unknown generalized coordinates, ξ_p and use this in (2.9) to derive a relationship between the applied forces and the first N generalized displacements. The solution to these equations is presented in the following chapters.

2.2 Translational and Rotational Invariance

Here we examine the structure of the stiffness matrix more closely. The properties of the stiffness matrix are integral to the behavior of the dynamical system. We determine the properties of the stiffness matrix, K_{ij}, by enforcing translational and rotational invariance on the quadratic potential energy function of the subsystem following [2].

2.2.1 Translational Invariance

The potential energy of the subsystem given by equation (2.2) should be invariant for an arbitrary translation of the entire subsystem. This is so because the potential energy of the subsystem as defined by the quadratic in equation (2.2) is derived from relative generalized displacements of the components of the subsystem from one another. We now denote a unit generalized displacement of the first N generalized coordinates, ξ_i in the 'a' direction by the vector $\zeta_i a$ and a unit generalized displacement of the next M generalized coordinates, ξ_p in the 'a' direction by the vector $\zeta_p a$. For example if ξ_i represent displacements in Cartesian coordinates, then ζ would be a $(M+N)\times(3)$ matrix, ζ_i^α and 'a' would be a vector in R^3. We now use the principle of translational invariance of the potential energy function to write:

$$V(\xi_i, \xi_p) = V\left(\xi_i + \zeta_i^\alpha a^\alpha, \xi_p + \zeta_p^\alpha a^\alpha\right). \tag{2.11}$$

We write the left hand side and the right hand side of equation (2.11) using the form of K_{ij} from (2.8) and equation (2.2) as:

$$V(\xi_i, \xi_p) = \frac{1}{2}\begin{pmatrix} \xi_i & \xi_p \end{pmatrix}\begin{pmatrix} K_{ij} & \kappa_{iq} \\ \kappa_{pj} & K_{pq} \end{pmatrix}\begin{pmatrix} \xi_j \\ \xi_q \end{pmatrix}. \tag{2.12}$$

Similarly the right hand side of equation (2.11) is written as:

$$V\left(\xi_i+\zeta_i^\alpha a^\alpha, \xi_p+\zeta_p^\alpha a^\alpha\right) = \frac{1}{2}\begin{pmatrix} \xi_i+\zeta_i^\alpha a^\alpha & \xi_p+\zeta_p^\alpha a^\alpha \end{pmatrix}\begin{pmatrix} K_{ij} & \kappa_{iq} \\ \kappa_{pj} & K_{pq} \end{pmatrix}\begin{pmatrix} \xi_j+\zeta_j^\alpha a^\alpha \\ \xi_q+\zeta_q^\alpha a^\alpha \end{pmatrix}. \tag{2.13}$$

The ranges of the indices in equation (2.12) and (2.13) are given by (2.7) and $\alpha = 1,2,3$. We now expand equation (2.12) and write:

$$\begin{aligned} V(\xi_i,\xi_p) &= \frac{1}{2}\begin{pmatrix} \xi_i K_{ij}+\xi_p\kappa_{pj} & \xi_i\kappa_{iq}+\xi_p K_{pq} \end{pmatrix}\begin{pmatrix} \xi_j \\ \xi_q \end{pmatrix} \\ &= \frac{1}{2}\left(\xi_i K_{ij}\xi_j+\xi_p\kappa_{pj}\xi_j+\xi_i\kappa_{iq}\xi_q+\xi_p K_{pq}\xi_q\right). \end{aligned} \tag{2.14}$$

Similarly we expand equation (2.13) to obtain:

$$\begin{aligned} &V\left(\xi_i+\zeta_i^\alpha a^\alpha, \xi_p+\zeta_p^\alpha a^\alpha\right) = \\ &\quad \frac{1}{2}\begin{pmatrix} \left(\xi_i+\zeta_i^\alpha a^\alpha\right)K_{ij}+\left(\xi_p+\zeta_p^\alpha a^\alpha\right)\kappa_{pj} & \left(\xi_i+\zeta_i^\alpha a^\alpha\right)\kappa_{iq}+\left(\xi_p+\zeta_p^\alpha a^\alpha\right)K_{pq} \end{pmatrix} \\ &\quad \begin{pmatrix} \xi_j+\zeta_j^\alpha a^\alpha \\ \xi_q+\zeta_q^\alpha a^\alpha \end{pmatrix} \\ &= \frac{1}{2}\Big[\left(\xi_i+\zeta_i^\alpha a^\alpha\right)K_{ij}\left(\xi_j+\zeta_j^\alpha a^\alpha\right)+\left(\xi_p+\zeta_p^\alpha a^\alpha\right)\kappa_{pj}\left(\xi_j+\zeta_j^\alpha a^\alpha\right)+ \\ &\quad \left(\xi_i+\zeta_i^\alpha a^\alpha\right)\kappa_{iq}\left(\xi_q+\zeta_q^\alpha a^\alpha\right)+\left(\xi_p+\zeta_p^\alpha a^\alpha\right)K_{pq}\left(\xi_q+\zeta_q^\alpha a^\alpha\right)\Big]. \end{aligned} \tag{2.15}$$

From equations (2.11, 2.14 and 2.15) we have:

$$\begin{aligned} &\xi_i K_{ij}\zeta_j^\alpha a^\alpha+\zeta_i^\alpha a^\alpha K_{ij}\xi_j+\zeta_i^\alpha a^\alpha K_{ij}\zeta_j^\alpha a^\alpha+ \\ &\xi_p\kappa_{pj}\zeta_j^\alpha a^\alpha+\zeta_p^\alpha a^\alpha\kappa_{pj}\xi_j+\zeta_p^\alpha a^\alpha\kappa_{pj}\zeta_j^\alpha a^\alpha+\xi_i\kappa_{iq}\zeta_q^\alpha a^\alpha+\zeta_i^\alpha a^\alpha\kappa_{iq}\xi_q+\zeta_i^\alpha a^\alpha\kappa_{iq}\zeta_q^\alpha a^\alpha+ \\ &\xi_p K_{pq}\zeta_q^\alpha a^\alpha+\zeta_p^\alpha a^\alpha K_{pq}\xi_q+\zeta_p^\alpha a^\alpha K_{p}q\zeta_q^\alpha a^\alpha=0. \end{aligned} \tag{2.16}$$

The principle of translational invariance holds for arbitrary translations, 'a'. Thus equation (2.16) splits into two parts, one with terms linear in 'a' and the other with terms quadratic in 'a':

$$\zeta_i^\alpha a^\alpha K_{ij}\zeta_j^\alpha a^\alpha + \zeta_p^\alpha a^\alpha \kappa_{pj}\zeta_j^\alpha a^\alpha + \zeta_i^\alpha a^\alpha \kappa_{iq}\zeta_q^\alpha a^\alpha + \zeta_p^\alpha a^\alpha K_{pq}\zeta_q^\alpha a^\alpha = 0 \tag{2.17}$$

$$\begin{aligned} &\xi_i K_{ij}\zeta_j^\alpha a^\alpha + \zeta_i^\alpha a^\alpha K_{ij}\xi_j + \xi_p \kappa_{pj}\zeta_j^\alpha a^\alpha + \zeta_p^\alpha a^\alpha \kappa_{pj}\xi_j \quad + \\ &\xi_i \kappa_{iq}\zeta_q^\alpha a^\alpha + \zeta_i^\alpha a^\alpha \kappa_{iq}\xi_q + \xi_p K_{pq}\zeta_q^\alpha a^\alpha + \zeta_p^\alpha a^\alpha K_{pq}\xi_q \quad = \quad 0. \end{aligned} \tag{2.18}$$

We note that equation (2.18) must hold for any displacement of the subsystem, (ξ_i, ξ_p). Thus equation (2.18) also splits into two parts:

$$\xi_i K_{ij}\zeta_j^\alpha a^\alpha + \zeta_i^\alpha a^\alpha K_{ij}\xi_j + \zeta_p^\alpha a^\alpha \kappa_{pj}\xi_j + \xi_i \kappa_{iq}\zeta_q^\alpha a^\alpha = 0 \tag{2.19}$$

$$\xi_p \kappa_{pj}\zeta_j^\alpha a^\alpha + \zeta_i^\alpha a^\alpha \kappa_{iq}\xi_q + \xi_p K_{pq}\zeta_q^\alpha a^\alpha + \zeta_p^\alpha a^\alpha K_{pq}\xi_q = 0. \tag{2.20}$$

We now use the fact that equation (2.19) should hold for each element of vector ξ_i because it holds for arbitrary ξ_i. We therefore can factor out ξ_i and ξ_j from equation (2.19) and write:

$$K_{ij}\zeta_j^\alpha a^\alpha + \zeta_j^\alpha a^\alpha K_{ji} + \zeta_p^\alpha a^\alpha \kappa_{pi} + \kappa_{iq}\zeta_q^\alpha a^\alpha = 0. \tag{2.21}$$

Similarly from equation (2.20) we get:

$$\kappa_{pj}\zeta_j^\alpha a^\alpha + \zeta_i^\alpha a^\alpha \kappa_{ip} + K_{pq}\zeta_q^\alpha a^\alpha + \zeta_q^\alpha a^\alpha K_{qp} = 0. \tag{2.22}$$

The stiffness matrix, $\boldsymbol{K}$, is symmetric. Therefore in equation (2.21) $K_{ij}\zeta_j^\alpha a^\alpha = \zeta_j^\alpha a^\alpha K_{ji}$ and $\zeta_p^\alpha a^\alpha \kappa_{pj} = \kappa_{jq}\zeta_q^\alpha a^\alpha$. We use this in equation (2.21) to get:

$$\left.\begin{aligned} K_{ij}\zeta_j^\alpha a^\alpha &= -\zeta_p^\alpha a^\alpha \kappa_{pi}^T \\ K_{ij}\zeta_j^\alpha a^\alpha &= -\kappa_{iq}\zeta_q^\alpha a^\alpha \\ \zeta_i^\alpha a^\alpha K_{ij} &= -\zeta_p^\alpha a^\alpha \kappa_{pj}^T \\ \zeta_i^\alpha a^\alpha K_{ij} &= -\kappa_{jq}\zeta_q^\alpha a^\alpha \end{aligned}\right\} \tag{2.23}$$

Similarly from equation (2.22) we get:

$$\left.\begin{aligned} K_{pq}\zeta_q^\alpha a^\alpha &= -\zeta_i^\alpha a^\alpha \kappa_{ip} \\ K_{pq}\zeta_q^\alpha a^\alpha &= -\kappa_{pj}^T \zeta_j^\alpha a^\alpha \\ \zeta_p^\alpha a^\alpha K_{pq} &= -\zeta_i^\alpha a^\alpha \kappa_{iq} \\ \zeta_p^\alpha a^\alpha K_{pq} &= -\kappa_{qj}^T \zeta_j^\alpha a^\alpha \end{aligned}\right\} \tag{2.24}$$

2.2.2 Rotational Invariance

In this discussion we consider the special case of a subsystem comprised of point masses attached to each other by linear spring elements. The generalized coordinates of such a subsystem can be the displacements of the point masses from their equilibrium positions. The potential energy of the subsystem as given by equation (2.2) is invariant for small rotations of the subsystem. For this subsystem we may represent a small rigid body rotation by a $(N+M)\times(N+M)$ transformation matrix, $\boldsymbol{Q}$, where $\boldsymbol{Q} = \boldsymbol{I} + \boldsymbol{\Omega}$. Here $\boldsymbol{I}$ is the identity matrix and $\boldsymbol{\Omega}$ is an antisymmetric matrix. We now use the principle of rotational invariance of the potential energy to derive further structure to the stiffness matrix.

We denote the position vector to the i^{th} attachment point by R_i and the position vector to the p^{th} point mass of the subsystem by R_p. We now subject the subsystem to a small rotation defined by the transformation matrix $\boldsymbol{Q}$. This rotation transforms the set of generalized coordinates of the subsystem as follows:

$$\hat{\xi}_i = Q_{ij}\left(R_j + \xi_j\right) - R_i \tag{2.25}$$

$$\hat{\xi}_p = Q_{pq}\left(R_q + \xi_q\right) - R_p. \tag{2.26}$$

Here $\hat{\xi}_i$ and $\hat{\xi}_p$ are the displacements of the attachment points and the point masses after the

rotation. We use the principle of rotational invariance to write:

$$V(\xi_i, \xi_p) = V\left(\hat{\xi}_i, \hat{\xi}_p\right). \tag{2.27}$$

Substituting equations (2.25) and (2.26) into (2.2) we get:

$$\begin{aligned} V\left(\hat{\xi}_i, \hat{\xi}_p\right) &= \frac{1}{2}\begin{pmatrix} (R_i + \xi_i) Q_{ij} - R_j & (R_p + \xi_p) Q_{pq} - R_q \end{pmatrix} \\ &\quad \begin{pmatrix} K_{jk} & \kappa_{jr} \\ \kappa_{qk}^T & K_{qr} \end{pmatrix} \begin{pmatrix} Q_{kl}(R_l + \xi_l) - R_k \\ Q_{rs}(R_s + \xi_s) - R_r \end{pmatrix}. \end{aligned} \tag{2.28}$$

In all that follows the transpose notation, κ^T, is implicit when the first index of κ is $p, q, r, \ldots$.

We note that for small rotations, $\boldsymbol{Q} = \boldsymbol{I} + \boldsymbol{\Omega}$, and small displacements, ξ_i and ξ_p, we may drop the quadratic terms, $\boldsymbol{\Omega\xi}$, in equations (2.25) through (2.28), therefore:

$$\hat{\xi}_i = \xi_i + \Omega_{ij} R_j \tag{2.29}$$

and

$$\hat{\xi}_p = \xi_p + \Omega_{pq} R_q. \tag{2.30}$$

We use equations (2.29) and (2.30) in equation (2.28) and expand to write:

$$\begin{aligned} V\left(\hat{\xi}_i, \hat{\xi}_p\right) &= \frac{1}{2}\Big[(\xi_j + R_i\Omega_{ij}) K_{jk} (\xi_k + \Omega_{kl} R_l) + (\xi_q + R_p\Omega_{pq}) \kappa_{qk} (\xi_k + \Omega_{kl} R_l) + \\ &\quad (\xi_j + R_i\Omega_{ij}) \kappa_{jr} (\xi_r + \Omega_{rs} R_s) + (\xi_q + R_p\Omega_{pq}) K_{qr} (\xi_r + \Omega_{rs} R_s)\Big]. \end{aligned} \tag{2.31}$$

We can now use equations (2.31) and (2.14) in (2.27) to write:

$$\begin{aligned} &\xi_j K_{jk}\Omega_{kl} R_l + R_i\Omega_{ij} K_{jk}\xi_k + R_i\Omega_{ij} K_{jk}\Omega_{kl} R_l + \xi_q\kappa_{qk}\Omega_{kl} R_l + R_p\Omega_{pq}\kappa_{qk}\xi_k + \\ &\quad R_p\Omega_{pq}\kappa_{qk}\Omega_{kl} R_l + \xi_j\kappa_{jr}\Omega_{rs} R_s + R_i\Omega_{ij}\kappa_{jr}\xi_r + R_i\Omega_{ij}\kappa_{jr}\Omega_{rs} R_s + \xi_q K_{qr}\Omega_{rs} R_s + \\ &\quad R_p\Omega_{pq} K_{qr}\xi_r + R_p\Omega_{pq} K_{qr}\Omega_{rs} R_s = 0. \end{aligned} \tag{2.32}$$

Equation (2.32) holds for arbitrary rotations, $\boldsymbol{\Omega}$. We use this to split equation (2.32) into two, one with terms linear in $\boldsymbol{\Omega}$ and the other with terms quadratic in $\boldsymbol{\Omega}$.

$$R_i\Omega_{ij}K_{jk}\Omega_{kl}R_l + R_p\Omega_{pq}\kappa_{qk}\Omega_{kl}R_l + R_i\Omega_{ij}\kappa_{jr}\Omega_{rs}R_s + R_p\Omega_{pq}K_{qr}\Omega_{rs}R_s = 0 \tag{2.33}$$

and similarly:

$$\begin{aligned} &\xi_j K_{jk}\Omega_{kl}R_l + R_i\Omega_{ij}K_{jk}\xi_k + \xi_q\kappa_{qk}\Omega_{kl}R_l + R_p\Omega_{pq}\kappa_{qk}\xi_k \quad + \\ &\xi_j\kappa_{jr}\Omega_{rs}R_s + R_i\Omega_{ij}\kappa_{jr}\xi_r + \xi_q K_{qr}\Omega_{rs}R_s + R_p\Omega_{pq}K_{qr}\xi_r \quad = \quad 0. \end{aligned} \tag{2.34}$$

We note that the principle of rotational invariance holds for arbitrary set of generalized displacements, (ξ_i, ξ_p). We use this fact to write:

$$K_{jk}\Omega_{kl}R_l + R_l\Omega_{lk}K_{kj} + R_p\Omega_{pq}\kappa_{qj} + \kappa_{jq}\Omega_{qp}R_q = 0 \tag{2.35}$$

and:

$$\kappa_{qk}\Omega_{kl}R_l + R_l\Omega_{lk}\kappa_{kq} + K_{qr}\Omega_{rs}R_s + R_s\Omega_{sr}K_{rq} = 0. \tag{2.36}$$

Since $\boldsymbol{\Omega}$ is antisymmetric we may use $\Omega_{ij} = -\Omega_{ji}$ in equations (2.35) and (2.36). Thus, we conclude that K_{ij} is symmetric, i.e. $K_{ij} = K_{ji}$.

Equation (2.33) however, may be written in the form of a matrix equation in order to exhibit another interesting property of the stiffness matrix, $\boldsymbol{K}$:

$$\begin{pmatrix} R_i & R_p \end{pmatrix} \begin{pmatrix} \Omega_{ij} & \Omega_{iq} \\ \Omega^T_{pj} & \Omega_{pq} \end{pmatrix} \begin{pmatrix} K_{jk} & \kappa_{jr} \\ \kappa^T_{qk} & K_{qr} \end{pmatrix} \begin{pmatrix} \Omega_{kl} & \Omega_{ks} \\ \Omega^T_{rl} & \Omega_{rs} \end{pmatrix} \begin{pmatrix} R_l \\ R_s \end{pmatrix} = 0. \tag{2.37}$$

We write equation (2.37) in symbolic form as $\boldsymbol{R\Omega K\Omega R^T} = 0$.

Chapter 3

The Exact Dirichlet to Neumann Map

In section 3.1 of this chapter we derive the solution of the equations of motion, (2.9) and (2.10). We write the solution in the form of a convolution integral using a Green's Function. In section 3.2 we use this solution to formulate a Dirichlet to Neumann Map or DtN [4]. The DtN map can be written as:

$$f_i = \tilde{\mathbf{F}}(\xi_i). \tag{3.1}$$

Here $\tilde{\mathbf{F}}$ is the Dirichlet to Neumann map. The forces f_i are the Neumann data and the displacements of the attachment points ξ_i are the Dirichlet data. Thus the DtN describes the forces exerted by the subsystem on its environment in terms of the displacements of its attachment points.

In section 3.3 we present a representation for the total mass of the subsystem and discuss the structure of the mass matrix. In section 3.4 we define the modal mass tensor in a manner similar to Pierce [3]. The modal mass tensors form the kernel of the convolution integral in the exact DtN map. We also derive some the properties of the modal mass tensors. In section 3.5 we define another quantity that we call the modal stiffness tensor and derive its properties. In the last section, we provide alternative representations of the Exact DtN map in terms of the modal mass tensors and the modal stiffness tensors.

3.1 Green's Function and Exact Solution

We shall now formulate the exact solution of equations (2.9 and 2.10) in terms two Green's functions, $g^{(\kappa)}$ and $g^{(M)}$. We introduce Green's function[1] $g_{qi}^{(\kappa)}(t-\tau)$ which satisfies the equation:

$$M_{pq}\ddot{g}_{qi}^{(\kappa)}(t-\tau) + K_{pq}g_{qi}^{(\kappa)}(t-\tau) = -\kappa_{pi}\delta(t-\tau) \tag{3.2}$$

[1]Here we use the same index convention as described in equation (2.7).

and the Green's function $g_{qi}^{(M)}(t-\tau)$ which satisfies the equation:

$$M_{pq}\ddot{g}_{qi}^{(M)}(t-\tau) + K_{pq}g_{qi}^{(M)}(t-\tau) = -M_{pi}\delta(t-\tau). \tag{3.3}$$

Here the causality condition can be written as:

$$g_{qi}^{(\kappa)}(t-\tau) = g_{qi}^{(M)}(t-\tau) = 0, \qquad \forall \quad t < \tau. \tag{3.4}$$

We now use equations (3.2), (3.3) and (3.4) in equation (2.10) to write the full solution:

$$\xi_p = \int_{-\infty}^{t} \left[\left(g_{pi}^{(\kappa)}(t-\tau)\xi_i(\tau)\right) + \left(g_{pi}^{(M)}(t-\tau)\ddot{\xi}_i(\tau)\right)\right] d\tau. \tag{3.5}$$

The structure of equations (3.2) and (3.3) are similar. We therefore need to solve for only one of the Green's functions. Henceforth we refer to this Green's function as $g_{qi}^{(A)}(t-\tau)$, while noting:

$$M_{pq}\ddot{g}_{qi}^{(A)}(t-\tau) + K_{pq}g_{qi}^{(A)}(t-\tau) = -A_{pi}\delta(t-\tau) \tag{3.6}$$

and

$$g_{qi}^{(A)}(t-\tau) = 0, \qquad \forall \quad t < \tau. \tag{3.7}$$

Physically the Green's function g_{pi} may be thought of as the generalized displacement of the p^{th} internal degree of freedom due to the i^{th} component of the generalized force.

We now introduce the change of variables

$$g_{qi}^{(A)}(t) = M_{qp}^{-1/2}y_{pi}(t). \tag{3.8}$$

Here we need not compute $M^{-1/2}$ explicitly. We only need to note that $M^{1/2}$ is the unique positive definite matrix that satisfies $M^{1/2}M^{1/2} = M$. Substituting equation (3.8) into (3.6) yields:

$$M_{pq}M_{qr}^{-1/2}\ddot{y}_{ri}(t) + K_{pq}M_{qr}^{-1/2}y_{ri}(t) = -A_{pi}\delta(t). \tag{3.9}$$

Left multiplying the free index of equation (3.9) with $M_{sp}^{-1/2}$ and noting that $M_{sp}^{-1/2} M_{pq} M_{qr}^{-1/2} = \delta_{sr}$, yields:

$$\ddot{y}_{si}(t) + \left(M^{-1/2} K M^{-1/2}\right)_{sr} y_{ri} = -M_{sp}^{-1/2} A_{pi} \delta(t). \tag{3.10}$$

In equation (3.10) we can see that $M_{sp}^{-1/2} K_{pq} M_{qr}^{-1/2}$ is a symmetric $M \times M$ matrix because $\mathbf{K}$ is symmetric. Further, $M_{sp}^{-1/2} K_{pq} M_{qr}^{-1/2}$ is positive definite; i.e., for any vector $\mathbf{x} \in R^{\mathrm{M}}$ we have:

$$\mathbf{x}^T \left(\mathbf{M}^{-1/2} \mathbf{K} \mathbf{M}^{-1/2}\right) \mathbf{x} > 0. \tag{3.11}$$

Since $\left(M_{sp}^{-1/2} K_{pq} M_{qr}^{-1/2}\right)$ is symmetric and positive definite, it has M positive eigenvalues, $(\omega^{(P)})^2$, $P = 1, ..., M$, and M distinct orthogonal eigenvectors, $\gamma^{(P)}$, $P = 1, ..., M$ (The range of indices are as defined in equation (2.7). Henceforth there is no implied summation on superscripted indices unless explicitly specified). We can use the properties of $\left(M_{sp}^{-1/2} K_{pq} M_{qr}^{-1/2}\right)$ to write y_{si} as a decomposition of normal modes:

$$y_{si}(t) = \sum_{P=1}^{M} (\gamma_s)^{(P)} z_i^{(P)}(t). \tag{3.12}$$

Using equation (3.12) in equation (3.10) yields:

$$\sum_{P=1}^{M} (\gamma_s)^{(P)} \ddot{z}_i^{(P)}(t) + \left(M^{-1/2} K M^{-1/2}\right)_{sr} \sum_{P=1}^{M} (\gamma_r)^{(P)} z_i^{(P)}(t) = -M_{sp}^{-1/2} A_{pi} \delta(t). \tag{3.13}$$

We now multiply equation (3.13) by $(\gamma_s)^{(Q)}$ and use the orthonormal property of the eigenvectors $\gamma^{(R)}$ to obtain:

$$\ddot{z}_i^{(Q)}(t) + (\gamma_s)^{(Q)} \left(M^{-1/2} K M^{-1/2}\right)_{sr} \sum_{Q=1}^{M} (\gamma_r)^{(Q)} z_i^{(Q)}(t) = -(\gamma_s)^{(Q)} M_{sp}^{-1/2} A_{pi} \delta(t). \tag{3.14}$$

By the definition of eigenvectors, $(\gamma_s)^{(Q)}$ we note that:

$$\left(M^{-1/2} K M^{-1/2}\right)_{sr} (\gamma_s)^{(Q)} = \left(M^{-1/2} K M^{-1/2}\right)_{rs} (\gamma_s)^{(Q)} = (\omega^2)^{(Q)} (\gamma_r)^{(Q)}. \tag{3.15}$$

Substituting equation (3.15) into equation (3.14) yields:

$$\ddot{z}_i^{(Q)}(t) + (\omega^2)^{(Q)} z_i^{(Q)}(t) = (\gamma_s)^{(Q)} \left[M_{sp}^{-1/2} A_{pi} \delta(t) \right]. \tag{3.16}$$

Equation (3.16) represents M equations for M time dependent vectors, $z_i(t)$. Further, causality condition (3.4) requires that $z_i^{(Q)}(t) = 0 \quad \forall \quad t < 0$. We use this to solve equation (3.16) to get:

$$z_i^{(Q)}(t) = -\frac{1}{\omega^{(Q)}} (\gamma_s)^{(Q)} \left[M_{sp}^{-1/2} A_{pi} \sin\left(\omega^{(Q)} t\right) \right]. \tag{3.17}$$

Substituting equation (3.17) into equation (3.12) yields:

$$y_{si}(t) = -\sum_{Q=1}^{M} (\gamma_s)^{(Q)} \frac{1}{\omega^{(Q)}} (\gamma_r)^{(Q)} \left[M_{rp}^{-1/2} A_{pi} \sin\left(\omega^{(Q)} t\right) \right]. \tag{3.18}$$

We obtain the Green's function, $g_{ti}^{(A)}(t)$, by using equation (3.18) in equation (3.8):

$$g_{ti}^{(A)}(t) = -M_{ts}^{-1/2} \sum_{Q=1}^{M} \frac{(\gamma_s \gamma_r)^{(Q)}}{\omega^{(Q)}} \left[M_{rp}^{-1/2} A_{pi} \sin\left(\omega^{(Q)} t\right) \right]. \tag{3.19}$$

We obtain $\mathbf{g}^{(\kappa)}(t)$ and $\mathbf{g}^{(M)}(t)$ by replacing A_{pi} in equation (3.19) with κ_{pi} and M_{pi}, respectively. Thus we obtain:

$$g_{ti}^{(\kappa)}(t) = -M_{ts}^{-1/2} \sum_{Q=1}^{M} \frac{(\gamma_s \gamma_r)^{(Q)}}{\omega^{(Q)}} \left[M_{rp}^{-1/2} \kappa_{pi} \sin\left(\omega^{(Q)} t\right) \right] \tag{3.20}$$

and

$$g_{ti}^{(M)}(t) = -M_{ts}^{-1/2} \sum_{Q=1}^{M} \frac{(\gamma_s \gamma_r)^{(Q)}}{\omega^{(Q)}} \left[M_{rp}^{-1/2} M_{pi} \sin\left(\omega^{(Q)} t\right) \right]. \tag{3.21}$$

The generalized displacements of the internal degrees of freedom are thus given by equations (3.5, 3.20 and 3.21) as:

$$\xi_p = -\int_{-\infty}^{t} M_{ts}^{-1/2} \sum_{Q=1}^{M} \frac{(\gamma_s \gamma_r)^{(Q)}}{\omega^{(Q)}} M_{rp}^{-1/2} \sin\left(\omega^{(Q)} t\right) \left\{ \kappa_{pi} \xi_i(\tau) + M_{pi} \ddot{\xi}_i(\tau) \right\} d\tau. \tag{3.22}$$

3.2 Exact DtN Map

Here we shall use the solution (3.22) in equation (2.9) to get the exact DtN map. Further we explore many alternative representations of the DtN map. Substituting equation (3.22) in equation (2.9) yields:

$$f_i = M_{ij}\ddot{\xi}_j + K_{ij}\xi_j - \left(\kappa_{ip} + M_{ip}\frac{d^2}{dt^2}\right)\int_{-\infty}^{t} M_{pq}^{-1/2}\sum_{P=1}^{M}\left[\frac{(\gamma_q\gamma_r)^{(P)}}{\omega^{(P)}}\right]M_{rs}^{-1/2}$$
$$\sin\left(\omega^{(P)}(t-\tau)\right)\left\{M_{sj}\ddot{\xi}_j(\tau) + \kappa_{sj}\xi_j(\tau)\right\}d\tau. \tag{3.23}$$

This is one form of the exact DtN map. We shall now simplify it. We denote the outer product, $\mathbf{M}^{-1/2}\boldsymbol{\gamma}\otimes\boldsymbol{\gamma}\mathbf{M}^{-1/2}$, in equation (3.23) by $\mathbf{A}$:

$$M_{pq}^{-1/2}\gamma_q^{(P)}\gamma_r^{(P)}M_{rs}^{-1/2} = A_{ps}^{(P)}. \tag{3.24}$$

We note that A_{pq} in equation (3.24) is not the same as A_{pi} corresponding to the Green's function g^A of the previous section. Thus, using the notation introduced in (3.24) in equation (3.23) yields:

$$f_i = M_{ij}\ddot{\xi}_j + K_{ij}\xi_j - \left(\kappa_{ip} + M_{ip}\frac{d^2}{dt^2}\right)\int_{-\infty}^{t}\sum_{P=1}^{M}\frac{A_{ps}^{(P)}}{\omega^{(P)}}\sin\left(\omega^{(P)}(t-\tau)\right)$$
$$\left\{M_{sj}\ddot{\xi}_j(\tau) + \kappa_{sj}\xi_j(\tau)\right\}d\tau. \tag{3.25}$$

We now integrate the terms containing 'ξ' in equation (3.25) twice by parts to obtain:

$$\int_{-\infty}^{t}\sum_{P=1}^{M}\frac{A_{ps}^{(P)}}{\omega^{(P)}}\kappa_{sj}\sin\left(\omega^{(P)}(t-\tau)\right)\xi_j(\tau)\,d\tau = \sum_{P=1}^{M}\frac{A_{ps}^{(P)}}{(\omega^{(P)})^2}\kappa_{sj}\xi_j(t)$$
$$-\int_{-\infty}^{t}\sum_{P=1}^{M}\frac{A_{ps}^{(P)}}{(\omega^{(P)})^3}\kappa_{sj}\sin\left(\omega^{(P)}(t-\tau)\right)\ddot{\xi}_j(\tau)\,d\tau \tag{3.26}$$

We use equation (3.26) in equation (3.25) to get:

$$f_i = M_{ij}\ddot{\xi}_j + K_{ij}\xi_j - \left(\kappa_{ip} + M_{ip}\frac{d^2}{dt^2}\right)\left\{\sum_{P=1}^{M}\frac{A_{ps}^{(P)}}{(\omega^{(P)})^2}\kappa_{sj}\xi_j(t) +\right.$$

$$\int_{-\infty}^{t} \sum_{P=1}^{M} \left(\frac{A_{ps}^{(P)}}{\omega^{(P)}} M_{sj} - \frac{A_{ps}^{(P)}}{(\omega^{(P)})^3} \kappa_{sj} \right) \sin\left(\omega^{(P)}(t-\tau)\right) \ddot{\xi}_j \, d\tau \Bigg\}. \tag{3.27}$$

Now we expand equation (3.26) by passing the time derivatives through the integrals, to obtain:

$$\begin{aligned} f_i = {} & M_{ij}\ddot{\xi}_j + K_{ij}\xi_j - \sum_{P=1}^{M} \kappa_{ip} \frac{A_{ps}^{(P)}}{(\omega^{(P)})^2} \kappa_{sj}\xi_j(t) - M_{ip} \sum_{P=1}^{M} \left(A_{ps}^{(P)} M_{sj} - \frac{A_{ps}^{(P)}}{(\omega^{(P)})^2} \kappa_{sj} + \frac{A_{ps}^{(P)}}{(\omega^{(P)})^2} \kappa_{sj} \right) \ddot{\xi}_j \\ & - \kappa_{ip} \int_{-\infty}^{t} \sum_{P=1}^{M} \left(\frac{A_{ps}^{(P)}}{\omega^{(P)}} M_{sj} - \frac{A_{ps}^{(P)}}{(\omega^{(P)})^3} \kappa_{sj} \right) \sin\left(\omega^{(P)}(t-\tau)\right) \ddot{\xi}_j \, d\tau \\ & + M_{ip} \int_{-\infty}^{t} \sum_{P=1}^{M} \left(\omega^{(P)} A_{ps}^{(P)} - \frac{A_{ps}^{(P)}}{\omega^{(P)}} \kappa_{sj} \right) \sin\left(\omega^{(P)}(t-\tau)\right) \ddot{\xi}_j \, d\tau \end{aligned} \tag{3.28}$$

We may simplify equation (3.28) by noting that $\sum_{P=1}^{M} M_{ip} A_{ps}^{(P)} M_{sj} = M_{ij}$ and writing the kernel of the integral in the form of a matrix product. This yields:

$$\begin{aligned} f_i = {} & K_{ij}\xi_j - \sum_{P=1}^{M} \kappa_{ip} \frac{A_{ps}^{(P)}}{(\omega^{(P)})^2} \kappa_{sj}\xi_j(t) + \int_{-\infty}^{t} \sum_{P=1}^{M} \omega^{(P)} \sin\left(\omega^{(P)}(t-\tau)\right) \\ & \frac{1}{(\omega^{(P)})^4} \begin{pmatrix} -\mathbf{M}(\omega^{(P)})^2 & \boldsymbol{\kappa} \end{pmatrix} \begin{pmatrix} \mathbf{A}^{(P)} & \mathbf{A}^{(P)} \\ \mathbf{A}^{(P)} & \mathbf{A}^{(P)} \end{pmatrix} \begin{pmatrix} -\mathbf{M}(\omega^{(P)})^2 \\ \boldsymbol{\kappa} \end{pmatrix} \ddot{\boldsymbol{\xi}}(\tau) \, d\tau \end{aligned} \tag{3.29}$$

Equation (3.29) represents the exact DtN map of the subsystem.

3.3 The Total Mass

The total mass of the system is given by:

$$M_{\text{Total}} = \begin{pmatrix} \zeta_i & \zeta_p \end{pmatrix} \begin{pmatrix} M_{ij} & M_{iq} \\ M_{pj} & M_{pq} \end{pmatrix} \begin{pmatrix} \zeta_j \\ \zeta_q \end{pmatrix} \tag{3.30}$$

Here $\boldsymbol{\zeta}$ is the unit translation vector as defined in section 2.2.1. This may be seen by considering the total kinetic energy of the subsystem in uniform translation.

It is, perhaps, more instructive to consider the approximate DtN map for very low frequencies. From equation (2.10) we get:

$$K_{pq}\xi_q = -\kappa_{pi}\xi_i - M_{pi}\ddot{\xi}_i - M_{pq}\ddot{\xi}_q. \tag{3.31}$$

For low frequency oscillations we may ignore the terms with time derivatives in $\boldsymbol{\xi}$, to obtain:

$$\xi_q \approx -K^{-1}_{qp}\kappa_{pi}\xi_i. \tag{3.32}$$

We may better our approximation of ξ_q by iterating, i.e. by substituting equation (3.32) back into equation (3.31) and left multiplying by $\mathbf{K}^{-1}$:

$$\xi_p \approx -K^{-1}_{pq}\kappa_{qi}\xi_i - K^{-1}_{pq}M_{qi}\ddot{\xi}_i + K^{-1}_{pq}M_{qr}K^{-1}_{rs}\kappa_{si}\ddot{\xi}_i. \tag{3.33}$$

We now use equation (3.33) in equation (2.9) and ignore terms containing fourth derivatives in $\boldsymbol{\xi}$, to obtain:

$$\begin{aligned} f_i \;&\approx\; M_{ij}\ddot{\xi}_j + K_{ij}\xi_j - M_{ip}K^{-1}_{pq}\kappa_{qj}\ddot{\xi}_j \\ &+\; \kappa_{ip}\left[-K^{-1}_{pq}\kappa_{qj}\xi_j - K^{-1}_{pq}M_{qj}\ddot{\xi}_j + K^{-1}_{pq}M_{qr}K^{-1}_{rs}\kappa_{sj}\ddot{\xi}_j\right] \end{aligned} \tag{3.34}$$

We rearrange equation (3.34) by grouping terms with corresponding derivatives in $\boldsymbol{\xi}$, to obtain:

$$\begin{aligned} f_i \;&\approx\; \left[M_{ij} - M_{ip}K^{-1}_{pq}\kappa_{qj} - \kappa_{ip}K^{-1}_{pq}M_{qj} + \kappa_{ip}K^{-1}_{pq}M_{qr}K^{-1}_{rs}\kappa_{sj}\right]\ddot{\xi}_j \\ &+\; \left[K_{ij} - \kappa_{ip}K^{-1}_{pq}\kappa_{qj}\right]\xi_j. \end{aligned} \tag{3.35}$$

Equation (3.35) holds for arbitrary displacements of the subsystem. We now consider unidirectional force and displacement such that:

$$\xi_i = \zeta_i x(t), \tag{3.36}$$

$$f_i = \zeta_i F(t). \tag{3.37}$$

Here $\boldsymbol{\zeta}$ is a generalized translation vector as defined in section (2.2.1).

We now use equation (3.36) in equation (3.35) along with the results of translational invariance, equations (2.23) and (2.24), to obtain:

$$f_i = \left[M_{ij}\zeta_j + M_{ip}\zeta_p - \kappa_{ip}K^{-1}_{pq}M_{qj}\zeta_j - \kappa_{ip}K^{-1}_{pq}M_{qr}\zeta_r\right]\ddot{x}(t) \tag{3.38}$$

We can left multiply the free index of equation (3.38) by ζ_i to get:

$$\zeta_i f_i = [\zeta_i M_{ij}\zeta_j + \zeta_i M_{ip}\zeta_p + \zeta_p M_{pi}\zeta_i + \zeta_p M_{pq}\zeta_q]\ddot{x}(t). \tag{3.39}$$

Equation (3.39) is a statement of Newton's Law for the entire translating subsystem. The left hand side is $\sum \mathbf{F}$ in the direction $\boldsymbol{\zeta}$. The right hand side "**Ma**". We observe that the total mass of the subsystem is given by:

$$M_{\text{Total}} = \zeta_i M_{ij}\zeta_j + \zeta_i M_{ip}\zeta_p + \zeta_p M_{pi}\zeta_i + \zeta_p M_{pq}\zeta_q. \tag{3.40}$$

This result shall be used in the following sections.

3.4 The Modal Mass Tensor and its Properties

We define our modal mass tensor as follows:

$$m^{(P)}_{ij} = \frac{1}{(\omega^{(P)})^4}\begin{pmatrix} -M_{ip}(\omega^{(P)})^2 & \kappa_{iq} \end{pmatrix}\begin{pmatrix} A^{(P)}_{pr} & A^{(P)}_{ps} \\ A^{(P)}_{qr} & A^{(P)}_{qs} \end{pmatrix}\begin{pmatrix} -M_{rj}(\omega^{(P)})^2 \\ \kappa_{sj} \end{pmatrix}. \tag{3.41}$$

Here $\mathbf{A}^{(P)}$ is defined in equation (3.24). We now show that summing the modal mass tensors over all modes, $P = 1, .., M$, yields the total mass of the subsystem.

$$\begin{aligned}\sum_{P=1}^{M} m^{(P)}_{ij} &= \sum_{P=1}^{M}\Bigg[M_{ip}A^{(P)}_{pr}M_{rj} - \frac{\kappa_{iq}}{(\omega^{(P)})^2}A^{(P)}_{qr}M_{rj} - \\ &\quad M_{ip}A^{(P)}_{ps}\frac{\kappa_{sj}}{(\omega^{(P)})^2} + \frac{\kappa_{iq}}{(\omega^{(P)})^2}A^{(P)}_{qs}\frac{\kappa_{sj}}{(\omega^{(P)})^2}\Bigg].\end{aligned} \tag{3.42}$$

We now expand each term on the right hand side of equation (3.42) using the definition of $\mathbf{A}^{(P)}$ from equation (3.24) to obtain:

$$\sum_{P=1}^{M} M_{ip} A_{pr}^{(P)} M_{rj} = \sum_{P=1}^{M} M_{ip} M_{pq}^{(-1/2)} \gamma_q^{(P)} \gamma_s^{(P)} M_{sr}^{(-1/2)} M_{rj}. \tag{3.43}$$

We know that the eigenvectors are orthonormal, and therefore:

$$\sum_{P=1}^{M} \gamma_q^{(P)} \gamma_s^{(P)} = \delta_{qs}. \tag{3.44}$$

We use this in equation (3.43) to get:

$$\begin{aligned} \sum_{P=1}^{M} M_{ip} A_{pr}^{(P)} M_{rj} &= M_{ip} M_{pq}^{(-1/2)} M_{qr}^{(-1/2)} M_{rj} \\ &= M_{ij}. \end{aligned} \tag{3.45}$$

Similarly we find:

$$\sum_{P=1}^{M} \frac{\kappa_{iq}}{(\omega^{(P)})^2} A_{qr}^{(P)} M_{rj} = \sum_{P=1}^{M} \frac{\kappa_{iq}}{(\omega^{(P)})^2} M_{qs}^{-1/2} \gamma_s^{(P)} \gamma_p^{(P)} M_{pr}^{-1/2} M_{rj}. \tag{3.46}$$

We left multiply both sides of equation (3.15) by $\mathbf{K}^{-1}\mathbf{M}^{1/2}$ to get:

$$M_{pq}^{-1/2} \gamma_q^{(P)} = (\omega^{(P)})^2 K_{pq}^{-1} M_{qr}^{1/2} \gamma_r^{(P)}. \tag{3.47}$$

Now we use equation (3.47) in equation (3.46) to obtain:

$$\begin{aligned} \sum_{P=1}^{M} \frac{\kappa_{iq}}{(\omega^{(P)})^2} A_{qr}^{(P)} M_{rj} &= \kappa_{iq} K_{qp}^{-1} M_{ps}^{1/2} \delta_{st} M_{tr}^{-1/2} M_{rj} \\ &= \kappa_{iq} K_{qp}^{-1} M_{pj}. \end{aligned} \tag{3.48}$$

The last two terms of equation (3.42) similarly yield:

$$\sum_{P=1}^{M} M_{ip} A_{ps}^{(P)} \frac{\kappa_{sj}}{(\omega^{(P)})^2} = M_{ip} K_{pq}^{-1} \kappa_{qj} \tag{3.49}$$

and

$$\sum_{P=1}^{M} \frac{\kappa_{iq}}{(\omega^{(P)})^2} A_{qs}^{(P)} \frac{\kappa_{sj}}{(\omega^{(P)})^2} = \kappa_{ip} K_{pq}^{-1} M_{qr} K_{rs}^{-1} \kappa_{sj}. \tag{3.50}$$

Note that we may also derive the relation:

$$\sum_{P=1}^{M} \frac{A_{ps}^{(P)}}{(\omega^{(P)})^2} = K_{ps}^{-1}. \tag{3.51}$$

We now use equations (3.45, 3.48, 3.49 and 3.50) in equation (3.42), multiply by ζ_i from the left and ζ_j from the right and use the results of translational invariance from equations (2.23 and 2.24) to obtain:

$$\sum_{P=1}^{M} \zeta_i m_{ij}^{(P)} \zeta_j = \zeta_i M_{ij} \zeta_j + \zeta_i M_{ip} \zeta_p + \zeta_p M_{pi} \zeta_i + \zeta_p M_{pq} \zeta_q. \tag{3.52}$$

We compare equation (3.52) with equation (3.40) and see that the modal mass tensors summed over all frequencies yield the total mass of the subsystem, i.e:

$$\sum_{P=1}^{M} \zeta_i m_{ij}^{(P)} \zeta_j = M_{\text{Total}}. \tag{3.53}$$

We can rewrite the exact DtN in terms of the modal mass tensors. Substituting equation (3.41) in equation (3.29) while noting (3.51) yields:

$$f_i = K_{ij}\xi_j - \kappa_{ip} K_{ps}^{-1} \kappa_{sj} \xi_j(t) + \int_{-\infty}^{t} \sum_{P=1}^{M} \omega^{(P)} m_{ij}^{(P)} \sin\left(\omega^{(P)}(t-\tau)\right) \ddot{\xi}_j(\tau)\, d\tau \tag{3.54}$$

In the subsequent chapters we utilize the properties of the modal mass tensors to provide approximate representations of the exact DtN (3.54). Note that the exact DtN as presented in equation (3.54) contains a discrete sum over all modes in the kernel of the convolution integral.

In the sequel we shall find it interesting to consider subsystems that contain small modal damping. The DtN for such a subsystem may be written approximately in the form:

$$f_i = K_{ij}\xi_j - \kappa_{ip} K_{ps}^{-1} \kappa_{sj} \xi_j(t) + \int_{-\infty}^{t} \sum_{P=1}^{M} \omega^{(P)} m_{ij}^{(P)} \sin\left(\omega^{(P)}(t-\tau)\right) e^{-\eta^{(P)}(t-\tau)} \ddot{\xi}_j(\tau)\, d\tau + O(\eta). \tag{3.55}$$

Here $\eta^{(P)} \ll 1$ is a small modal damping factor. We emphasize that equation (3.54) is exact, however, equation (3.55) is an approximate representation.

3.5 Modal Stiffness Tensor and its Properties

In what follows we find it convenient to define another modal quantity that we call the *Modal Stiffness Tensor.* The modal stiffness tensors are M in number and have the dimensions of stiffness. We define the modal stiffness tensors in terms of the modal mass tensors. The modal stiffness tensors, like the modal mass tensors contain some inherent physical properties of the system. Here we list some of the properties that the modal stiffness tensors exhibit.

We define the modal stiffness tensors in terms of the modal mass tensors as follows:

$$\mathcal{K}_{ij}^{(P)} = m_{ij}^{(P)}(\omega^{(P)})^2. \tag{3.56}$$

We now use the properties of the modal mass tensors to obtain some of the properties of the modal stiffness tensors.

Multiplying equation (3.41) by $(\omega^{(P)})^2$ and summing the result over all the modes yields:

$$\sum_{P=1}^{M}(\omega^{(P)})^2 m_{ij}^{(P)} = \sum_{P=1}^{M}\left[(\omega^{(P)})^2 M_{ip}A_{pr}^{(P)}M_{rj} - \kappa_{iq}A_{qr}^{(P)}M_{rj} - M_{ip}A_{ps}^{(P)}\kappa_{sj} + \kappa_{iq}\frac{A_{qs}^{(P)}}{(\omega^{(P)})^2}\kappa_{sj}\right]. \tag{3.57}$$

We now sum each term of equation (3.57) by applying relations (3.44) and (3.51). This yields:

$$\sum_{P=1}^{M}(\omega^{(P)})^2 m_{ij}^{(P)} = M_{ip}M_{pq}^{-1}K_{qr}M_{rs}^{-1}M_{sj} - M_{ip}M_{pq}^{-1}\kappa_{qj} - \kappa_{ip}M_{pq}^{-1}M_{qj} + \kappa_{ip}K_{pq}^{-1}\kappa_{qj}. \tag{3.58}$$

Equations (3.58) and (3.56) show an important property of the modal stiffness tensors, namely:

$$\sum_{P=1}^{M}\mathcal{K}_{ij}^{(P)} = M_{ip}M_{pq}^{-1}K_{qr}M_{rs}^{-1}M_{sj} - M_{ip}M_{pq}^{-1}\kappa_{qj} - \kappa_{ip}M_{pq}^{-1}M_{qj} + \kappa_{ip}K_{pq}^{-1}\kappa_{qj}. \tag{3.59}$$

Further, we multiply equation (3.59) from the left by ζ_i and from the right by ζ_j and use the results of translational invariance from (2.23) and (2.24) to obtain:

$$\zeta_i\sum_{P=1}^{M}\mathcal{K}_{ij}^{(P)}\zeta_j = \zeta_i K_{ij}\zeta_j + \zeta_i M_{ip}M_{pq}^{-1}K_{qr}M_{rs}^{-1}M_{sj}\zeta_j - \zeta_i M_{ip}M_{pq}^{-1}\kappa_{qj}\zeta_j - \zeta_i\kappa_{ip}M_{pq}^{-1}M_{qj}\zeta_j. \tag{3.60}$$

We can use the form of the modal stiffness tensors and their properties to write the exact DtN map in an alternative form. Integrating equation (3.54) by parts twice in time and using the definition of the modal stiffness tensors yields:

$$f_i = K_{ij}\xi_j - \kappa_{ip}K_{ps}^{-1}\kappa_{sj}\xi_j(t) + \sum_{P=1}^{M} \mathcal{K}_{ij}^{(P)}\xi_j - \int_{-\infty}^{t} \sum_{P=1}^{M} \omega^{(P)}\mathcal{K}_{ij}^{(P)} \sin\left(\omega^{(P)}(t-\tau)\right) \xi_j(\tau)\, d\tau. \tag{3.61}$$

Note that equation (3.61) is an exact relation. Equations (3.54) and (3.61) are two important forms of representing the exact DtN map of the subsystem.

Chapter 4

Approximate Dirichlet to Neumann Maps

In this chapter we introduce the modal mass function $\mathbf{m}(\omega)$. In section 4.1 we re-express the exact DtN map by replacing the modal mass tensors by the modal mass function. This substitution is motivated by the work of Pierce [3]. In the following sections we obtain representations for approximate DtN's by approximating the modal mass function. We calculate the error incurred by approximating the exact but discontinuous $\mathbf{m}(\omega)$ with a continuous approximation $\bar{\mathbf{m}}(\omega)$. We show that by imposing certain restrictions on $\bar{\mathbf{m}}(\omega)$, the error can be bounded for all time. The restrictions thus determined lead us to a hierarchy of approximations that we discuss at the end of the chapter.

4.1 Modal Mass Function and Its Properties

We introduce the modal mass function $\mathbf{m}(\omega)$ to exactly replace the modal mass tensors as follows:

$$\mathbf{m}(\omega) = \sum_{P=1}^{M} \mathbf{m}^{(P)} H(\omega - \omega^{(P)}). \tag{4.1}$$

Here H is the Heaviside step function. Differentiating equation (4.1) with respect to ω yields:

$$\frac{d\mathbf{m}(\omega)}{d\omega} = \sum_{P=1}^{M} \mathbf{m}^{(P)} \delta(\omega - \omega^{(P)}). \tag{4.2}$$

Equation (4.1) and (4.2) are equivalent. This definition of the modal mass function is similar though not identical to that of Pierce [3]. We note that the modal mass function $\mathbf{m}(\omega)$ as defined in equation (4.1) and (4.2) is highly discontinuous. Some of the general properties of the modal mass function are [5]:

$$\begin{aligned} &\mathbf{m}(0) = \mathbf{0} \\ &\frac{d\mathbf{m}(\omega)}{d\omega} \geq \mathbf{0} \end{aligned} \tag{4.3}$$

Another property of the modal mass function is obtained from its definition and the property of the modal mass tensors (3.53). i.e.:

$$\zeta_i^\alpha \int_0^\infty \frac{dm_{ij}(\omega)}{d\omega} \zeta_j^\beta \, d\omega = M_{\text{Total}} \delta^{\alpha\beta} \tag{4.4}$$

Further, we use the definition of the modal stiffness tensors and equations (3.56) through (3.60) with the definition of the modal mass function to obtain the following results:

$$\int_0^\infty \omega^2 \frac{dm_{ij}(\omega)}{d\omega} \, d\omega = \int_0^\infty \frac{dK_{ij}(\omega)}{d\omega} \, d\omega$$

$$\int_0^\infty \omega^2 \frac{dm_{ij}(\omega)}{d\omega} \, d\omega = M_{ip} M_{pq}^{-1} K_{qr} M_{rs}^{-1} M_{sj} - M_{ip} M_{pq}^{-1} \kappa_{qj} - \kappa_{ip} M_{pq}^{-1} M_{qj} + \kappa_{ip} K_{pq}^{-1} \kappa_{qj} \tag{4.5}$$

$$\zeta_i \int_0^\infty \omega^2 \frac{dm_{ij}(\omega)}{d\omega} \zeta_j \, d\omega = \begin{array}{l} \zeta_i K_{ij} \zeta_j + \zeta_i M_{ip} M_{pq}^{-1} K_{qr} M_{rs}^{-1} M_{sj} \zeta_j - \\ \zeta_i M_{ip} M_{pq}^{-1} \kappa_{qj} \zeta_j - \zeta_i \kappa_{ip} M_{pq}^{-1} M_{qj} \zeta_j \end{array}$$

Here we have introduced the quantity $K_{ij}(\omega) = \omega^2 m_{ij}(\omega)$. We call this the modal stiffness function.

4.2 The Approximate DtN Map and Error Bounds

In the previous section we introduced the modal mass function $\mathbf{m}(\omega)$. In this section we use the properties of the modal mass function to find an approximate modal mass function $\bar{\mathbf{m}}(\omega)$. We then approximate the exact DtN (3.54) by using the approximate modal mass function $\bar{\mathbf{m}}(\omega)$. The error made in approximating the exact DtN is bounded by imposing conditions on the choice of the approximate modal mass function.

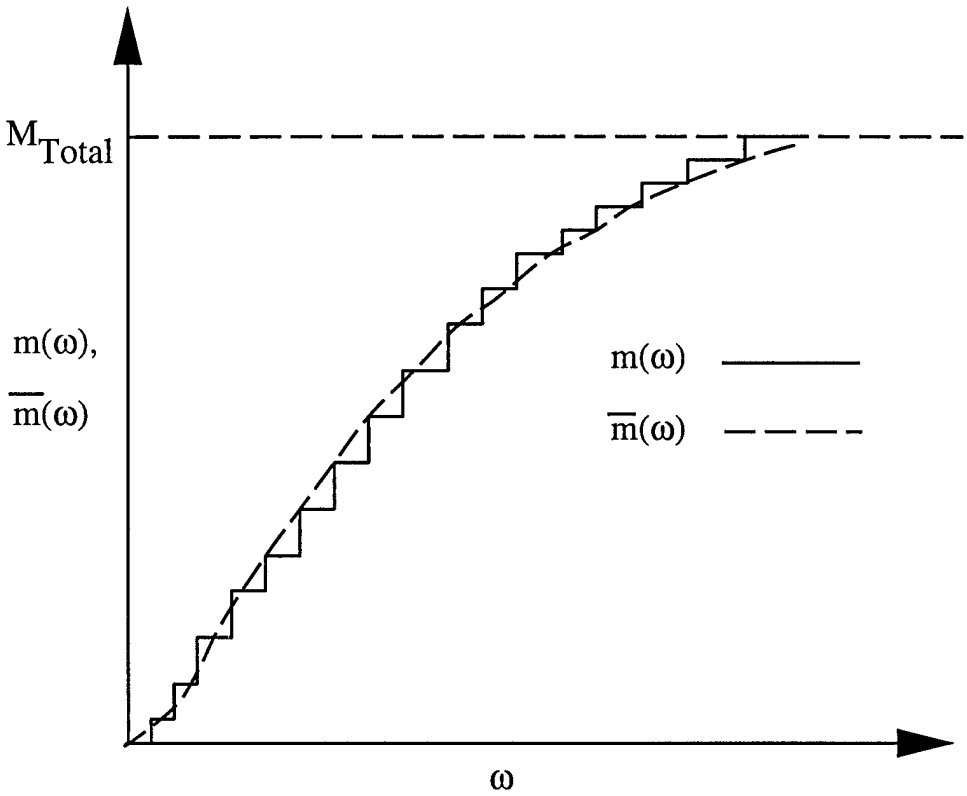

Figure 4.1: Exact and Approximate modal mass functions

We use the definition of the modal mass function (4.1) in the exact DtN (3.54) to obtain:

$$f_i(t) = K_{ij}\xi_j(t) - \kappa_{ip}K^{-1}_{pq}\kappa_{qj}\xi_j + \int_0^t \int_0^\infty \omega \frac{d\mathbf{m}(\omega)}{d\omega} \sin\omega(t-\tau)\boldsymbol{\xi}''(\tau)\, d\omega\, d\tau. \tag{4.6}$$

Here we emphasize that equation (4.6) is exact in the absence of damping and no approximations have as yet been made. Note that the time integration starts at $t = 0$ because we assume that the subsystem has no displacement history prior to this. When the number of modes is high we expect that the discontinuous modal mass function $\mathbf{m}(\omega)$ is well approximated by a smooth function $\bar{\mathbf{m}}(\omega)$ such that:

$$\mathbf{m}(\omega) = \bar{\mathbf{m}}(\omega) + \epsilon \mathbf{m}^e\left(\frac{\omega}{\epsilon}\right), \qquad \epsilon \ll 1. \tag{4.7}$$

Here $\epsilon\mathbf{m}^e\left(\frac{\omega}{\epsilon}\right)$ is a small but rapidly varying function which represents the error in approximating $\mathbf{m}(\omega)$ by $\bar{\mathbf{m}}(\omega)$. The parameter ϵ represents the non-dimensional modal spacing. The relation

(4.7) is demonstrated pictorially in figure 4.1. The stair step line represents an example $\mathbf{m}(\omega)$ while the smooth curve represents $\bar{\mathbf{m}}(\omega)$.

We obtain the approximate Dirichlet to Neumann map by substituting equation (4.7) into (4.6). This yields:

$$\begin{aligned} f_i(t) &= K_{ij}\xi_j(t) - \kappa_{ip}K^{-1}_{pq}\kappa_{qj}\xi_j + \\ &\int_0^t \int_0^\infty \omega \frac{d\bar{\mathbf{m}}(\omega)}{d\omega} \sin\omega(t-\tau)\boldsymbol{\xi}''(\tau)\, d\omega\, d\tau + \mathbf{error}(t). \end{aligned} \tag{4.8}$$

The error term in equation (4.8) is given by:

$$\begin{aligned} \mathbf{error}(t) &= \int_0^t \int_0^\infty \omega \frac{d\mathbf{m}^e\left(\frac{\omega}{\epsilon}\right)}{d\omega} \sin\omega(t-\tau)\boldsymbol{\xi}''(\tau)\, d\omega\, d\tau \\ &= Im\left\{ \int_0^t \int_0^\infty \omega \frac{d\mathbf{m}^e\left(\frac{\omega}{\epsilon}\right)}{d\omega} e^{i\omega(t-\tau)}\boldsymbol{\xi}''(\tau)\, d\omega\, d\tau \right\}. \end{aligned} \tag{4.9}$$

Here we have written the trigonometric function $\sin\omega(t-\tau)$ as the imaginary part of the exponent $e^{i\omega(t-\tau)}$. We now find error bounds by integrating equation (4.9) by parts once in time and twice in frequency.

Integrating equation (4.9) once in time yields:

$$\begin{aligned} \mathbf{error}(t) &= Im\left\{ \int_0^\infty \omega \frac{d\mathbf{m}^e\left(\frac{\omega}{\epsilon}\right)}{d\omega} \frac{e^{i\omega(t-\tau)}}{-i\omega}\boldsymbol{\xi}''(\tau)\Big|_0^t d\omega \right\} - \\ &\quad Im\left\{ \int_0^\infty \int_0^t \frac{d\mathbf{m}^e\left(\frac{\omega}{\epsilon}\right)}{d\omega} \frac{e^{i\omega(t-\tau)}}{-i\omega}\boldsymbol{\xi}'''(\tau)\, d\omega\, d\tau \right\}. \end{aligned} \tag{4.10}$$

We now use the relation $e^{i\theta} = \cos\theta + i\sin\theta$ in equation (4.10). This yields:

$$\begin{aligned} \mathbf{error}(t) &= \boldsymbol{\xi}''(t) \int_0^\infty \frac{d\mathbf{m}^e\left(\frac{\omega}{\epsilon}\right)}{d\omega} d\omega - \boldsymbol{\xi}''(0) \int_0^\infty \frac{d\mathbf{m}^e\left(\frac{\omega}{\epsilon}\right)}{d\omega} \cos\omega(t-\tau)\, d\omega - \\ &\quad - \int_0^t \int_0^\infty \frac{d\mathbf{m}^e\left(\frac{\omega}{\epsilon}\right)}{d\omega} \cos\omega(t-\tau)\boldsymbol{\xi}'''(\tau)\, d\omega\, d\tau. \end{aligned} \tag{4.11}$$

We assume that the subsystem is initially at rest with $\xi_i''(0) = 0$ and choose the approximate modal mass function $\bar{\mathbf{m}}(\omega)$ such that:

$$\int_0^\infty \frac{d\bar{\mathbf{m}}(\omega)}{d\omega}\, d\omega = \sum_{P=1}^{M} \mathbf{m}^{(P)} H(\omega - \omega^{(P)}); \qquad \bar{\mathbf{m}}(0) = \mathbf{0}. \tag{4.12}$$

We now use equation (4.12) with (4.1) and (4.7) to obtain:

$$\begin{aligned} &\int_0^\infty \frac{d\mathbf{m}^e(\omega')}{d\omega'}\, d\omega' = \mathbf{0} \\ &\Rightarrow \mathbf{m}^e(0) = \mathbf{0}, \quad \mathbf{m}^e(\infty) = \mathbf{0}. \end{aligned} \tag{4.13}$$

Conditions (4.13) enables us to eliminate the first term in equation (4.11). Thus, we get:

$$\mathbf{error}(t) = -Re\left\{ \int_0^t \int_0^\infty \frac{d\mathbf{m}^e\left(\frac{\omega}{\epsilon}\right)}{d\omega} e^{i\omega(t-\tau)} \boldsymbol{\xi}'''(\tau)\, d\omega\, d\tau \right\}. \tag{4.14}$$

We integrate equation (4.14) once in frequency to get:

$$\begin{aligned} \mathbf{error}(t) &= -\epsilon \mathbf{m}^e\left(\frac{\omega}{\epsilon}\right) \int_0^t \cos\omega(t-\tau) \Big|_{\omega=0}^{\omega=\infty} \boldsymbol{\xi}'''(\tau)\, d\tau \\ &- \epsilon \int_0^t \int_0^\infty \mathbf{m}^e\left(\frac{\omega}{\epsilon}\right) (t-\tau) \sin\omega(t-\tau) \boldsymbol{\xi}'''(\tau)\, d\omega\, d\tau. \end{aligned} \tag{4.15}$$

The conditions in (4.13) eliminate the first term in equation (4.15). We integrate the remaining term by parts once more in frequency. Thus we obtain:

$$\begin{aligned} \mathbf{error}(t) &= -\epsilon^2 \mathbf{m}^e_{-1}\left(\frac{\omega}{\epsilon}\right) \int_0^t (t-\tau) \sin\omega(t-\tau) \Big|_{\omega=0}^{\omega=\infty} \boldsymbol{\xi}'''(\tau)\, d\tau \\ &+ \epsilon^2 \int_0^t \int_0^\infty \mathbf{m}^e_{-1}\left(\frac{\omega}{\epsilon}\right) (t-\tau)^2 \cos\omega(t-\tau) \boldsymbol{\xi}'''(\tau)\, d\omega\, d\tau. \end{aligned} \tag{4.16}$$

Here we have introduced the integral of $\mathbf{m}^e(\omega)$:

$$\mathbf{m}^e_{-1}(\omega) = \int_0^\omega \mathbf{m}^e(\omega')\, d\omega'. \tag{4.17}$$

We now impose the following conditions on the choice of the approximate modal mass function $\bar{\mathbf{m}}(\omega)$:

$$\begin{aligned} \mathbf{m}^e_{-1}(0) &= \mathbf{0} \\ \mathbf{m}^e_{-1}(\infty) &= \mathbf{0} \end{aligned} \tag{4.18}$$

We use (4.18) in equation (4.16) to get:

$$\mathbf{error}(t) = \epsilon^2 \int_0^t \int_0^\infty \mathbf{m}^e_{-1}\left(\frac{\omega}{\epsilon}\right)(t-\tau)^2 \cos\omega(t-\tau)\boldsymbol{\xi}'''(\tau)\, d\omega\, d\tau. \tag{4.19}$$

We shall show that $\mathbf{error}(t)$ is bounded in the next section.

4.2.1 Error Bounds

In this section we examine the functions in the integrand of the error term in equation (4.19) to determine their maxima. We use these maxima and integrate the error term once in time and once in frequency. By doing this we obtain the maximum value of the integral and thus a bound on the error.

We first examine the function $(t-\tau)^2$ for values of $\tau < t$ in the range $0 < t < \infty$. This yields:

$$(t-\tau)^2 \leq t^2. \tag{4.20}$$

In addition, we have:

$$\left|\cos\omega(t-\tau)\right| \leq 1. \tag{4.21}$$

We can use equations (4.20) and (4.21) in equation (4.19) to obtain:

$$\left\|\mathbf{error}(t)\right\| \leq \epsilon^2 t^2 \left\|\boldsymbol{\xi}''(t)\right\| \left\| \int_0^\infty \mathbf{m}^e_{-1}\left(\frac{\omega}{\epsilon}\right) d\omega \right\|. \tag{4.22}$$

We now impose:

$$\int_0^\infty \mathbf{m}_{-1}^e\left(\frac{\omega}{\epsilon}\right) d\omega = \epsilon \int_0^\infty \mathbf{m}_{-1}^e(\omega')\, d\omega' \triangleq \epsilon \mathbf{C} = \text{constant} < \infty. \tag{4.23}$$

Here we have assumed:

$$\mathbf{C} = \int_0^\infty \mathbf{m}_{-1}^e(\omega)\, d\omega < \infty. \tag{4.24}$$

We use (4.23) in (4.22) to bound the error as follows:

$$\left\|\mathbf{error}(t)\right\| \leq \epsilon^3 t^2 \left\|\mathbf{C}\right\| \left\|\boldsymbol{\xi}''(t)\right\|; \qquad \forall\ \epsilon\ >\ 0. \tag{4.25}$$

From equation (4.25) we see that the error is bounded for simulation times $t = O(1/\epsilon^{3/2})$. We stress that this result is not an asymptotic error estimate. Equation (4.25) holds for any ϵ and not just the limit as $\epsilon \to 0$.

If there were damping present in the subsystem, then we might expect that the damping drives the total response to zero before the error can accumulate. We show this by considering the error made in approximating the DtN with damping (3.55). In that case the error is given by:

$$\mathbf{error}(t) = \epsilon^2 \int_0^t \int_0^\infty \mathbf{m}_{-1}^e\left(\frac{\omega}{\epsilon}\right) (t-\tau)^2 \cos\omega(t-\tau) e^{-\eta(t-\tau)} \boldsymbol{\xi}'''(\tau)\, d\omega\, d\tau + O(\eta). \tag{4.26}$$

We now examine the function $f(t) = t^2 e^{-\eta t}$ in the range $0 \leq t \leq \infty$, $0 \leq \eta \ll 1$. To obtain the maximum of $f(t)$ we differentiate it with respect to time and set the result equal to zero. This yields $t = 2/\eta$. Further, this stationary point is a maximum. Thus $f(t)$ is bounded and we have:

$$\begin{aligned} (t-\tau)^2 e^{-\eta(\omega)(t-\tau)} &\leq (t-\tau)^2 e^{-\eta_{min}(t-\tau)} \\ &\leq \left(\frac{2}{\eta_{\min}}\right)^2 e^{-2}. \end{aligned} \tag{4.27}$$

We use equations (4.27), (4.21), (4.23) and (4.24) in equation (4.26) to bound the error in the presence of damping. This yields:

$$\left\|\mathbf{error}(t)\right\| \leq \epsilon^3 \left\|\mathbf{C}\right\| \left(\frac{2}{\eta_{\min}}\right)^2 e^{-2} \left\|\boldsymbol{\xi}''(t)\right\|; \qquad \forall\ \epsilon\ >\ 0,\ \lim_{\eta \to 0+}. \tag{4.28}$$

Here $\mathbf{C}$ is a constant and we assume that $\left\|\boldsymbol{\xi}''(t)\right\|$ is bounded. Again, we emphasize that the error bound (4.28) holds for all ϵ, and not just in the limit as $\epsilon \to 0$.

The special case of a subsystem comprised of a number of unidirectional oscillators attached to a single unidirectional oscillator was recently considered by Weaver [12]. Weaver numerically simulated this system to obtain several response curves. His numerical results for this special system show behavior that is consistant with the general results derived in this chapter (c.f. equations (4.25) and (4.28)).

4.3 Levels of Approximation of $\mathbf{m}(\omega)$

Here we enumerate a hierarchy of approximations of the modal mass function (matrix). These approximations are based on the structure of the modal mass tensors and the properties that the modal mass function exhibit. In each case we list the restrictions on the approximate modal mass function such that the error is bounded.

4.3.1 Case 1

The crudest form of approximating the modal mass function is to assume an isotropic form. This yields:

$$\bar{\mathbf{m}}(\omega) = m_{(c)}(\omega)\, \delta_{ij}. \tag{4.29}$$

We note that the modal mass function must satisfy (4.4). We may use this to get:

$$\zeta_i^\alpha \int_0^\infty \frac{dm_{(c)}(\omega)}{d\omega} \delta_{ij} \zeta_j^\beta \, d\omega = M_{\text{Total}} \delta^{\alpha\beta}. \tag{4.30}$$

Therefore at this level we only need to choose one smooth function $m_{(c)}(\omega)$ such that it satisfies the relation:

$$\zeta_i \int_0^\infty \frac{dm_{(c)}(\omega)}{d\omega} \zeta_i \, d\omega = M_{\text{Total}}. \tag{4.31}$$

We note that equations (4.31) and (4.5) imply that the attachment point stiffness matrix K_{ij} should be isotropic. If we approximate the modal mass function using (4.29) the error is bounded only if (4.3) through (4.5) are satisfied and in addition, K_{ij} is isotropic and the coupling mass $M_{ip} = M_{qj} = 0$. We note that this level of approximation seems unrealistic, especially when the number of modes in the subsystem is low. The only physical property that this approximation captures is the total mass of the subsystem.

4.3.2 Case 2

We may use the properties of the modal mass function to form a better approximation of it. In particular from equation (4.5) we note that the modal mass function is related to the low frequency stiffness matrix $\kappa_{ip} K_{pq}^{-1} \kappa_{qj}$ of the attachment points. i.e:

$$\int_0^\infty \omega^2 \frac{dm_{ij}(\omega)}{d\omega} \, d\omega = \kappa_{ip} K_{pq}^{-1} \kappa_{qj} + M_{ip} M_{pq}^{-1} K_{qr} M_{rs}^{-1} M_{sj} - M_{ip} M_{pq}^{-1} \kappa_{qj} - \kappa_{ip} M_{pq}^{-1} M_{qj} \tag{4.32}$$

In the special case where the coupling masses M_{ip} and M_{qj} are zero, equation (4.32) reduces to:

$$\int_0^\infty \omega^2 \frac{dm_{ij}(\omega)}{d\omega} \, d\omega = \kappa_{ip} K_{pq}^{-1} \kappa_{qj} \triangleq K_{ij}^0. \tag{4.33}$$

We could choose the approximate modal mass function $\bar{\mathbf{m}}(\omega)$ to have the same eigenvectors as that of the low frequency attachment stiffness matrix K^0_{ij}. Then the approximate modal mass function satisfies the relation:

$$\int_0^\infty \omega^2 \frac{d\bar{m}_{ij}(\omega)}{d\omega}\, d\omega = \kappa_{ip} K^{-1}_{pq} \kappa_{qj} = K^0_{ij}. \tag{4.34}$$

We also choose the approximate modal mass function to satisfy the relation (4.4). We may write the low frequency attachment stiffness matrix K^0_{ij} in terms of its N distinct, orthogonal [1] eigenvectors $\psi^{(I)}_i$ and its positive eigenvalues $(\lambda^{(I)})^2$ as follows:

$$K^0_{ij} = \sum_{I=1}^{N} (\lambda^{(I)})^2 \left[\psi^{(I)}_i \otimes \psi^{(I)}_j\right]. \tag{4.35}$$

We now approximate the modal mass function using the known eigenvectors $\psi^{(I)}_i$. Thus we obtain:

$$\bar{m}_{ij}(\omega) = \sum_{I=1}^{N} (\mu^{(I)}(\omega))^2 \left[\psi^{(I)}_i \otimes \psi^{(I)}_j\right]. \tag{4.36}$$

From equation (4.36) we can see that we need to choose only N smooth functions $\mu^{(I)}(\omega)$ in order to approximate the modal mass function. We note that these functions have to be chosen so as to satisfy equations (4.3), (4.4) and (4.33).

This is a more realistic approximation for the modal mass function. It not only captures the total mass of the system but also possesses some information as to how the mass is partitioned amongst the attachment points.

4.3.3 Case 3

Finally we may form an approximation of the modal mass function that takes into account all the systems internal degrees of freedom and dynamics. We note that the modal mass matrix

[1] Note that K^0_{ij} is symmetric and positive definite.

$m_{ij}(\omega)$ is symmetric. Thus we need to have $\frac{1}{2}N(N+1)$ functions of ω to completely define the modal mass matrix $\mathbf{m}(\omega)$. We choose these functions $m_{(1)}(\omega)$ through $m_{\left(\frac{1}{2}N(N+1)\right)}(\omega)$ such that conditions (4.3) through (4.5) are satisfied.

We have explicit error bounds on this approximation subject to conditions (4.13) and (4.18). This would be the most accurate approximation for the modal mass function. This approximation would account for all the internal dynamics of the subsystem. Note that the error analysis of sections 4.2 and 4.2.1 are valid for this approximation and thus the error would be bounded for all time in the presence of a small amount of system damping.

Chapter 5

Implementation Methods: A Special Case

In this chapter we discuss methods of efficiently implementing our approximate DtN's in a numerical simulation. For the purpose of this discussion we shall consider the special case of a subsystem that interacts with the environment through a single massless attachment point. The internal components of this subsystem are allowed unidirectional motion only. The formulation presented here is taken from Barbone [5]. In section 5.1 we interpret this special case based on the notation and results of the earlier chapters. We then derive methods to implement the DtN's for such a subsystem. In section 5.2 we discuss the implementation of an approximate DtN map for the case where the natural frequencies of the subsystem are low compared to the time scale of the excitation. In section 5.3 we derive methods for implementing high modal density approximate DtN's for a subsystem whose strong resonant frequencies are known.

5.1 Special Example

We consider a subsystem that has a quadratic potential energy function in M degrees of freedom. This subsystem is attached to the outside world at only one attachment point. This subsystem is assumed to have M internal components. We assume that the internal components of the subsystem move in a single Cartesian direction only. All the results that were derived in the previous chapters apply to this case.

The equations of motion (2.9) and (2.10) for this subsystem reduce to:

$$M_{pq}\ddot{\xi}_q + K_{pq}\xi_q = -\kappa_p \xi_0. \tag{5.1}$$

and

$$\kappa_p (\xi_p - \zeta_p \xi_0) = f_0. \tag{5.2}$$

These equations are obtained from (2.9) and (2.10) by noting that the mass of the single attachment point is zero. The index notation in (2.7) still holds with $N = 1$. Here we have denoted the displacement of the attachment point by ξ_0 and the force at the attachment point by f_0. Note that the generalized unit displacement vector, in this case, takes the form of a vector in $\mathbf{R}^M$ with each of its entries equal to unity. i.e. $\zeta_q = 1, q = 1, 2, \cdots, M$. The results for translational invariance (2.23) and (2.24) for this case yield:

$$K_{pq}\zeta_q = -\kappa_p \tag{5.3}$$

and

$$k_0 = -\zeta_p \kappa_p = \zeta_p K_{pq} \zeta_q. \tag{5.4}$$

Here we have denoted the stiffness of the single attachment point by k_0. i.e. $K_{11} = k_0$.

5.1.1 Exact DtN Map

We may obtain the exact DtN map of the subsystem for this case from equation (3.29) as:

$$f_0(t) = k_0 \xi_0(t) - \int_{-\infty}^{t} \sum_{P=1}^{M} m^{(P)} (\omega^{(P)})^3 \sin\left(\omega^{(P)}(t-\tau)\right) \xi_0(\tau)\, d\tau. \tag{5.5}$$

Note that the modal mass is no longer a tensor but rather a scalar. As before we may write (5.5) exactly in the continuous form as:

$$f_0(t) = k_0 \xi_0(t) - \int_{-\infty}^{t} \int_{0}^{\infty} \omega^3 \frac{dm(\omega)}{d\omega} \sin\omega(t-\tau) \xi_0(\tau)\, d\omega\, d\tau. \tag{5.6}$$

The conditions (4.3) through (4.5) now become:

$$\begin{aligned} &m(0) = 0 && m(\infty) = M_{\text{Total}} \\ &\int_0^\infty \frac{dm(\omega)}{d\omega} d\omega = M_{\text{Total}} && \int_0^\infty \omega^2 \frac{dm(\omega)}{d\omega} d\omega = k_0 \end{aligned} \tag{5.7}$$

5.1.2 Approximate DtN map

An approximate DtN map is proposed for this special case in [5]. A function which is representative of the class of functions satisfying (5.7) is used to approximate the modal mass function $m(\omega)$ to get the approximate DtN map. For this special case, the approximate modal mass function proposed is:

$$\bar{m}(\omega) = M_{\text{Total}}\, erf\left(\frac{\omega}{\sqrt{2}\Omega}\right). \tag{5.8}$$

Here $erf(z)$ is the error function of z [6]. Requiring (5.8) to satisfy (5.7) yields:

$$\Omega = \sqrt{\frac{k_0}{M_{\text{Total}}}}. \tag{5.9}$$

Using (5.8) and (5.9) in (5.6) and integrating repeatedly with respect to omega yields the approximate DtN map for this special case as:

$$f_0(t) = k_0\xi_0(t) - M_{\text{Total}}\Omega^4 \int_0^t \left[3 - \Omega^2(t-\tau)^2\right](t-\tau)e^{-(t-\tau)^2\Omega^2/2}\xi_0(\tau)\, d\tau. \tag{5.10}$$

Here we have assumed that the subsystem has no displacement history prior to $t = 0$. This approximate DtN map has no added damping. According to equation (4.25), the error in this approximation is bounded for $t < O(1/\epsilon^{3/2})$, provided (5.7), (4.13), (4.18) and (4.23) hold.

We now suggest implementation methods for the approximate DtN (5.10) map when the natural frequency scale of the subsystem Ω is either low or high compared to the excitation time scale.

5.1.3 Low Ω Implementation of The Approximate DtN

When the natural frequency scale of the subsystem Ω is low the kernel of the integral does not vanish quickly and thus equation (5.10) is difficult to integrate numerically. We may, however,

use the first few terms of the asymptotic expansion of the Laplace transform of equation (5.10) for implementing the approximate DtN in a numerical scheme.

Integrating (5.10) once in time yields:

$$f(t) = \int_0^t k(t-\tau)\xi_0'(\tau)\,d\tau. \tag{5.11}$$

Here the kernel $k(t-\tau)$ is given by:

$$k(t-\tau) = M_{\text{Total}}\Omega^2\left[1-\Omega^2(t-\tau)^2\right]e^{-(t-\tau)^2\Omega^2/2}. \tag{5.12}$$

Since $\xi'(t) = 0, \forall t \in (-\infty, 0]$ we can take the Laplace transform [6] of equation (5.11) to get:

$$\mathcal{L}[f(t)] = \mathcal{L}[k(t)]\mathcal{L}[\xi_0'(t)]. \tag{5.13}$$

Here $\mathcal{L}[f(t)], \mathcal{L}[k(t)]$ and $\mathcal{L}[\xi_0'(t)]$ are the respective functions in the transform domain. In addition, assuming $\xi_0(0) = 0$, from the definition of the Laplace Transform, we get $\mathcal{L}[\xi_0'(t)] = s\mathcal{L}[\xi_0(t)]$.

To compute the Laplace transform of the kernel (5.12) we use the substitution $\tilde{t} = t - \tau$ and drop the tildes on the argument to write:

$$\mathcal{L}[k(t)] = \int_0^\infty M_{\text{Total}}\Omega^2\left(1-\Omega^2t^2\right)e^{-t^2\Omega^2/2}e^{-st}\,dt. \tag{5.14}$$

We now complete the square in the exponent and use the definition of the complimentary error function of z, $erfc(z)$ from [6] to get:

$$\mathcal{L}[k(t)] = \sqrt{\frac{\pi}{2}}M_{\text{Total}}\Omega e^{s^2/2\Omega^2}erfc\left(\frac{s}{\sqrt{2}\Omega}\right) - M_{\text{Total}}\Omega^4 e^{s^2/2\Omega^2}\int_0^\infty t^2 e^{-\left(\frac{t\Omega}{\sqrt{2}}-\frac{s}{\sqrt{2}\Omega}\right)^2}\,dt. \tag{5.15}$$

We now use the substitution $\dfrac{t\Omega}{\sqrt{2}} - \dfrac{s}{\sqrt{2}\Omega} = y$ in the integral of equation (5.15) and integrate repeatedly by parts to obtain:

$$\mathcal{L}[k(t)] = M_{\text{Total}}\,s - \sqrt{\frac{\pi}{2}}\,M_{\text{Total}}\,\frac{s^2}{\Omega}\,e^{s^2/2\Omega^2}erfc\left(\frac{s}{\sqrt{2}\Omega}\right). \tag{5.16}$$

We now employ the asymptotic expansion of the complementary error function from [6]:

$$\sqrt{\pi} z e^{z^2} erfc(z) \sim 1 + \sum_m (-1)^m \frac{1.3 \cdots (2m-1)}{(2z^2)^m}; \qquad z \to \infty, |arg(z)| < \frac{3\pi}{4}. \tag{5.17}$$

Using (5.17) in (5.16) with $z = \frac{s}{\sqrt{2}\Omega}$ and ignoring terms of $O\left(\frac{\Omega}{s}\right)^6$ and higher we obtain:

$$s^3 \mathcal{L}[k(t)] = M_{\text{Total}} \Omega^2 s^2 - 3 M_{\text{Total}} \Omega^4. \tag{5.18}$$

We now use equation (5.18) in (5.13) to obtain:

$$s^2 \mathcal{L}[f_0(t)] = \mathcal{L}[\xi_0(t)] \left[M_{\text{Total}} \Omega^2 s^2 - 3 M_{\text{Total}} \Omega^4 \right]. \tag{5.19}$$

We can now take the inverse Laplace transform [6] of (5.19) and use the result for implementing the approximate DtN in the time domain. Assuming homogeneous initial conditions the inverse Laplace transform of (5.19) is:

$$f_0''(t) = M_{\text{Total}} \Omega^2 \xi_0''(t) - 3 M_{\text{Total}} \Omega^4 \xi_0(t). \tag{5.20}$$

Note that when we ignore terms of order $O\left(\frac{\Omega}{s}\right)^4$ and higher in equation (5.16), we obtain:

$$f_0(t) = M_{\text{Total}} \Omega^2 \xi_0(t) = k_0 \xi_0(t). \tag{5.21}$$

Equation (5.20) requires taking two time derivatives of the attachment point displacement $\xi_0(t)$ and relating it to the second time derivative of the force $f_0(t)$ in the time domain. Equation (5.21) would be the simplest form of implementing the approximate DtN map (5.10) for the case when Ω is small.

5.1.4 Implementation When a Known Resonant Frequency Exists

When Ω is not small, the kernel in equation (5.10) decays quickly. Therefore we can use (5.10) directly for efficient implementation. Trouble may arise, however, if there is a single strong

resonance that decays slowly. A model for such a scenario is:

$$\bar{m}(\omega) = M_1 erf\left(\frac{\omega}{\sqrt{2}\Omega_1}\right) + M_2 H(\omega - \Omega_2). \tag{5.22}$$

Here H is the Heaviside step function and $erf(z)$ is the error function of z as defined in [6]. $M_2 H(\omega - \Omega_2)$ exactly represents the single strong mode of the subsystem that we assume to be known. M_2 is the modal mass of the mode which has resonant frequency Ω_2. In equation (5.22) $M_1 + M_2 \equiv M_{\text{Total}}$. Further, we let $k_1 = M_1\Omega_1^2$. We use equation (5.22) with (5.6) to obtain the approximate DtN map as:

$$\begin{aligned} f_0(t) &= (k_0 - k_1)\xi_0(t) + M_1\Omega_1^2 \int_0^t e^{-(t-\tau)^2\Omega_1^2/2}\left[1 - \Omega_1^2(t-\tau)^2\right]\xi_0'(\tau)\,d\tau \\ &+ M_2 \int_0^t \int_0^\infty \Omega_2^3 \delta(\omega - \Omega_2)\sin\Omega_2(t-\tau)\xi_0(\tau)\,d\omega\,d\tau. \end{aligned} \tag{5.23}$$

When the natural frequency scale of the subsystem Ω_1 is not small, the kernels in the integrals of (5.23) that contain the error function vanish quickly. The trigonometric kernel does not decay at all. We treat this trigonometric kernel here. To do this we take two time derivatives of equation (5.23). Treating each term individually, we have:

$$\begin{aligned} &\frac{d^2}{dt^2}\left\{M_1\Omega_1^2 \int_0^t e^{-(t-\tau)^2\Omega_1^2/2}\left[1 - \Omega_1^2(t-\tau)^2\right]\xi_0'(\tau)\,d\tau\right\} = \\ &\quad M_1\Omega_1^2\xi_0''(t) - M_1\Omega_1^4 \int_0^t e^{-(t-\tau)^2\Omega_1^2/2}\left[3 - 6\Omega_1^2(t-\tau)^2 + \Omega_1^4(t-\tau)^4\right]\xi_0'(\tau)\,d\tau, \end{aligned} \tag{5.24}$$

and

$$\begin{aligned} &\frac{d^2}{dt^2}\left\{M_2 \int_0^t \int_0^\infty \Omega_2^3\delta(\Omega - \Omega_2)\sin\Omega_2(t-\tau)\xi_0(\tau)\,d\omega\,d\tau\right\} = \frac{d^2}{dt^2}\left\{M_2\Omega_2^3 \int_0^t \sin\Omega_2(t-\tau)\xi_0(\tau)\,d\tau\right\} \\ &= M_2\Omega_2^4\xi_0(t) - M_2\Omega_2^5 \int_0^t \sin\Omega_2(t-\tau)\xi_0(\tau)\,d\tau. \end{aligned} \tag{5.25}$$

We now eliminate the integral containing the trigonometric kernel in (5.23) by using (5.24) and (5.25) to obtain an equation for $f_0''(t) + \Omega_2^2 f_0(t)$. This yields:

$$f_0''(t) + \Omega_2^2 f_0(t) = k_0 \xi_0''(t) + \left[(k_0 - k_1)\Omega_2^2 + M_2\Omega_2^4\right] \xi_0(t) +$$
$$M_1\Omega_1^2 \int_0^t e^{-(t-\tau)^2\Omega_1^2/2} \left[\left(\Omega_2^2 - 3\Omega_1^2\right) + \left(6\Omega_1^2 - \Omega_2^2\right) \Omega_1^2(t-\tau)^2 - \Omega_1^6(t-\tau)^4 \right] \xi_0'(\tau)\, d\tau. \quad (5.26)$$

Equation (5.26) may be used for implementing the approximate DtN map when Ω_1 is not small. The integral in equation (5.26) has a quickly vanishing kernel. Thus efficient numerical integration of (5.26) is possible.

Chapter 6

Numerical Simulations and Results

In this chapter we describe a numerical experiment designed to test the analytical results from the previous chapters. To do this, we consider the special type of subsystem described in chapter 5. We know the exact and an approximate DtN map for such a subsystem from the previous chapter. Here we replace the dynamical subsystem in the simulation by the force it exerts on a superstructure as predicted by the exact and approximate DtN maps. This is shown schematically in figures 6.1 and 6.2. Note that the number of modes in the subsystem is inversely related to the small parameter ϵ introduced in section 4.2; specifically $\epsilon \stackrel{\Delta}{=} \frac{1}{M}$. Thus we compare the force predicted by the exact DtN to that predicted by the approximate DtN.

In section 6.1 we describe the particular problem being considered. In section 6.2 we discuss the numerical schemes by which the analytical results of the previous chapters are implemented in this problem. In section 6.3 we describe the method by which the subsystem parameters are chosen in the simulation. Finally, in section 6.4 we show the results of our comparisons.

6.1 Example Problem

We consider an elastic rod (superstructure) of length L and a unit square cross section. A dynamical subsystem (*fuzzy structure*) is attached to the end of the rod at $x = L$. The components of the subsystem are allowed unidirectional motion only. The rod interacts with the dynamical subsystem through a single attachment point. Figure 6.1 shows a schematic of the setup. We model the rod using ten elastic finite elements. We prescribe a unit step displacement at the end of the rod $x = 0$ at time $t = 0$. The displacement wave propagates through the elastic rod and interacts with the fuzzy subsystem through the attachment point.

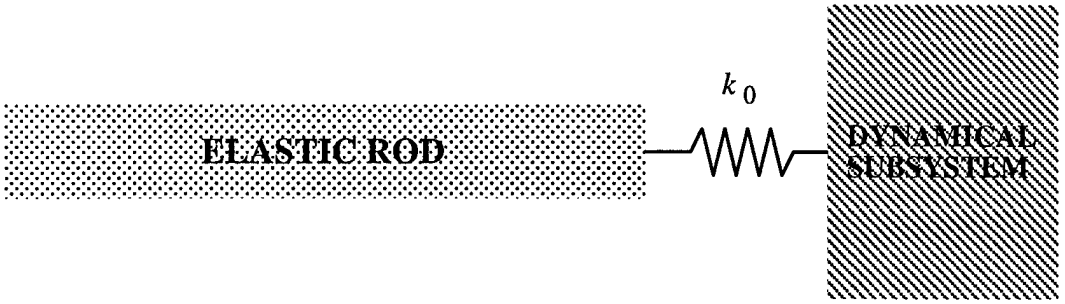

Figure 6.1: Dynamical subsystem attached to super structure.

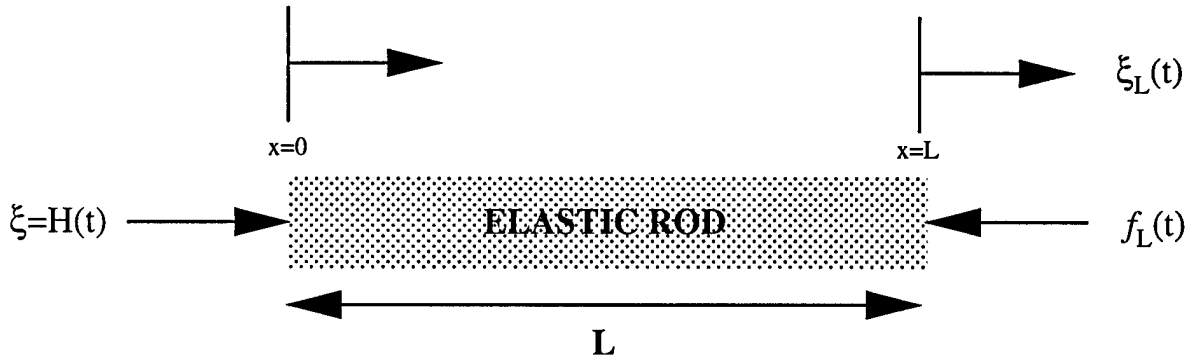

Figure 6.2: Dynamical subsystem is replaced by DtN condition.

We replace the dynamical subsystem in the simulation by the force it exerts on the rod as predicted by the exact (5.6) and approximate (5.10) DtN maps. We compare results of the simulations using both the DtN's. Our basis of comparison is the force between the rod and the equipment.

6.2 Numerical Implementation

The numerical results are obtained using DLEARN [7]. The time marching scheme employed in DLEARN is the α-method. We refer the reader to chapter 9 of [8] for details of the time

marching in the rod. We modify the DLEARN program to accommodate the DtN boundary condition at the end of the rod that accounts for the fuzzy subsystem. We divide the discussion of the modifications into two parts. In section 6.2.1 we discuss the dynamics in the rod and in section 6.2.2 we discuss the implementation of the DtN map.

6.2.1 Numerical Integration In The Rod

We use an explicit time marching algorithm to propagate the displacement wave in the elastic rod. It is incorporated in the DLEARN program.

The discrete finite element equations of motion describing the response of the elastic rod may be expressed in the form:

$$\mathbf{M}\ddot{\boldsymbol{\xi}} + \mathbf{C}\dot{\boldsymbol{\xi}} + \mathbf{K}\boldsymbol{\xi} = \mathbf{F}. \tag{6.1}$$

Here the vector $\boldsymbol{\xi}$ contains the nodal displacements in the elastic rod. $\mathbf{M}$ is the symmetric positive definite mass matrix of the rod. $\mathbf{C}$ is the symmetric positive semidefinite viscous damping matrix and $\mathbf{K}$ is the symmetric positive definite stiffness matrix of the rod. In addition we have $\xi(0)$ and $\dot{\xi}(0)$ specified at the end of the rod at $x = 0$. In the α - method the time-discrete equation of motion is [8].

$$\mathbf{M}\ddot{\boldsymbol{\xi}}^{n+1} + (1+\alpha)\mathbf{C}\dot{\boldsymbol{\xi}}^{n+1} - \alpha\mathbf{C}\dot{\boldsymbol{\xi}}^{n} + (1+\alpha)\mathbf{K}\boldsymbol{\xi}^{n+1} - \alpha\mathbf{K}\boldsymbol{\xi}^{n} = \mathbf{F}(t_{n+\alpha}). \tag{6.2}$$

Here n is the number of the time step and α is a numerical dissipation parameter. In equation (6.2):

$$t_{n+\alpha} = t_{n+1} + \alpha\Delta t. \tag{6.3}$$

We now use the following finite difference formulas to compute the displacements and velocities

at the next time step t_{n+1}. Note that these formulas comprise an explicit form of implementing the α - method.

$$\boldsymbol{\xi}^{n+1} = \boldsymbol{\xi}^n + \Delta t \dot{\boldsymbol{\xi}}^n + \frac{\Delta t^2}{2}(1-2\beta)\ddot{\boldsymbol{\xi}}^n, \tag{6.4}$$

and

$$\dot{\boldsymbol{\xi}}^{n+1} = \dot{\boldsymbol{\xi}}^n + \Delta t(1-\gamma)\ddot{\boldsymbol{\xi}}^n. \tag{6.5}$$

Implicit methods of implementation are also possible. These are discussed in [8]. To start the process, $\ddot{\boldsymbol{\xi}}^0$ may be calculated from:

$$\mathbf{M}\ddot{\boldsymbol{\xi}}^0 = \mathbf{F} - \mathbf{C}\dot{\boldsymbol{\xi}}^0 - \mathbf{K}\boldsymbol{\xi}^0. \tag{6.6}$$

We then compute the velocities and displacements at t_{n+1} from equations (6.5) and (6.4), respectively. We use these results to compute the acceleration at the next time step from equation (6.2) and then repeat the iterative process. The above scheme allows us to compute a force at the end of the rod at $x = L$ at the end of each time step. We call this force $\mathbf{F}^R(t)$.

6.2.2 Numerical Integration Of The DtN

In the previous section we described the scheme to compute $\boldsymbol{\xi}_0(t)$. We store the time history of displacements $\boldsymbol{\xi}_0(t)$ at the attachment point. At the end of each time step we employ this time history to integrate either equation (5.6) or (5.10)[1] and obtain the force due to the subsystem $f_0(t)$. From (5.6):

$$f_0^n = k_0\xi_0^n - F(\xi_0^0, \xi_0^1, \cdots, \xi_0^n). \tag{6.7}$$

[1]Note that the time histories are different for the exact and the approximate DtN's

Similarly for the approximate DtN, from (5.10) we get:

$$\bar{f}_0^n = k_0\bar{\xi}_0^n - \bar{F}(\bar{\xi}_0^0, \cdots, \bar{\xi}_0^n). \tag{6.8}$$

The functions $F(\xi_0^0, \xi_0^1, \cdots, \xi_0^n)$ and $\bar{F}(\bar{\xi}_0^0, \cdots, \bar{\xi}_0^n)$ are time convolutions of the displacements of the attachment point. To compute these we store the displacement history of the attachment point for the exact and approximate DtN's separately. We use the Trapezoid Rule to integrate the exact DtN (5.6) or the approximate DtN (5.10) at the end of each time step to obtain $F(\xi_0^0, \xi_0^1, \cdots, \xi_0^n)$ and $\bar{F}(\bar{\xi}_0^0, \cdots, \bar{\xi}_0^n)$, respectively. Note that we integrate the DtN's at the end of each time step using the displacement history of the attachment point till that time step. We then update the forces $\mathbf{F}^R(t)$ in the rod by adding to it either the exact force $f_0(t)$ or the approximate force $\bar{f}_0(t)$ due to the subsystem and then use the updated force to compute the displacement at the next time step.

6.3 Determination of Equipment Parameters

Here we describe the process by which we select our equipment parameters. We select a random distribution of masses and frequencies to approximate the error function distribution in (5.8). To do this, we first choose the number of modes in the subsystem M. We then use a pseudo random number generator to choose a random number between zero and one. We scale this distribution of random numbers to give us a frequency distribution in the range $0 < \omega < \omega_{max}$. Here we choose $\omega_{max} = 2\Omega$, with Ω given by:

$$\Omega = \sqrt{\frac{k_0}{M_{\text{Total}}}}. \tag{6.9}$$

We choose the attachment stiffness k_0 and the total mass of the system M_{Total}. We choose M_{Total} such that it is of the order of the mass of the rod. We denote the p^{th} frequency by ω_p.

The mass corresponding to ω_p is given by:

$$m_p = M_{\text{Target}} \frac{d\bar{m}(\omega)}{d\omega}\bigg|_{\omega=\omega_p} \Delta\omega. \tag{6.10}$$

In equation (6.10) $\bar{m}(\omega)$ is given by (5.8) and $\Delta\omega = \frac{\omega_{max}}{M}$. We then compute the stiffness of each individual component of the subsystem using the relation:

$$K_p = m_p \omega_p^2. \tag{6.11}$$

We verify that the total mass satisfies the relation:

$$M_{\text{Total}} = \sum_{p=1}^{M} \frac{K_p}{\omega_p^2} \neq M_{\text{Target}}. \tag{6.12}$$

We simulate the subsystem using the above choice of parameters. This subsystem corresponds to the one described in the previous chapter. We can thus validate our analytic results using this simulated subsystem. We compare the results obtained by using M_{Total} rather than M_{Target} in our approximate DtN's.

6.4 Evaluating Approximate DtN's

In this section we compare the forces predicted by the exact DtN (5.6) to those predicted by the approximate DtN (5.10). In different simulations, we vary the number of modes in the subsystem and the amount of damping in the subsystem. In figures 6.3 through 6.8 the thick curves represent the exact DtN results and the thin curves represent the approximate DtN results. In each figure the x-axis represents time t and the y-axis represents the force at the attachment point due to the dynamical subsystem $f_0(t)$. Note that as the small parameter $\epsilon \to 0$, as the number of modes $M \to \infty$. Figures 6.3 through 6.5 represent exact and approximate DtN's for subsystems with ten, one hundred and five hundred internal degrees of freedom respectively.

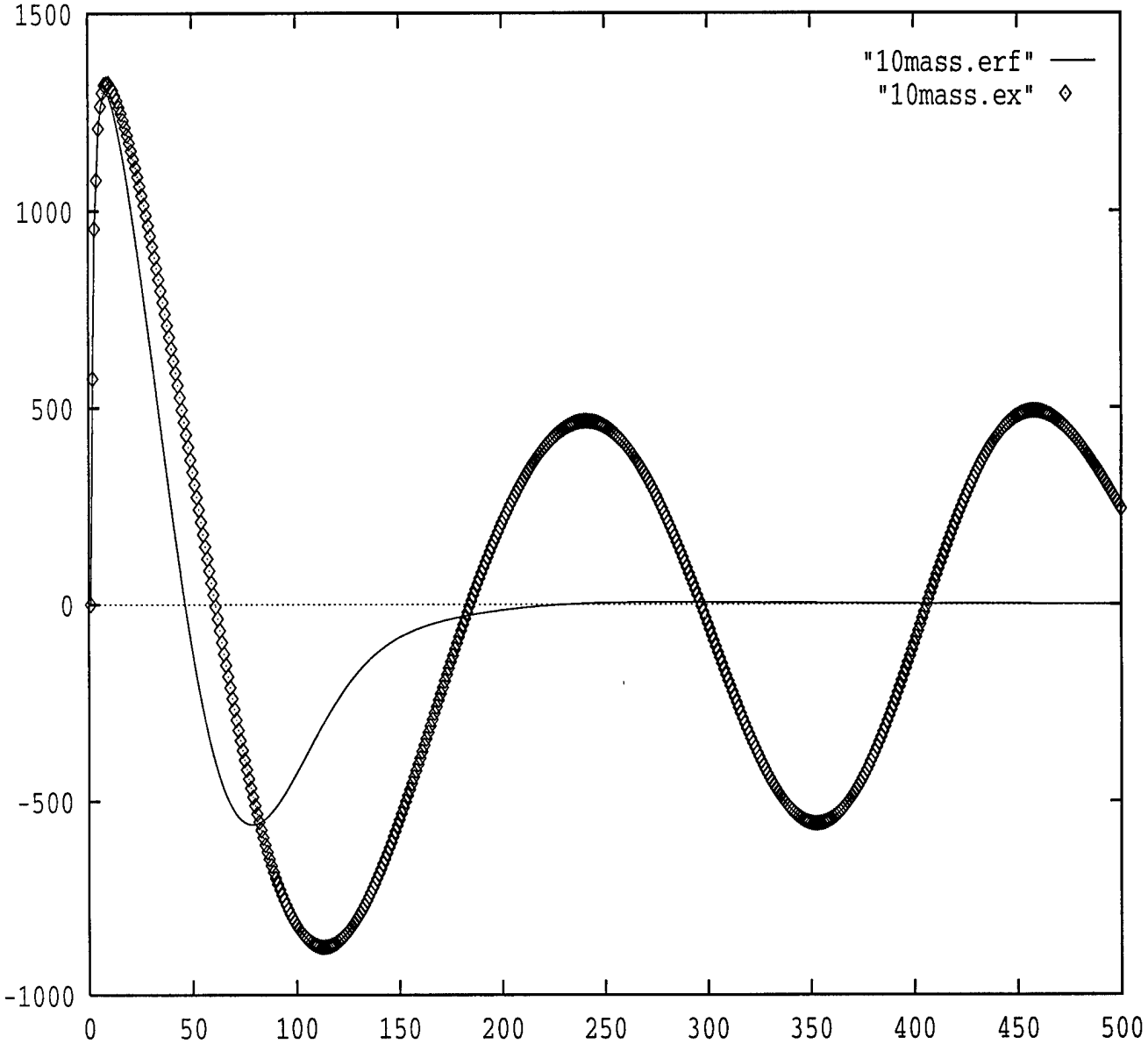

Figure 6.3: Dynamical subsystem with 10 internal degrees of freedom.

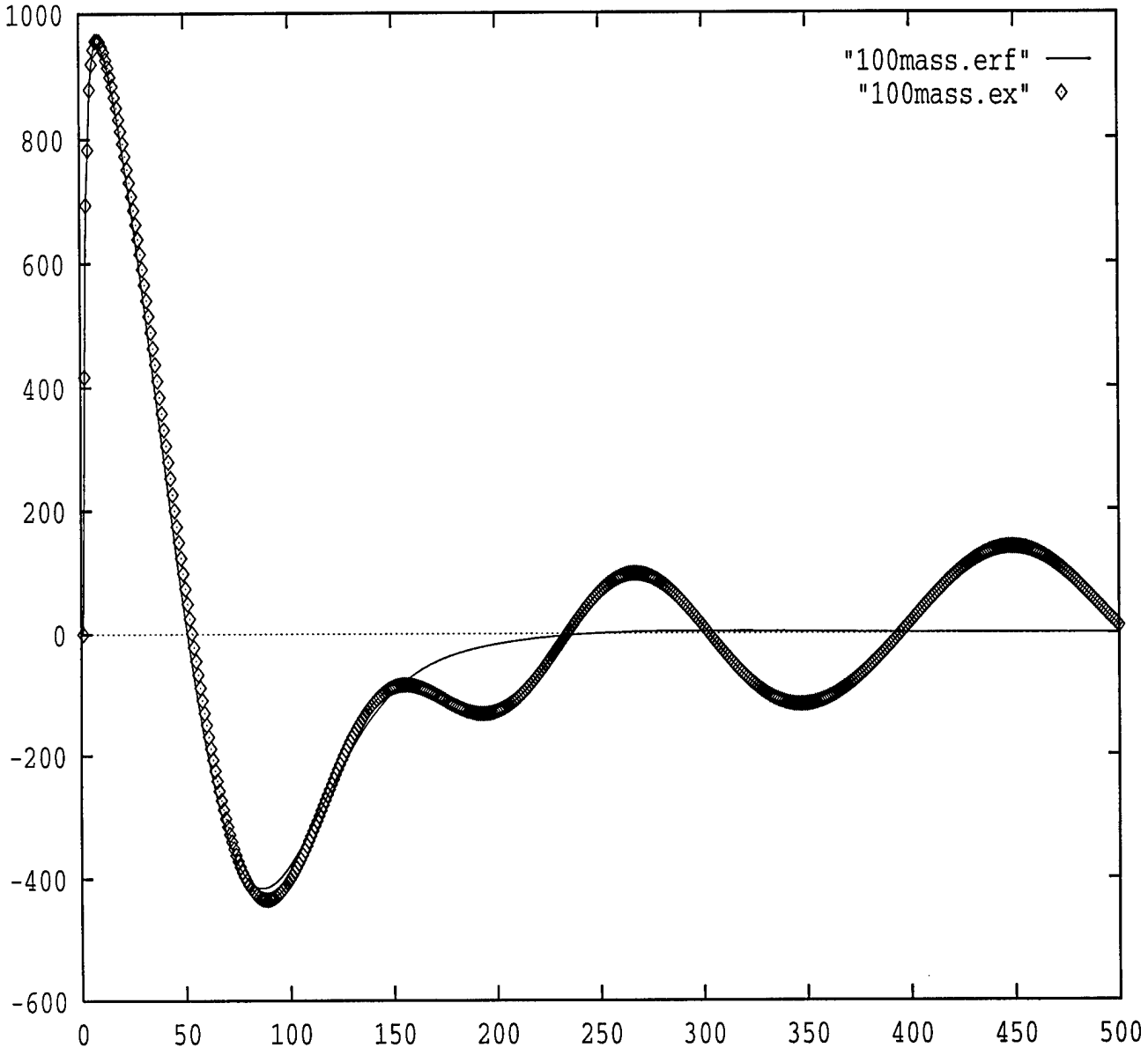

Figure 6.4: Dynamical subsystem with 100 internal degrees of freedom.

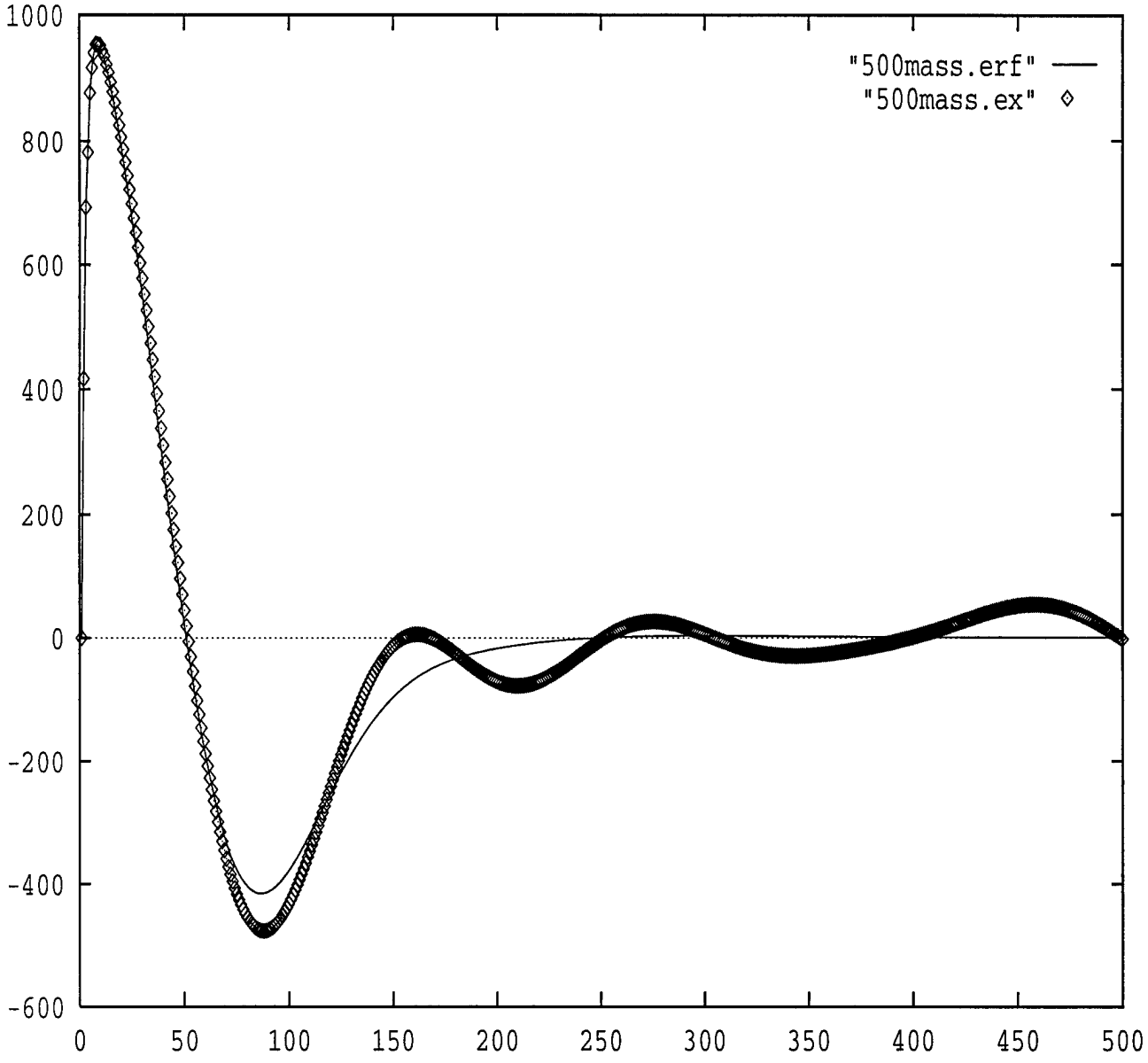

Figure 6.5: Dynamical subsystem with 500 internal degrees of freedom.

In figures 6.3 through 6.5 we see the effect of the number of internal degrees of freedom (modes) on the exact and approximate DtN's (5.6) and (5.10) respectively. Note that in these plots neither the exact DtN nor the approximate DtN have any added damping. As the number of modes M increases we expect the forces predicted by the approximate DtN in (5.10) to better approximate the forces predicted by the exact DtN (5.6). From these figures we see that the approximate DtN indeed provides a better representation of the exact DtN as the number of modes increase from ten (figure 6.3) to five hundred (figure 6.5).

We now demonstrate the effects of subsystem damping on the performance of the approximate DtN (5.10). In figures 6.6 through 6.8 we keep the number of degrees of freedom M fixed and vary the damping η. Figures 6.6 through 6.8 contain representations of subsystems with one hundred internal degrees of freedom. The damping in the exact DtN of these figures is one percent, five percent and ten percent of critical damping, respectively. Note that the approximate DtN's in these figures are identical and contain no damping.

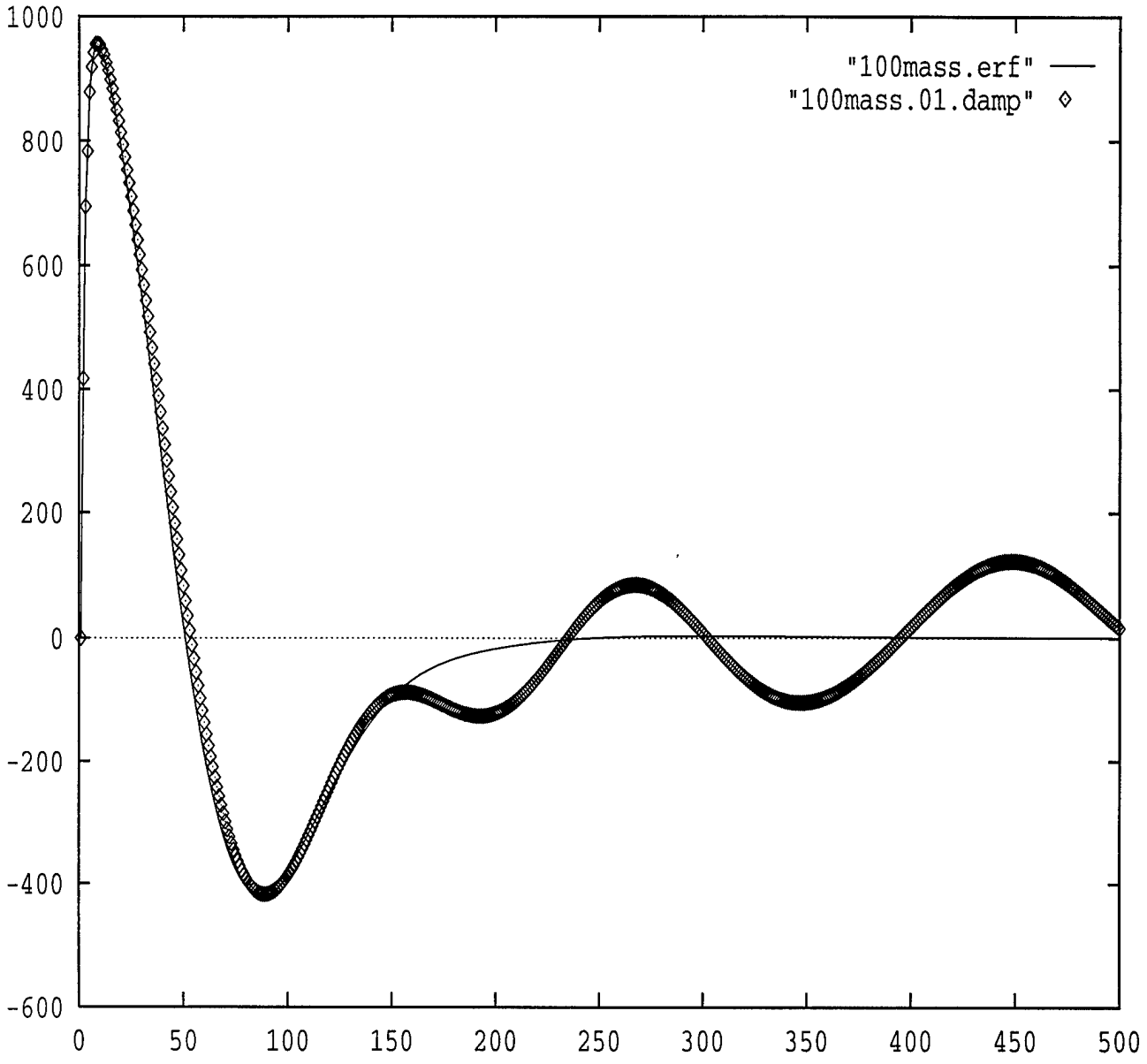

Figure 6.6: Subsystem with 100 degrees of freedom and 1% damping.

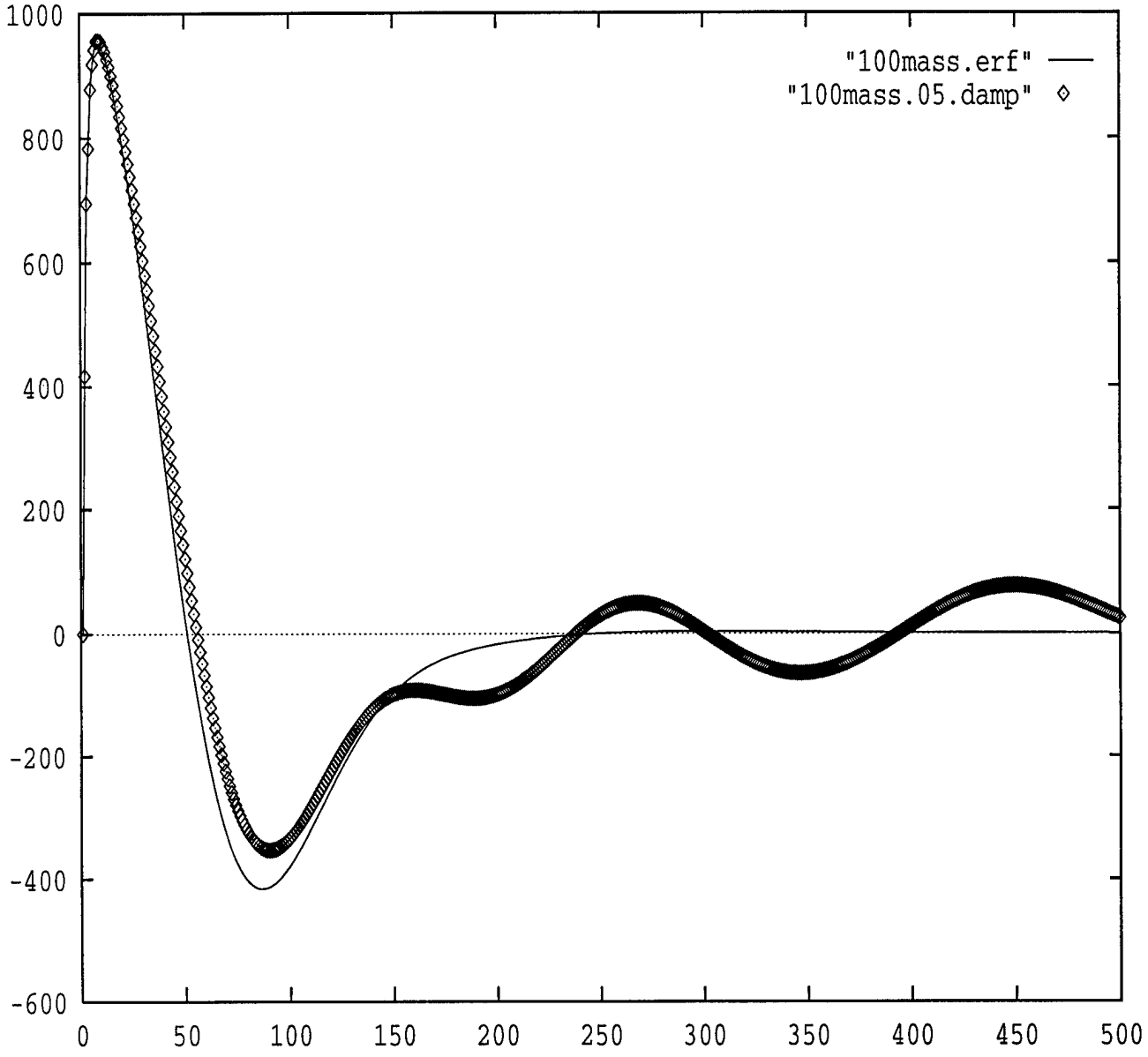

Figure 6.7: Subsystem with 100 degrees of freedom and 5% damping.

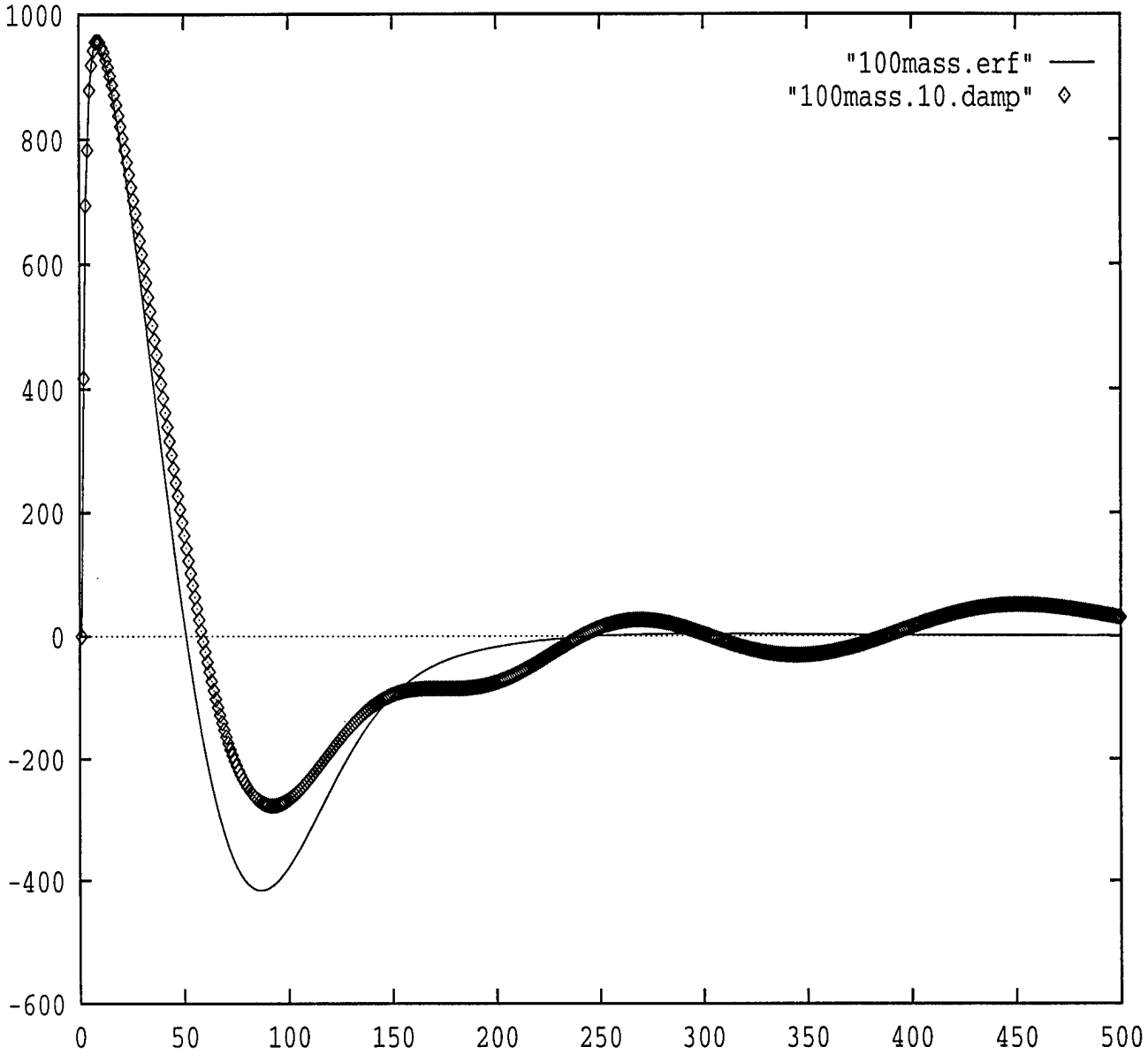

Figure 6.8: Subsystem with 100 degrees of freedom and 10% damping.

Based on the results from chapter 4 we should expect that increased damping with fixed M would control the long time error in the simulations. In these figures we see precisely this behavior as η is increased from 1% to 10% of critical damping. We can also compare figures 6.4 and 6.6 to see that a small amount of damping (1%) has increased the agreement between the exact and approximate DtN's for a subsystem with one hundred internal degrees of freedom.

Chapter 7

Conclusions

In chapter 2 we formulated the equations of motion for a general dynamical subsystem. In chapter 3 we showed that a general dynamical subsystem can be represented by an exact Dirichlet to Neumann map. The map can be used to replace the subsystem in a dynamical simulation. In developing the DtN we find a generalization of the modal mass tensor of Cunniff and O'Hara [3] and Pierce [2]. In chapter 4 we provided approximate representations for a general dynamical subsystem. We proved that the error in approximating the exact DtN map of a general dynamical subsystem can be bounded for all time in the presence of subsystem damping. We also showed that in the absence of damping the error can be bounded for times of the order $O(1/\epsilon^{3/2})$, where ϵ is a small parameter that is inversely proportional to the number of modes in the subsystem. We then showed three levels of approximations for the modal mass function (tensor) $\mathbf{m}(\omega)$, of a general dynamical subsystem. In chapter 5 we discussed implementation methods for certain approximate DtN maps based on the natural frequency scale of the components of the subsystem. Finally, in chapter 6 we studied an example problem and performed a dynamical simulation using both our exact and approximate DtN's. The simulation demonstrates the validity of our results when the number of modes is high or when there is some small amount of damping.

Bibliography

[1] C. Lanczos. *The Variational Principles of Mechanics.* Dover, reprint of fourth (1970) edition, 1986.

[2] A.D. Pierce. Resonant-frequency-distribution of internal mass inferred from mechanical impedance matrices, with application to fuzzy structure theory. In *Proceedings of ASME Symposium on Acoustics of Submerged Structures and Transduction Systems.* ASME Press, New York, September 17-21 1995.

[3] G.J. O'Hara and P.F. Cunniff. Elements of Normal Mode Theory.*Naval Research Laboratory Report*, 6002, 1963.

[4] D. Givoli. *Numerical Methods for Problems on Infinite Domains.* Elsevier, Amsterdam, first edition, 1992.

[5] Paul E. Barbone. Equipment Representations for Shock Calculations: Time Domain Dirichlet to Neumann Maps. *Boston University, Department of Aerospace and Mechanical Engineering Technical Report No. AM-95-012*, April 1995.

[6] M. Abramowitz and I. A. Stegun. *Handbook of Mathematical Functions.* Dover Publications, New York, 1972.

[7] Thomas J.R. Hughes, R.M. Ferencz, A.M. Raefsky. DLEARN: A Linear Static And Dynamic Finite Element Analysis Program. *Chapter 10: The Finite Element Method.* Prentice-Hall, Inc., New Jersey, 1987.

[8] Thomas J.R. Hughes. *The Finite Element Method (Linear Static and Dynamic Finite Element Analysis).* Prentice-Hall, Inc., New Jersey, 1987.

[9] J.S. Przemieniecki. *Theory of Matrix Structural Analysis.* Dover, reprint of (1968) edition, 1985.

[10] Roy R. Craig Jr. and Mervyn C.C. Bampton. Coupling of Substructures for Dynamic Analyses. *AIAA Journal.* Vol. 6, No. 7, July 1968.

[11] A. L. Hale and L. Meirovitch. A General Substructure Synthesis Method for the Dynamic Simulation of Complex Structures. *Journal of Sound and Vibration.* Vol. 69, 309-326, 1980.

[12] Richard Weaver and J. Turner. Radiative Transfer in Structural Acoustics. *Office of Naval Research: Structural Dynamics and Structural Acoustics Program Review; Part 1.* Luise Couchman, Ed. Orlando, FL, February 12-15, 1996.

C.6 Equipment Representations for Shock Calculations: Time Domain Dirichlet to Neumann Maps

"Equipment Representations for Shock Calculations: Time Domain Dirichlet to Neumann Maps," Paul E. Barbone, *Acoustics, Vibrations, and Rotating Machines*, Vol. 3, Part B, pp. 223–228, Proceedings of the 1995 Design Engineering Technical Conferences, Sept. 17–20, 1995. ASME Press, New York.

DE-Vol. 84-2, 1995 Design Engineering Technical Conferences
Noise Control and Acoustics Divsion
ASME 1996

Equipment representations for shock calculations: Time domain Dirichlet to Neumann Maps

Paul E. Barbone
Department of Aerospace and Mechanical Engineering
Boston University
Boston, Massachusetts

ABSTRACT

Large scale dynamic simulations can often be simplified by appropriately replacing large portions of the domain by a Dirichlet to Neumann, or DtN map (Givoli, 1992). Here we consider the problem of representing a dynamical subsystem, a piece of equipment aboard a naval vessel for example, in terms of an equivalent time domain DtN map. The exact DtN map is computed as a modal summation. The exact map is then approximated in both the low and high modal density regimes. The approximate DtN in the high modal density limit is computed utilizing fuzzy-structures concepts recently developed by Pierce, Sparrow and Russel (1993) and others. The resulting DtN map depends on just two easily determined system parameters: the total mass and the high-frequency stiffness.

INTRODUCTION

Large scale dynamic simulations can often be simplified by appropriately replacing large portions of the domain by a Dirichlet to Neumann, or *DtN* Map (Givoli, 1992) . Here we consider the problem of representing a dynamical subsystem, a piece of equipment aboard a naval vessel for example, in terms of an equivalent DtN Map. In this contribution, we use the term "DtN" to denote the map that takes displacement histories into current forces. Here, we consider the force to be Neumann data, and the displacement to be Dirichlet data.

We shall consider a subsystem to be attached to a main structure at distinct points. The DtN map yields the forces at the attachment points in terms of the displacement histories of the attachment points. Thus, given the DtN map for a piece of equipment, the effect of that piece of equipment on the dynamics of a structure is fully taken into account.

Though exact representations of equipment models may be available, approximate representations are often attractive. There are at least two reasons for this. First, the approximate representation may provide sufficient accuracy at greatly reduced computational expense. Second, and perhaps more importantly, an approximate representation involves only a few gross parameters of the dynamical system, sometimes as few as two. These parameters can be easily estimated, thus permitting simulations to be performed with relatively little knowledge of the dynamic equipment parameters.

In the next section, we formulate the problem of determining the DtN in the context of an equipment model proposed by Pierce (1995). We then solve the equations of motion of the system and derive an exact expression for the DtN. After examining two simple limiting cases, we consider two main simplifications to the exact DtN. The first simplification is applicable in the limit of low modal density. The second is valid in the limit of high modal density. It represents a time-domain application of Pierce, Sparrow and Rus-

sel's (1993) fuzzy-structures concepts. Both simplifications depend on relatively few dynamical parameters.

FORMULATION

We consider a dynamical subsystem which has a quadratic potential energy function in the N degrees of freedom, x_n, $n = 1, \ldots, N$. We shall assume that the dynamical system is attached to the outside world at only one attachment point. The displacement of the attachment point from equilibrium is denoted by $x_0(t)$, and we further assume that the attachment point has no associated mass. We will denote by $f_0(t)$ the force that is applied to the attachment point. The "DtN" condition that we will derive represents a map from $x_0(t)$ to $f_0(t)$. Thus, the effect of the dynamical subsystem can be included in a dynamical simulation by employing the following boundary condition at the attachment point

$$f_0(t) = M\, x_0(t). \tag{1}$$

Here, M denotes the DtN map.

In what follows, x_0 and x_n are purely unidirectional. The extension to many attachment points and three dimensional displacements follows as an exercise.

In the case when $f_0 = 0$, we can write the potential energy function as

$$V(x_0, \mathbf{x}) = \frac{1}{2}[\mathbf{x} \cdot \mathbf{K}\mathbf{x} + 2x_0\, \check{} \cdot \mathbf{x} + k_o {x_0}^2]. \tag{2}$$

Here, $\mathbf{x}$ is an N dimensional displacement vector, $\mathbf{K}$ is an $N \times N$ positive definite matrix, $\check{}$ is an N dimensional vector of spring constants, and k_o is a coupling spring constant. The potential energy function must be invariant to rigid body translation (Pierce, 1995). Therefore, for all α

$$V(x_0 + \alpha, \mathbf{x} + \alpha p) = V(x_0, \mathbf{x}). \tag{3}$$

In (3), p is an N dimensional vector with each component equal to unity. Substituting (2) into (3) yields

$$\mathbf{K}p = -\check{} \tag{4}$$

$$k_o = -p \cdot \check{} = p \cdot \mathbf{K}p. \tag{5}$$

We introduce the positive definite mass matrix $\mathbf{M}$ which allows us to write the kinetic energy function as:

$$T(\dot{\mathbf{x}}) = \dot{\mathbf{x}} \cdot \mathbf{M}\dot{\mathbf{x}}. \tag{6}$$

After applying Lagrange's dynamical equations of motion (Lanczos, 1986), we write the equations of motion for our system as:

$$\mathbf{M}\ddot{\mathbf{x}} + \mathbf{K}\mathbf{x}(t) = -\check{}\, x_0(t) \tag{7}$$

$$\check{} \cdot (\mathbf{x}(t) - p x_0(t)) = f_0(t). \tag{8}$$

LOCAL (IN TIME) APPROXIMATIONS

The DtN map is obtained by solving (7) for $\mathbf{x}(t)$, and substituting the result into (8). In this section we shall consider approximate solutions of (7) in both the high and low frequency limits.

Low frequency limit

When the time scale of the excitation is much slower than the natural frequencies of the subsystem, then the inertia of the subsystem is negligible to a first approximation. To obtain an approximate DtN in this case, we rewrite (7) as

$$\mathbf{K}\mathbf{x}(t) = -\check{}\, x_0(t) - \mathbf{M}\ddot{\mathbf{x}}. \tag{9}$$

Solving (9) by iteration yields

$$\mathbf{x}(t) = -\mathbf{K}^{-1}\check{}\, x_0(t) + \mathbf{K}^{-1}\mathbf{M}\mathbf{K}^{-1}\check{}\, \ddot{x}_0(t) - \mathbf{K}^{-1}\mathbf{M}\mathbf{K}^{-1}\mathbf{M}\mathbf{K}^{-1}\check{}\, \frac{d^4 x_0(t)}{dt^4} + \ldots \tag{10}$$

We now substitute (10) into (8) and simplify using (5) to obtain

$$f_0(t) = M_T\, \ddot{x}_0(t) - p \cdot \mathbf{M}\mathbf{K}^{-1}\mathbf{M}p\, \frac{d^4 x_0(t)}{dt^4} + \ldots. \tag{11}$$

Here, we have introduced the symbol $M_T = p \cdot \mathbf{M}p$ which represents the total mass in the subsystem. We note that to leading order, the force is merely accelerating the subsystem as a rigid body.

High frequency limit

Alternatively, the time scale of the excitation may be much higher than any of the natural frequencies of the dynamical subsystem. In this case, the inertia term in equation (7) dominates. We rewrite (7), therefore, as

$$\mathbf{M}\ddot{\mathbf{x}}(t) = -\check{}\, x_0(t) - \mathbf{K}\mathbf{x} \tag{12}$$

$$\mathbf{M}\ddot{\mathbf{x}}(t) \approx -\check{}\, x_0(t) \tag{13}$$

Taking two time derivatives of (8) and simplifying using (13) yields

$$\ddot{f}_0(t) = k_o\, \ddot{x}_0(t) - \check{} \cdot \mathbf{M}\check{}\, \ddot{x}_0(t). \tag{14}$$

At very high frequencies, the last term in (14) can be neglected yielding

$$\ddot{f}_0(t) = k_o\, \ddot{x}_0(t). \tag{15}$$

From (15), we see that in this regime the force is resisted primarily by the elasticity in the equipment mount. Based on the interpretation of (15), we refer to the quantity k_o as the "high-frequency stiffness."

EXACT DtN MAP

An exact DtN map can be constructed by solving (7) exactly and substituting the result into (8). An exact solution of (7) can be constructed in terms of a Green's function. The Green's function itself shall be found in terms of the modes of vibration of the dynamical subsystem.

The Green's function

The Green's function, $g(t-\tau)$ satisfies

$$\mathbf{M}\,\ddot{g}(t-\tau) + \mathbf{K}\,g(t-\tau) = -\delta(t-\tau), \tag{16}$$

$$g(t-\tau) = 0 \qquad t < \tau. \tag{17}$$

Equation (7), together with equations (16) and (17) show that $\mathbf{x}(t)$ is given by

$$\mathbf{x}(t) = \int_{-\infty}^{t} g(t-\tau)\, x_0(\tau)\, d\tau. \tag{18}$$

We now solve (16) for g in terms of a normal mode expansion. We begin by introducing a change of dependent variables

$$g(t) = \mathbf{M}^{-1/2}\, y(t). \tag{19}$$

Here, $\mathbf{M}^{1/2}$ is the unique positive definite matrix which satisfies $\mathbf{M}^{1/2}\,\mathbf{M}^{1/2} = \mathbf{M}$. (We shall not have the need to calculate $\mathbf{M}^{1/2}$ explicitly here.) Substituting (19) into (16) and left multiplying both sides by $\mathbf{M}^{-1/2}$ yields

$$\ddot{y}(t) + \mathbf{M}^{-1/2}\mathbf{K}\mathbf{M}^{-1/2}\, y(t) = -\mathbf{M}^{-1/2}\,\delta(t). \tag{20}$$

The matrix $\mathbf{M}^{-1/2}\mathbf{K}\mathbf{M}^{-1/2}$ is $N \times N$, symmetric and positive definite. It therefore possesses N distinct, orthonormal eigenvectors $\phi^{(n)}$ $n = 1, \ldots, N$, and N (not necessarily distinct) positive eigenvalues ω_n^2. Since $\phi^{(n)}$ are orthonormal and span R^N, we can write

$$y(t) = \sum_{n=1}^{N} \phi^{(n)}\, z_n(t). \tag{21}$$

We now substitute (21) into (20) and make use of the orthonormality of $\phi^{(n)}$ to obtain

$$\ddot{z}_n(t) + \omega_n^2\, z_n(t) = -\phi^{(n)} \cdot \mathbf{M}^{-1/2}\,\delta(t). \tag{22}$$

Further, causality requires

$$z_n(t) = 0 \qquad t < 0. \tag{23}$$

Solving (22) subject to the condition (23) yields

$$z_n(t) = -\frac{1}{\omega_n}\,\phi^{(n)} \cdot \mathbf{M}^{-1/2}\,\sin(\omega_n t) \qquad t \geq 0. \tag{24}$$

We obtain $g(t)$ by using (24) in (21) and (19) to find, for $t > 0$

$$g(t) = -\mathbf{M}^{-1/2} \sum_{n=1}^{N} \frac{1}{\omega_n}\,\phi^{(n)}[\phi^{(n)} \cdot \mathbf{M}^{-1/2}]\,\sin(\omega_n t). \tag{25}$$

With $g(t)$ determined, the exact DtN condition follows directly using (18) and (8):

$$f_0(t) = -\delta \cdot p x_0(t) - \int_{-\infty}^{t} \Big\{ \delta \cdot \mathbf{M}^{-1/2} \times \sum_{n=1}^{N} \frac{1}{\omega_n}\,\phi^{(n)}[\phi^{(n)} \cdot \mathbf{M}^{-1/2}\delta] \times \sin\omega_n(t-\tau)\, x_0(\tau) \Big\} d\tau. \tag{26}$$

Equation (26) can be simplified by utilizing the concept of modal mass. O'Hara and Cunniff (1963) define the modal mass as (see also Pierce (1995))

$$m_n = (p \cdot \mathbf{M}^{1/2}\phi^{(n)})^2. \tag{27}$$

From the definition of $\phi^{(n)}$, we note that

$$\mathbf{M}^{-1/2}\mathbf{K}\mathbf{M}^{-1/2}\phi^{(n)} = \omega_n^2\,\phi^{(n)}. \tag{28}$$

We left multiply (28) by $\delta \cdot \mathbf{K}^{-1}\mathbf{M}^{1/2}$, and use (4) to find

$$\delta \cdot \mathbf{M}^{-1/2}\phi^{(n)} = -\omega_n^2 p \cdot \mathbf{M}^{1/2}\phi^{(n)}. \tag{29}$$

We now use (29) and (27) to simplify (26) and obtain

$$f_0(t) = k_o x_0(t) - \int_{-\infty}^{t} \sum_{n=1}^{N} m_n \omega_n^3\, \sin\omega_n(t-\tau)\, x_0(\tau)\, d\tau. \tag{30}$$

Equation (30) represents the exact DtN for the dynamical subsystem under consideration. In general, $2N$ parameters are required to characterize the subsystem. In practice, N can be arbitrarily large, or

even infinite. In such situations, it is often beneficial to consider approximations to (30) in which the DtN can be accurately represented by relatively few effective parameters. Two such approximations will be discussed in the next sections.

LOW MODAL DENSITY

The exact DtN map (30) above can simplified by taking explicit account of the time scales of the excitation. Already in an earlier section, we addressed the case when the excitation time scale was either long or short, respectively. Here, we can use similar approximations for each mode independently. Thus, high frequency modes will contribute predominantly stiffness, low frequency modes will contribute predominantly mass, and we will find that "mid-frequency" modes will contribute predominantly damping.

To make the approximations just described more precise, we shall introduce the short (long) time scale t_0 (T_0). t_0 corresponds to the highest frequency contained in $x_0(t)$. T_0, on the other hand, corresponds to the support of $x_0(t)$, or equivalently, the lowest frequency it contains. With these definitions, we can write the force $f_0(t)$ as the sum of four contributions:

$$f_0(t) = k_o x_0(t) + f_1(t) + f_2(t) + f_3(t) \tag{31}$$

$$f_1(t) = -\sum_{\omega_n < 2\pi/T_o} m_n \omega_n^3 \int_{-\infty}^{t} \sin\omega_n(t-\tau)\; x_0(\tau) d\tau \tag{32}$$

$$f_2(t) = -\sum_{2\pi/t_o < \omega_n} m_n \omega_n^3 \int_{-\infty}^{t} \sin\omega_n(t-\tau)\; x_0(\tau) d\tau \tag{33}$$

$$f_3(t) = -\sum_{2\pi/T_o \le \omega_n \le 2\pi/t_o} m_n \omega_n^3 \int_{-\infty}^{t} \sin\omega_n(t-\tau)\; x_0(\tau) d\tau. \tag{34}$$

We now find local approximations to $f_1(t)$ and $f_2(t)$ similar to those found earlier, but here applied to time scales characterizing individual modes rather than the equipment overall.

Low frequency modes

Local approximations to $f_1(t)$ are obtained by successive differentiation of (32), treating ω_n as a small parameter relative to $2\pi/T_0$. Upon taking two time derivatives of (32), we find

$$\ddot{f}_1(t) = -\sum_{\omega_n < 2\pi/T_o} m_n \omega_n^3 \Big[\omega_n x_0(t) - \omega_n^2 \int_{-\infty}^{t} \sin\omega_n(t-\tau)\; x_0(\tau)\, d\tau\Big]. \tag{35}$$

In this range of frequencies, we may neglect the second term in (35) relative to the first term and write

$$\ddot{f}_1(t) \sim -\frac{k_L}{T_o^2} x_0(t)\big(1 + O(\omega_n^2 T_o^2)\big). \tag{36}$$

Here, k_L is defined as

$$k_L = T_o^2 \sum_{\omega_n < 2\pi/T_o} m_n \omega_n^4. \tag{37}$$

Higher approximations can be obtained by taking higher order derivatives of (32) and using intermediate results to simplify. For example, taking four time derivatives of (32) and using (36) yields

$$\frac{d^4 f_1(t)}{dt^4} + \sum_{\omega_n < 2\pi/T_o} m_n \omega_n^6 T_o^2/k_L \frac{d^2 f_1(t)}{dt^2} \sim -\frac{k_L}{T_o^2} \ddot{x}_0(t)\big(1 + O(\omega_n^4 T_0^4)\big). \tag{38}$$

High frequency modes

Local approximations to $f_2(t)$ are obtained by successive integrations by parts. Integrating (33) by parts twice yields

$$f_2(t) \sim -\left[k_H x_0(t) + m_H \ddot{x}_0(t)\right]\left(1 + O(\omega_n t_o)^{-4}\right). \tag{39}$$

Here, we define k_H and m_H to be

$$k_H = \sum_{2\pi/t_o < \omega_n} m_n \omega_n^2, \tag{40}$$

$$m_H = \sum_{2\pi/t_o < \omega_n} m_n \tag{41}$$

We note that when $t_o \to \infty$, $k_H \to k_o$, and $m_H \to M_T$, thus reproducing the local mass limit (11).

Low modal density: summary

When the modal density is such that clear distinct modes of vibration exist within the frequency ranges of interest, the exact DtN can be broken up into four individual contributions (c.f. equation (31)). Three of those contributions can be written approximately in a form which is local in time. We summarize those results here, using equations (31-34), (36) and (39):

$$f_0(t) = k_o x_0(t) + f_1(t) + f_2(t) + f_3(t) \tag{42}$$

$$f_1(t) \sim -\frac{k_L}{T_0^2} x_0(t) \tag{43}$$

$$f_2(t) \sim -k_H x_0(t) + m_H \ddot{x}_0(t) \tag{44}$$

$$f_3(t) = -\sum_{2\pi/T_o \le \omega_n \le 2\pi/t_o} m_n \omega_n^3 \int_{-\infty}^{t} \sin\omega_n(t-\tau) x_0(\tau) d\tau. \tag{45}$$

The fourth contribution, f_3, can not be simplified beyond the form of (45). The number of terms in the sum, however, can be quite small. For some applications, as few as one term will be sufficient. Thus, a subsystem may be well represented by as few as five parameters (one term in (45)), and probably not many more than 17 (seven terms in (45)). We emphasize, however, that *these parameters depend explicitly on the time scales present in the excitation.*

If a large number of frequencies are within the excitation time scales, then a large number of terms are required in equation (45). In this case, however, the dynamics of the subsystem may be approximated using a high modal density assumption. In the next section, we discuss the high modal density limit, and show that the number of system parameters can be reduced to two; they are excitation independent and can be easily measured.

HIGH MODAL DENSITY

In the last section, we simplified the form of the exact DtN map (30) by making assumptions regarding the form of the excitation. In this section, we instead make an assumption regarding the complexity of the dynamical subsystem and thereby simplify the DtN map. Specifically, we assume that the modes are closely spaced in frequency. We also make use of Pierce's (1995) notion of mass as a function of natural frequency. Therefore, we introduce the function, $m(\omega)$, such that

$$(\omega_{n+1} - \omega_n)\frac{dm(\omega_n)}{d\omega} = m_n. \tag{46}$$

Substituting (46) into the exact DtN condition (30), we obtain

$$\begin{aligned} f_0(t) &= k_o x_0(t) - \int_{-\infty}^{t} \sum_{n=1}^{N} (\omega_{n+1} - \omega_n)\frac{dm(\omega_n)}{d\omega}\omega_n^3 \\ &\times \sin\omega_n(t-\tau)\, x_0(\tau)\, d\tau. \end{aligned} \tag{47}$$

The assumption of high modal density, or closely spaced modes, allows us to replace the summation over natural frequencies in (47) with an integration over all frequencies

$$\begin{aligned} f_0(t) &\approx k_o x_0(t) - \int_{-\infty}^{t} \int_{0}^{\infty} \frac{dm(\omega)}{d\omega}\omega^3 \\ &\times \sin\omega(t-\tau)\, d\omega\, x_0(\tau)\, d\tau. \end{aligned} \tag{48}$$

Form of $m(\omega)$

In general, the function $m(\omega)$ must have the following properties (Pierce, 1995):

- $m(0) = 0.$
- $\lim_{\omega\to\infty} m(\omega) = M_T.$
- $\frac{dm}{d\omega} \geq 0.$

A function which is representative of the class of functions satisfying the above properties is

$$m(\omega) = M_T \,\mathrm{erf}(\omega/\sqrt{2}\Omega). \tag{49}$$

Here, $\mathrm{erf}(z)$ is the error function of z (Abramowitz & Stegun, 1972). Besides being representative of other similar functions, it is reasonable to assume that the error function will be a limiting case for infinite modal density, independent of the particular characteristics of the dynamical subsystem. Therefore, it is of particular interest to focus on the specific form of $m(\omega)$ as described in (49).

Equation (49) contains two parameters which describe the dynamical subsystem. The first is the total mass, M_T. The second parameter is Ω, which is a natural frequency scale of the dynamical subsystem. We shall show later that

$$\Omega = \sqrt{\frac{k_o}{M_T}}. \tag{50}$$

High modal density: time domain fuzzy-structure

Equation (48) simplifies considerably with the assumed form of $m(\omega)$, equation (49). Substituting (49) into (48) and integrating by parts repeatedly with respect to ω yields

$$\begin{aligned} f_0(t) = k_o x_0(t) - \frac{M_T\Omega^3\sqrt{2}}{\sqrt{\pi}}\int_{-\infty}^{t}(t-\tau)[3-\Omega^2(t-\tau)^2] \\ \times \int_0^{\infty} e^{-\omega^2/8\Omega^2}\cos\omega(t-\tau)\, d\omega\; x_0(\tau)\, d\tau. \end{aligned} \tag{51}$$

We evaluate the remaining integral with respect to ω by writing $\cos\omega(t-\tau) = \mathcal{R}\{e^{i\omega(t-\tau)}\}$, completeing the square in the exponent, then taking the real part:

$$f_0(t) = k_o x_0(t) - \int_{-\infty}^{t} k_f(t-\tau)\, x_0(\tau)\, d\tau, \tag{52}$$

$$k_f(t) = M_T\Omega^3\, \Omega t\,[3-\Omega^2 t^2]\, e^{-t^2\Omega^2/2} \tag{53}$$

Equation (52) is the simplified representation of the DtN Map under the assumptions of high modal density, and an error function modal mass distribution as a function of natural frequency. The three parameters appearing in (52), M_T, k_o, and Ω, are related to each other as shown in the next section.

Relation between M_T, k_o, and Ω

We shall now determine a relation between M_T, k_o, and Ω by considering the special case of

$$x_0(t) = A_0\, H(t). \tag{54}$$

Here, $H(t)$ is the Heaviside step function, and A_0 is the magnitude of the step. As a result of moving the attachment point suddenly an amount A_0, the force $f_0(t)$ will change suddenly, and then relax. On physical grounds, we can expect that

$$\lim_{t\to\infty} f_0(t) = 0. \tag{55}$$

That is, we expect that the system will eventually relax back to an unstressed equilibrium.

Substituting (54) into (52) yields

$$\begin{aligned} f_0(t) &= A_0 k_o H(t) - A_0 \int_0^t k_f(t-\tau)\, d\tau H(t) && (56)\\ &= A_0 k_o H(t) - A_0 M_T \Omega^2 [1 \\ &\qquad -(1-\Omega^2 t^2)\, e^{-t^2\Omega^2/2}] H(t) && (57)\\ &\to A_0 [k_o - M_T \Omega^2] \qquad t\to\infty && (58) \end{aligned}$$

Employing condition (55) with (58), we find

$$\Omega^2 = k_o / M_T. \tag{59}$$

High modal density: summary

When the modal density is so high (or when damping is such that sufficient modal overlap exists) that distinct modes of vibration become "blurred" in the frequency domain, then the exact DtN map, (30) can be greatly simplified. The result is (52), repeated here for convenience:

$$\begin{aligned} f_0(t) &= k_o x_0(t) - \int_{-\infty}^{t} k_f(t-\tau)\; x_0(\tau)\, d\tau, && (60)\\ k_f(t) &= M_T \Omega^3\; \Omega t\, [3 - \Omega^2 t^2]\, e^{-t^2\Omega^2/2} && (61) \end{aligned}$$

The assumptions leading to (60 and 61) are high modal density and an error function modal mass distribution as a function of natural frequency. The three parameters appearing in (60), M_T, k_o, and Ω, are related to each other by $\Omega = \sqrt{k_o/M_T}$. Here, as described earlier, M_T is the total mass of the dynamical subsystem and k_o is the equivalent high-frequency stiffness of the subsystem. Thus, in order to model the effects of a dynamical subsystem on the dynamic response of a larger structure, one needs only two easily determined parameters.

ACKNOWLEDGEMENTS

This work is financially supported by the Office of Naval Research. The author is grateful to Dr. Geoff Main and Professor Allan D. Pierce for helpful discussions.

REFERENCES

Abramowitz, M. and Stegun, I.A., 1972, *Handbook of Mathematical Functions.* Dover Publications, New York.

Givoli, D., 1992, *Numerical Methods for Problems on Infinite Domains.* first edition, Elsevier, Amsterdam.

Lanczos, C., 1986, *The Variational Principles of Mechanics* reprint of fourth (1970) edition, Dover.

O'Hara, G.J. and Cunniff P.F., 1963, "Elements of normal mode theory," *Naval Research Laboratory Report*, 6002.

Pierce, A.D., 1995, "Resonant-frequency distribution of internal mass inferred from mechanical impedance matrices, with application to fuzzy structure theory," In *Proceedings of the ASME Symposium on Acoustics of Submerged Structures and Transduction Systems*, ASME Press, New York, September 17–21 1995; In this issue.

Pierce, A.D., Sparrow, V.W., and Russel D.A., 1993, "Fundamental structural-acoustic idealizations for structures with fuzzy internals," *ASME Transactions*, Paper No. 93-WA/NCA-17 (ASME Winter Annual Meeting, New Orleans), November 1993.